

Methodological Improvements in Combining TMS and Functional MRI

Dissertation

zur Erlangung des Grades eines Doktors
der Naturwissenschaften

der Mathematisch-Naturwissenschaftlichen Fakultät
und
der Medizinischen Fakultät
der Eberhard-Karls-Universität Tübingen

vorgelegt

von

Marius Moisă
aus Bacău, Rumänien

Januar 2011

Tag der mündlichen Prüfung: 06.07.2011

Dekan der Math.-Nat. Fakultät: Prof. Dr. W. Rosenstiel

Dekan der Medizinischen Fakultät: Prof. Dr. I. B. Autenrieth

1. Berichterstatter: Prof. Dr. Uwe Klose

2. Berichterstatter: Prof. Dr. Klaus Scheffler

Prüfungskommission: Prof. Dr. Wolfgang Grodd

Prof. Dr. Uwe Klose

Prof. Dr. Klaus Scheffler

Prof. Dr. Fritz Schick

Prof. Dr. Hartwig Siebner

I hereby declare that the dissertation entitled:

“Methodological improvements in combining TMS and functional MRI”

submitted for the award of a doctorate has been completed by me the undersigned and that I have not used any other than permitted reference sources or materials nor engaged in any plagiarism. All references and other sources used by me have been appropriately acknowledged in the work.

Tübingen, 31.01.2011

Marius Moisă

Table of Contents

Abstract	5
Synopsis.....	7
1. Introduction	8
2. Methodological Developments.....	13
2.1 New Coil Positioning Method for Interleaved TMS/fMRI.....	13
2.2 Validation of the Interleaved TMS/fMRI Setup.....	14
2.3 Interleaved TMS/CASL: General Setup and Quality Measurements	16
3. Interleaved TMS/CASL: Applications in Neuroscience	17
3.1 Comparison of the Effects of Two Stimulation Protocols: Continuous 2Hz rTMS and Short 10Hz rTMS Trains	17
3.2 State Dependence of rTMS Effects on the Dorsal Premotor Cortex.....	19
4. Discussion	24
5. Summary	29
6. Outlook.....	30
7. References	32
Abbreviations	37
Acknowledgements	38
Personal Contributions to the Publications	39
Manuscripts	41
M1. New Coil Positioning Method for Interleaved Transcranial Magnetic Stimulation (TMS)/Functional MRI (fMRI) and Its Validation in a Motor Cortex Study.....	42
M2. Interleaved TMS/CASL: Comparison of Different rTMS Protocols.....	52
M3. Remote Motor Cortical Areas Acutely Compensate for a Transient Lesion of Left Dorsal Premotor Cortex during Arbitrary Visuomotor Mapping.....	66

Abstract

Since 1997, when Bohning and colleagues demonstrated for the first time the feasibility of interleaving transcranial magnetic stimulation (TMS) with functional magnetic resonance imaging (fMRI), this combination became a very promising techniques to study brain connectivity. However, the implementation of a reliable setup for interleaved TMS/fMRI is still technically challenging. In this thesis, I intended to further explore and develop methodological improvements and to apply them in order to better understand the neural underpinnings of the behavioral TMS effects and to study brain connectivity. First, I developed and validated a new hardware/software coil positioning method for interleaved TMS/fMRI and demonstrated the feasibility of our overall setup. Second, a setup for combining TMS with continuous arterial spin labeling (CASL) was implemented and I tested the feasibility of this novel combination. Third, I demonstrated that this combination is sensitive enough to reliably measure rCBF changes induced by TMS, and that interleaved TMS/CASL can detect differences between the effects on regional cerebral flow (rCBF) of two different stimulation protocols. Fourth, it was shown that interleaved TMS/CASL is suitable to target questions from cognitive neuroscience. It was demonstrated that TMS applied over left dorsal premotor cortex (PMd) has different effects on the remote rCBF activation depending on the motor task. Overall, the results presented in this thesis suggest that interleaved TMS/CASL can become an interesting complement to interleaving TMS with normal blood oxygenation level dependency (BOLD) fMRI, and that this combination can be considered for studying the impact of fully-fledged repetitive TMS protocols.

Synopsis

1. Introduction

In 1985 Barker and his colleagues performed the first successful transcranial magnetic stimulation (TMS) experiment (Barker et al., 1985). Since then, TMS became a well-established noninvasive tool for stimulating the cortex of the brain, with a broad range of applications from the experimental treatment of different brain disorders to the study of the processes involved in action, cognition and perception. On the methodological level, single-pulse TMS was complemented by more complex stimulation protocols such as the “classical” repetitive TMS (rTMS) protocols (Pascual-Leone et al., 1994; Chen et al., 1997a) or theta burst protocols (Huang et al., 2005). rTMS protocols can modulate cortical excitability beyond the duration of the stimulation itself and, depending on the stimulation parameters, can induce inhibitory or facilitatory effects on the brain activity. These modulatory effects are not limited to the directly targeted cortical area, but can affect a wider neural network transynaptically. Modulation of cortical excitability by rTMS may be useful not only as a research tool but also as potential treatment of neurological and psychiatric disorders like stroke (Nowak et al., 2010; Dimyan et al., 2010) or major depression (Lam et al., 2008; Schutter et al., 2009). Thus, there is a great interest in developing novel and more effective rTMS protocols. Combining rTMS with neuroimaging is one promising way of investigating the underlying neural mechanisms and the affected networks.

In the mid-1990s TMS started to be combined with different neuroimaging methods, most commonly with positron emission tomography (PET) and functional magnetic resonance imaging (fMRI). This offers three main advantages (Siebner et al., 2001a). First, brain imaging before the TMS intervention helps to accurately position the TMS coil over a distinct cortical area which is targeted by TMS. Since TMS can be used to interfere with regional cortical function during a given task, the TMS effects on task performance can help to clarify the task-specific functional contribution of a given cortical area which has previously shown task-related activation in a functional imaging study (e.g. Sack et al., 2009). Second, brain imaging can be used to assess the aftereffects of rTMS protocols, allowing us to study the plasticity of the human cortex and to better understand their putative therapeutical effects (e.g. Speer et al., 2000; Lee et al., 2003; Siebner et al., 2003; O’Shea et al. 2007). Third, imaging the brain during TMS is a promising approach for assessing cortical excitability and intracerebral functional connectivity.

In 1997 Bohning and colleagues (Bohning et al., 1997) demonstrated for the first time the feasibility of interleaving TMS with BOLD (blood oxygenation level dependency) fMRI. Since then, interleaved TMS/fMRI proved to be a promising technique to assess brain connectivity. For example, it was used to demonstrate activity changes in remote areas of the brain induced by stimulation of the motor cortex (Bohning et al., 1998; Bestmann et al., 2003), dorsal premotor cortex (Bestmann et al., 2005), dorsolateral prefrontal cortex (Nahas et al., 2001), or the frontal eye fields (Ruff et al., 2006). In addition, TMS was used to disturb task-related activity in a brain region of interest while fMRI allowed monitoring the effects on both local and remote BOLD activations (Sack et al., 2007). This represents a substantial

extension to the classical “virtual lesion approach” (Cowey 2005) which can be used to demonstrate the causal involvement of the directly stimulated area to the task under study.

The potential advantages offered by the combination of TMS with fMRI motivated me to further explore and develop methodological improvements and to apply them in order to better understand the TMS effects on brain activity and brain connectivity. In particular, large parts of my thesis were motivated by a specific disadvantage of BOLD-based fMRI, namely its low temporal stability. This prevented the usage of interleaved TMS/fMRI in studying longer lasting rTMS effects up to now. As a result, rTMS effects were mostly studied using PET. These studies either assessed regional cerebral blood flow (rCBF) using H_2^{15}O PET (e.g. Paus et al., 1997; Siebner et al., 2001c; Speer et al., 2003) or regional cerebral metabolic rate of glucose consumption (rCMRglc) using [^{18}F]deoxyglucose PET (e.g. Siebner et al., 2001b; Siebner et al., 1998). While PET offers high sensitivity and specificity and provides absolute measurements, it has also substantial limitations such as its low temporal resolution and, in particular, the subjects’ exposure to radiation, which limits the number of measurements per subject. As an alternative to BOLD-based fMRI, I explored the possibility to combine TMS with ASL imaging. ASL provides a direct quantitative measure of perfusion (i.e., rCBF), thereby complementing the information offered by BOLD imaging in characterizing the brain responses to TMS stimulation. In particular, ASL offers better temporal stability and opens the possibility to study slow modulatory rTMS effects. Hence, during my PhD project, I had the following agenda: 1) to develop and validate a new hardware/software coil positioning method for interleaved TMS/fMRI, 2) to develop a setup and to investigate the feasibility of combining TMS with continuous arterial spin labeling (CASL), 3) to investigate if this novel combination is sensitive enough to measure the regional cerebral blood flow (rCBF) changes induced by the TMS and if it can be used to distinguish the impact of two different rTMS protocols, namely continuous 2Hz rTMS and short 10Hz rTMS trains, and 4) to investigate if interleaved TMS/CASL is suitable for targeting questions from cognitive neuroscience and if it can be used for studying brain connectivity.

The first goal of my PhD was to implement a reliable setup for interleaved TMS/fMRI (see Fig. 1a). A MR-compatible figure-8 coil (MRi-B88) is connected through a high current filter to the TMS stimulator (MagPro X100, MagVenture, Denmark) that is placed outside MR cabin in order to avoid interferences with the scanner. Custom-written software controlled by trigger signals coming from the scanner is used for interleaving the TMS pulses with the echo planar imaging (EPI) acquisition, thus preventing the TMS pulses to disturb the EPI images. The timing between the TMS pulses and the EPI acquisition is presented in Fig. 1b. First, it was checked in phantom studies if the EPI data quality was affected by the interleaved TMS pulses. An important practical challenge is the accurate positioning of the coil inside the MR scanner. Therefore, in a second step, I developed and validated a positioning method for interleaved TMS/fMRI that for the first time allows the exchange of TMS coil positions between a neuronavigation system and a MR-compatible holding device. This allows easy and precise TMS coil placement inside the MR scanner using pre-planned positions that were previously recorded using the neuronavigation system. The first part of my PhD project was

rounded off by a motor cortex study in order to demonstrate the feasibility of our overall interleaved TMS/fMRI setup.

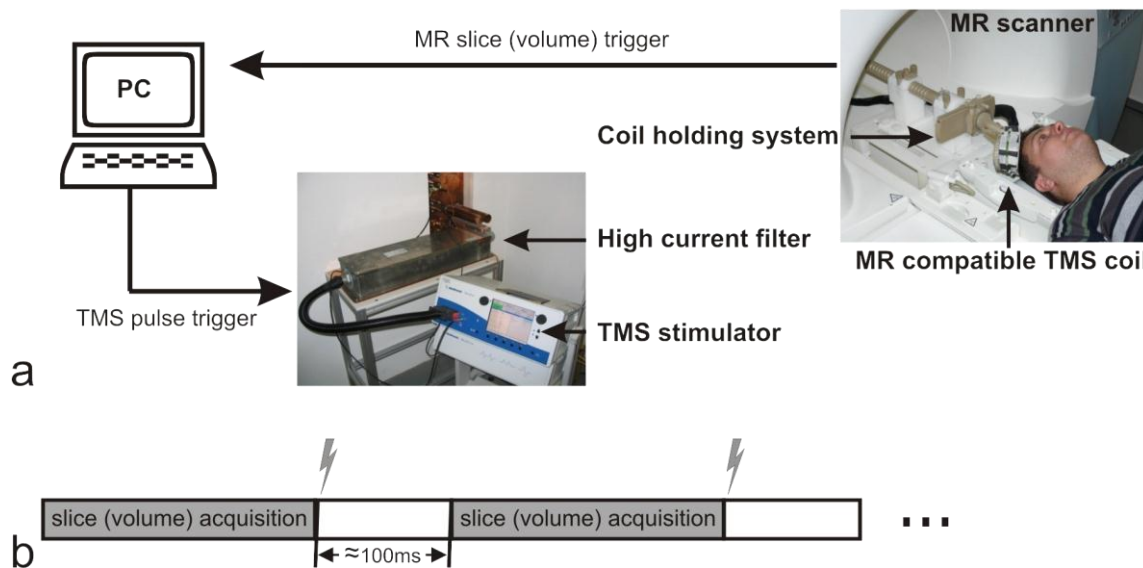


Fig. 1 a) General setup for interleaved TMS/fMRI. b) The timing between the TMS pulses and the EPI acquisition. In order to prevent the TMS pulses to disturb the EPI images a sufficiently long gap between TMS and fMRI data acquisition has to be applied ($\approx 100\text{ms}$; Bestmann et al., 2003).

The second goal of my PhD was to extend our setup to combine for the first time TMS with CASL. In ASL imaging, rCBF is assessed based on the subtraction of tag images in which an radio frequency (RF) pulse is used to tag the inflowing blood from unaltered control images (see Fig. 2). Both types of images are acquired in an alternating sequence, so that image variations caused by scanner instabilities like field drifts or subject motion effectively cancel out after subtraction, allowing the acquisition of quantitative and constant signals during long term measurements and even different sessions. This allows us to determine baseline perfusion values and to measure rCBF quantitatively and, in turn, opens the possibility to assess both the immediate and the more long-term effects of rTMS stimulation on brain baseline state and activation. In contrast to PET imaging, the subjects are not exposed to radiation and the spatial and temporal resolutions are in the range of normal fMRI experiments. However, compared both with PET and BOLD imaging, ASL offers a lower signal to noise ratio (SNR) and a limited field of view. Also, in order to combine TMS with ASL, one has to consider and to mitigate new technical challenges, besides the ones implied by the combination of TMS with BOLD fMRI.

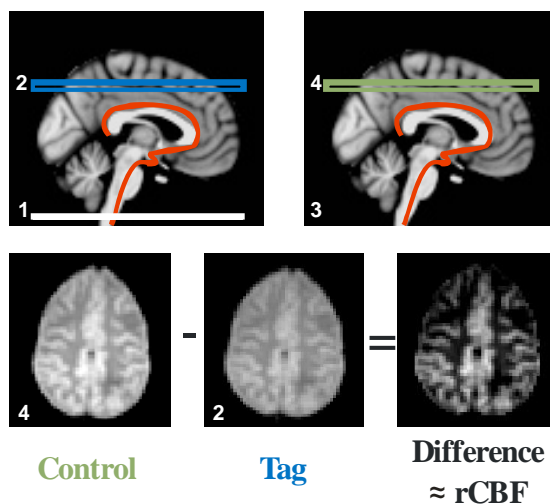


Fig. 2 Quantitative measurement of rCBF using CASL: 1 – An RF pulse is tagging the inflowing arterial blood; 2 - The tag image is acquired; 3 – The experiment is repeated without tagging; 4 – The control image is acquired. RCBF is assessed based on the subtraction of the tag image from the control image.

After the implementation of the interleaved TMS/CASL setup and after performing quality measurements, I used this technique to investigate and to compare the effects of two different stimulation protocols on rCBF (continuous 2Hz rTMS and short 10Hz rTMS trains, respectively). We choose to investigate these two protocols since combined TMS-PET studies have previously shown that periods of continuous rTMS and periods of short successive rTMS trains applied to the motor cortex act differently onto rCBF in motor and remote regions: rCBF was positively correlated with stimulation intensity for continuous 1Hz rTMS (Speer et al., 2003), while it was negatively correlated with the number of 10Hz rTMS trains (Paus et al., 1998). The two different rTMS protocols were applied to the motor cortex and the effect on rCBF was measured using CASL. Continuous 2Hz rTMS was applied at 3 different intensities while short 10Hz rTMS trains were applied at constant intensity but with varying numbers of trains per stimulation block. Our hypothesis was that motor and premotor areas will exhibit rCBF intensity dependent increases for continuous 2Hz rTMS stimulation while during the stimulation with 10Hz rTMS trains the rCBF will decrease with increasing the number of trains. We directly compared the rCBF time courses in response to these protocols, thereby capitalizing on the higher temporal resolution of CASL compared to PET imaging. The activated network due to the two stimulation protocols was also compared with the activation map elicited by volitional movement (acoustically triggered by 50% rMT stimuli).

In my last PhD project, I used interleaved TMS/CASL to investigate the task-dependency of the local and remote rCBF activations in response to stimulation of the dorsal premotor cortex (PMd). Based on studies in non-human primates, a functional distinction between the medial and lateral premotor areas is suggested: Medial areas are thought to be more involved in internally generated movements while the lateral regions (in particular their dorsal part; PMd) might preferentially contribute to tasks involving sensory-motor mappings (Mushiake et al. 1991; Passingham et al. 2004). The goal was to test the involvement of left PMd in

internally and externally generated movements performed with the ipsilateral hand, by assessing the functional effective connectivity, with the driving idea that the specialization of an area should also be reflected in its connectivity pattern (Passingham et al. 2004). Using a block design, short bursts of TMS were delivered to left PMd during three different motor states (i.e., during associative or freely selected sequential key presses with the ipsilateral hand, or during passive viewing as control). The key presses were cued by abstract visual stimuli under two different conditions corresponding to internally and externally guided movements: Subjects were asked to freely select the finger and make a fresh choice upon each new trial in one condition whereas they were required to use a prelearned arbitrary visuomotor association in the other condition.

2. Methodological Developments

2.1 New Coil Positioning Method for Interleaved TMS/fMRI

Neuronavigation systems as used in many TMS studies for the precise targeting of cortical areas (Schönfeldt-Lecuona et al., 2005) cannot be utilized inside the MR cabin. To circumvent this limitation, Bohning et al. developed a mechanical holding device in combination with a simple software program which enabled positioning of the TMS coil over a desired target area (Bohning et al., 2003) within the MRI scanner. Critically, the target had to be manually located in a structural scan acquired directly before the start of the interleaved TMS/fMRI experiment, based on the individual brain anatomy. In order to eliminate the need for the manual and time-consuming identification of individual brain structures, I developed an improved positioning method which allows accurate TMS coil placement inside the MR scanner using pre-planned coil positions previously determined with a neuronavigation system. Initially, a T₁-weighed high-resolution (1mm iso-voxel) structural image is acquired once for each subject for usage in our neuronavigation system (BrainView, Fraunhofer IPA, Stuttgart, Germany). In BrainView, coil positions-of-interest are saved with respect to the coordinate system defined by the high resolution image. In the combined TMS/fMRI experiment, the position of the subject's head is then determined using a fast structural image (FLASH) lasting ~1 min, which is automatically coregistered to the high resolution image using custom-written software (MATLAB, Natick, USA) and SPM5 (Wellcome Department, UCL, GB) functions. The software automatically determines the parameters of the coil holding device corresponding to the pre-planned coil position, thereby preventing the need to manually identify brain structures. Further software features are presented in Table 1. The accuracy of the positioning method was assessed using an agar phantom, demonstrating that pre-planned coil positions can be reached within 2.9 ± 1.3 (SD) mm (6 mm maximum offset) which is in a comparable range of spatial accuracy as reported for neuronavigation systems used outside of the MRI scanner (Schönfeldt-Lecuona et al., 2005).

<ul style="list-style-type: none"> • The high-resolution structural image is displayed together with the coregistered FLASH image to visually verify the coregistration result.
<ul style="list-style-type: none"> • A list of coil positions is provided. The user has the possibility to add a position, to restore it, and to save the overall list as MATLAB file.
<ul style="list-style-type: none"> • Head movements in the course of an experiment displace the originally targeted cortical area with respect to the fixed TMS coil. The amount of displacement can be monitored by regularly acquiring FLASH images. For each new image, the software computes an updated coil position and compares it with the positions in the list, so that the (apparent) change of coil position indicates the amount of displacement.
<ul style="list-style-type: none"> • A set of coil holding parameters can be transformed back into a coil position for usage in the neuronavigation system, or in a further interleaved TMS/fMRI session.
<ul style="list-style-type: none"> • It automatically determines the orientation of the EPI slices parallel to the TMS coil plane. This is necessary to minimize the susceptibility artifacts induced by the TMS coil (Baudewig et al., 2000).

Table 1 Features of the positioning software for the TMS coil placement inside the MR scanner.

2.2 Validation of the Interleaved TMS/fMRI Setup

Phantom measurements were acquired according to the functional biomedical informatics research network (fBIRN) protocol (Friedman et al., 2006) to test for the potential impact of the TMS pulses on the EPI image quality. Three different measurements have been performed using an agar phantom: (i) Without the TMS coil, (ii) with TMS coil, but without stimulation, and (iii) with TMS stimulation at 80% of the maximal intensity. The EPI parameters and the stimulation protocol were the same as in the motor cortex study described in the next paragraph. For each EPI slice, the mean across volumes was determined to check for static signal dropout and distortions. Additionally, the signal-to-fluctuation-noise ratio (SFNR) was determined by dividing the mean by the standard deviation across volumes. Low SFNR values signal a high temporal variability of the EPI signal, hinting, e.g. towards an unwanted impact of the TMS pulses on the EPI measurements. The SFNR calculation showed that the temporal stability was not affected by the stimulation itself. As expected, static signal dropouts could be observed due to the presence of the coil inside the MR scanner in the three slices in direct vicinity to the coil. Importantly, these slices are closer to the coil than the cortex is in normal experiments (slice thickness 4 mm, gap between slices 1 mm). Static distortions could be observed in slices up to 35 mm away from the coil on the surface of the phantom.

In order to quantify the amount of distortions in the EPI brain images, phase maps were recorded for two subjects using the standard Siemens gradient-echo field map sequence, with and without the TMS coil being positioned over the motor cortex. The voxel shifts in the images were estimated using FSL 4.0 PRELUDE and FUGUE (FMRIB, Oxford University, Oxford, UK). The analysis revealed moderate distortions that were mainly restricted to the first 4 slices underneath the coil. In both subjects, the estimated maximal pixel shifts for the corresponding EPI slices were 1.4 and -1.8 voxels, respectively. The central brain region directly underneath the TMS coil (corresponding to the stimulated M1/S1) exhibited hardly any distortions.

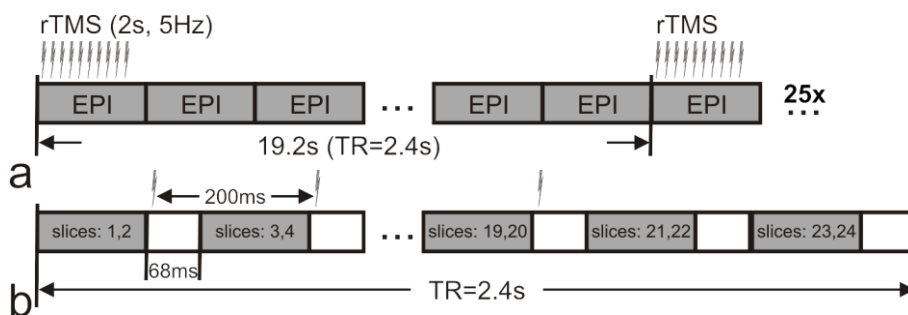


Fig. 3 RTMS stimulation protocol. a) Short 5Hz rTMS trains (10 pulses) were followed by rest periods of 17.2 s. b) Pauses of 68 ms were introduced after every 132 ms in the EPI sequence, i.e. after every second slice. The TMS pulses were applied at the beginning of these pauses, thus preventing the interference with the EPI acquisition (Bestmann et al., 2003).

In order to test the viability of our overall interleaved TMS/fMRI experimental setup, the BOLD activity induced by short 5Hz rTMS trains (10 pulses) on the motor cortex was investigated in 5 subjects. The TMS “Hot Spot” of a particular finger muscle (abductor pollicis brevis; APB) in the motor cortex (M1) was determined offline and its position was saved using the neuronavigation system. In the MR scanner, the TMS coil was placed on the “Hot Spot” using our positioning method. Subsequently, the lowest TMS intensity resulting in activation of the finger muscle (the resting motor threshold, rMT) was determined using electromyographical recordings. The TMS stimulation was interleaved with the MRI acquisition using custom-written software. Pauses of 68 ms were introduced after every 132 ms in the EPI sequence, i.e. after every second slice. The pauses were used to interleave the EPI sequence with trains of 10 biphasic TMS pulses applied every 200 ms for 2 s at 110% rMT, followed by rest periods of 17.2 s. This was repeated 25 times (see Fig. 3). Two runs with TMS stimulation at 110% rMT were acquired. In one additional run, the TMS intensity was set to 50% rMT and the subjects performed volitional thumb movements, acoustically triggered by the TMS coil clicks. The results of the supra-threshold stimulation are in concordance with previous findings (Bohning et al., 2000; Bestmann et al., 2004). Significant BOLD responses were observed in the motor system (stimulated primary sensorimotor area [M1/S1_i], cingulate and supplementary motor areas [CMA, SMA], thalamus ipsilateral to stimulated M1, bilateral putamen, bilateral cerebellum), in the bilateral auditory cortices, the ipsilateral inferior colliculus and the bilateral insula (Fig. 4a). Volitional movement resulted in stronger BOLD effects, but in a similar spatial activation pattern (Fig. 4b). Taken together, these findings and the results of the quality assurance measurements demonstrates a good EPI signal quality and validate our overall setup.

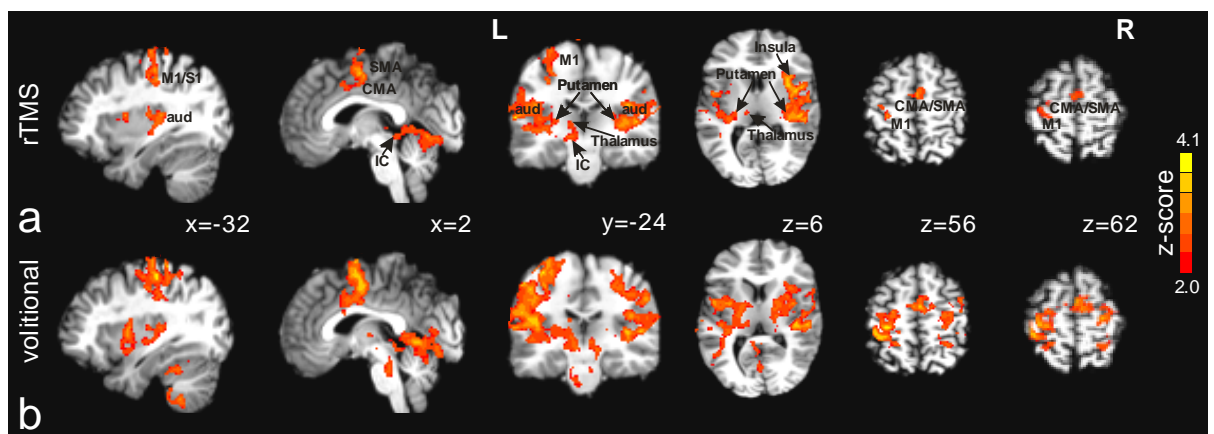


Fig. 4 a) Group activation map for rTMS stimulation (N=5, voxel threshold $z=2.3$, cluster threshold $p=0.05$ corrected, MNI space) shown on an individual structural image. b) Group activation map for volitional movement (same threshold level as used for rTMS).

2.3 Interleaved TMS/CASL: General Setup and Quality Measurements

Fig. 5 shows a schematic diagram of the interleaved TMS/CASL setup. An in-house written CASL sequence with EPI readout (2D gradient-echo echo planar imaging) and separate RF coils placed on the subject neck for labeling the inflowing blood in the right and left carotid (Zaharchuk et al., 1999) were used for assessing the rCBF. Custom written software controlled by trigger signals coming from the scanner was used for interleaving the TMS pulses with the MRI acquisition. The same software was used to interrupt the tagging phase 5 ms before and 15 ms after applying a TMS pulse in order to prevent putative TMS effects on the labeling of the inflowing blood. These temporal gaps were also applied in the rest periods.

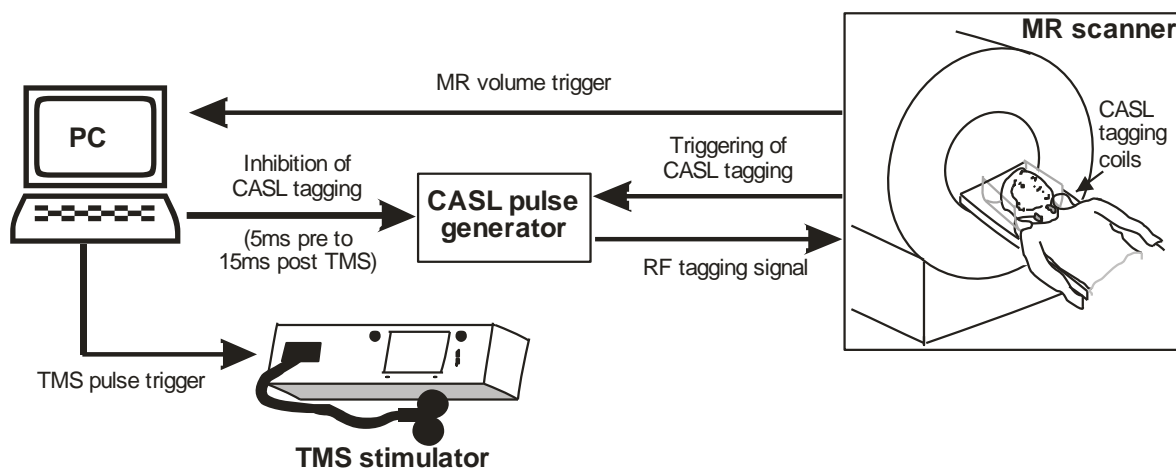


Fig. 5 Schematic diagram of the combined TMS/CASL setup.

Phantom quality measurements and phase maps images for two subjects were acquired using the procedure described in section 2.2, in order to test the feasibility of our interleaved TMS/CASL setup. Phantom measurements were performed without TMS coil, with the coil attached to the phantom but not connected to the stimulator, and during two stimulation protocols (continuous 2 Hz rTMS and 10Hz rTMS trains, 2 seconds gaps, both at 100% stimulator output). The two stimulation protocols and the CASL sequence parameters were the same as for the motor cortex study described in section 3.1. The phantom quality measurements revealed no signal drop out. Only moderate distortions in the first 3 slices at the rim of the phantom were detected due to the presence of the TMS coil. The stimulation itself had no influence on the image quality. The analysis of the phase maps measurements revealed a maximal amount of shifts of 1.3 and -2.3 voxels, respectively. The maximal voxel shifts occurred at some positions at the rim of the brain and, in general, only few voxels exhibited shifts greater than 1 or smaller than -1. Based on these results, we decided not to apply distortion correction to the CASL images in next studies. Taken together, the results of the quality assurance measurements and the findings of the phase maps measurements demonstrate that with our setup we can acquire ASL images with good quality.

3. Interleaved TMS/CASL: Applications in Neuroscience

3.1 Comparison of the Effects of Two Stimulation Protocols: Continuous 2Hz rTMS and Short 10Hz rTMS Trains

After the implementation of the interleaved TMS/fMRI setup it was investigated whether ASL imaging is sensitive enough to reliably measure TMS-induced rCBF changes and whether this combination can be used to distinguish between the impacts of two different rTMS protocols.

Interleaved TMS/CASL was performed on 10 right-handed healthy subjects at our 3T Siemens scanner. Inside the scanner, the TMS coil was positioned over the representation of a finger muscle (abductor pollicis brevis; APB) in the primary motor cortex using our positioning method (Moisa et al., 2009) and the resting motor threshold (rMT) was determined. Three different conditions were investigated in each subject: 2 Hz continuous rTMS, short 10 Hz rTMS trains and volitional movement. In total, 16 experimental runs were conducted in two different sessions, at least one week apart. The order of intervention was counterbalanced between sessions and between subjects. Each run consisted of 8 blocks and each block consisted of 24 s of rTMS followed by 52 s of rest. 2 Hz continuous rTMS was investigated for three different stimulation intensities: 100%, 110% and 120% rMT (in total 6 runs, 2 runs for each stimulation intensity). The 10 Hz rTMS trains consisted of 8 pulses which were delivered at 110% rMT intensity and were applied with three different intertrain intervals: 2, 4 and 12 s corresponding to a number of 12, 6 and respectively 2 trains per stimulation block (in total 6 runs, 2 runs for each different intertrain interval). Finally, 4 experimental runs were performed with volitional movement which was acoustically triggered by 50% rMT stimuli. Each experimental run contained 158 volumes and one volume consisted of 8 slices covering the motor and premotor areas.

In a control experiment performed in the TMS lab, the time courses of the motor evoked potentials (MEPs) were investigated for two of the rTMS protocols, namely continuous 2Hz rTMS and 10Hz rTMS trains with 4 s intervals (both at 110% rMT; same protocol as used inside the scanner). Twenty test pulses were applied before the first stimulation block and again after the last block (pulse interval: 8 s). Additionally, six test pulses (8 s spacing) were applied between each two successive stimulation blocks, resulting in altogether 82 test pulses. MEPs were recorded from the right APB muscle and quantified as peak-to-peak amplitudes. The MEP amplitudes were first normalized to the mean of the 82 test pulses. Subsequently, in order to compare the MEPs with the rCBF time courses, the rTMS blocks were divided in 4 s time intervals (corresponding to the TR of one CASL volume) and the amplitudes were averaged across these intervals. Finally, averaging across blocks and across subjects was performed.

The rTMS stimulation elicited robust rCBF and BOLD signal increases in motor and premotor areas: Stimulated M1/S1_i, CMA/SMA, as well as medial and lateral parts of PMd. The positive group rCBF and BOLD activations largely overlap. The activation rCBF clusters

for volitional movement overlap well with those due to rTMS stimulation, but are smaller in extent and are restricted to the ipsilateral M1/S1, ipsilateral PMd, CMA and SMA.

Next, we investigated which regions exhibit parametrical changes in rCBF with increasing stimulation intensity (continuous 2 Hz rTMS) and increasing number of trains (10Hz rTMS), respectively (Fig. 6). A positive relationship between the number of 10Hz trains and rCBF was observed in most of the areas that showed general rCBF activations due to rTMS stimulation. For 2Hz stimulation, increasing rCBF with increasing stimulation intensity occurred only in the stimulated M1/S1 and, to a lesser extent, in CMA, the medial part of the ipsilateral PMd and the lateral part of the contralateral PMd.

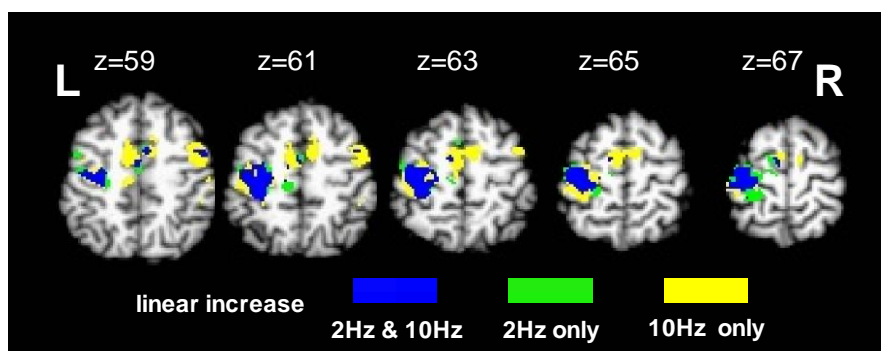


Fig. 6 Regions exhibiting increasing rCBF with increasing stimulation intensity for continuous 2Hz rTMS (green), with increasing number of trains for 10Hz rTMS (yellow), and overlap between both (blue).

The perfusion time courses elicited by different stimulation conditions were assessed in eight regions of interest (ROIs) corresponding to the motor and premotor systems. The relative rCBF signal change obtained from 2 representative regions (ipsilateral M1/S1 and SMA) is illustrated in Fig. 7a&b for all six stimulation conditions. For 10Hz rTMS trains, the time courses consistently show a clear-cut peak at the beginning of the stimulation period and then fall off. In contrast, the rCBF increase is rather constant during continuous 2 Hz stimulation. This difference was formerly tested for two of the stimulation protocols, namely continuous 2 Hz rTMS and 10 Hz rTMS trains with 4 s intervals, both at 110% rMT. The data was reanalyzed using separate regressors for the first and second halves of the stimulation and the two halves compared on the group level (Fig. 7c). For 10 Hz trains, most of the affected motor and premotor regions were more strongly activated during the first half compared to the second half of stimulation (yellow and blue areas in Fig. 7c). In contrast, for 2 Hz rTMS, higher rCBF values during the first half were almost completely restricted to the directly stimulated M1/S1 (blue and green areas). None of the regions exhibited the opposite effect, i.e. stronger activation during the second rather the first half of stimulation. For 2 Hz stimulation, the MEPs recorded in the control experiment showed an increasing trend, while the MEPs in response to the 10 Hz trains were constant throughout the stimulation period. That is, we observed a clear-cut dissociation between MEP and rCBF time courses for the 10 Hz trains.

To conclude, the rCBF in motor and premotor areas correlated positively both with stimulation intensity (continuous 2Hz rTMS) and the number of 10 Hz trains. Interestingly, the two rTMS protocols yielded markedly different rCBF time courses, which did not correlate with the amplitudes of the peripheral muscle responses.

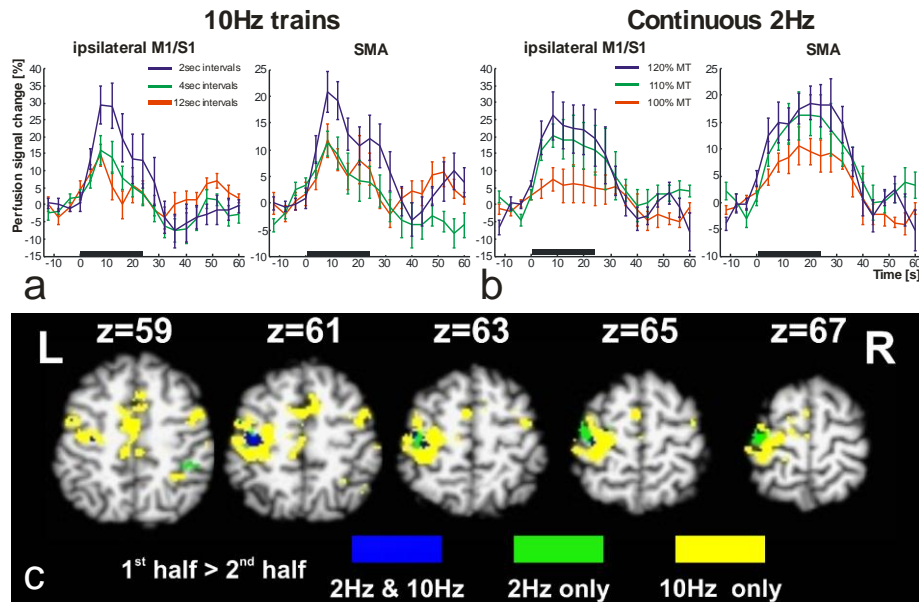


Fig. 7 RCBF signal changes in 2 representative regions for 10 Hz rTMS trains (a) and for continuous 2 Hz rTMS (b). c) Regions with higher CBF in the first 12 s compared to the second 12 s of stimulation; for 2 Hz 110% stimulation (green), for 10Hz trains – 4 s gaps (yellow), and overlap between both (blue). The stimulation intensity and the number of pulses were matched between these two protocols. Only the temporal arrangement (continuous vs. bursts) was different.

3.2 State Dependence of rTMS Effects on the Dorsal Premotor Cortex

In the last project of my PhD it was investigated if interleaved TMS/CASL is suitable to target questions from cognitive neuroscience. Specifically, I investigated the task-dependency of the local and remote rCBF activations in response to stimulation of the dorsal premotor cortex.

Motivated by prior studies demonstrating that the effects of rTMS protocols depend on the activation state of the stimulated cortex (e.g., Bestmann et al., 2008; O’shea et al., 2007), we used interleaved TMS/CASL to assess the effects of short bursts of TMS delivered to left PMd during three different motor states (i.e., during associative or freely selected sequential key presses with the ipsilateral hand, or during passive viewing as control).

Interleaved TMS/CASL was performed on 9 subjects at our 3T Siemens scanner. Fig. 8 illustrates the experimental design. The stimulation site above the left PMd was determined offline using a procedure described previously (see Bestmann et al., 2008; Schluter et al., 1998). Inside the scanner, the TMS coil was positioned over the “Hot Spot”, the resting and active motor thresholds (rMT and aMT) were determined and then the coil was repositioned

over the left PMd. A 2 x 3 factorial block design was used with TMS over left PMd (TMS high = 110% rMT, TMS low = 70% aMT) and motor state (associative key presses [AK] vs. freely selected key presses [FK] vs. passive viewing [PV]) as experimental factors. Each subject underwent two sessions which differed in terms of the motor task. Sessions were separated by at least one week. Prior to a session, they were trained on one of the two tasks (associative or freely selected key presses). Subsequently, 8 experimental runs were acquired, 4 runs during which the subject performed the task and 4 runs with passive viewing. Using a block design, each run contained 3 successive blocks with 60 seconds of task followed by 120 seconds of rest. During the task phases, subjects viewed a randomized sequence of 5 geometrical figures. In the associative finger tapping session, each figure instructed a response with a specific finger. In the free selection session, subjects had to respond with a freely selected finger when a figure was displayed. In the control runs, subjects had to passively view the figures. The figures were presented at a rate of 0.8 Hz. During the rest periods the subjects had to fixate a white cross presented in the central visual field. TMS was applied as successive short 10Hz trains during the task periods (5 pulses per train, 4 sec gap between trains).

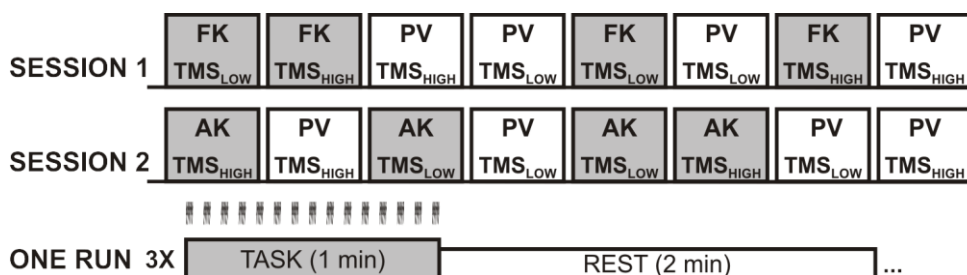


Fig. 8 Schematic diagram of the experimental design. One motor task was tested per session (either associative or freely selected key presses) while passive viewing was assessed in both sessions. One condition was investigated per experimental run. The order of runs within one session was pseudo-randomized across subjects and the order of sessions was counterbalanced across subjects. Each run consisted of three alternating epochs of task and rest with task epochs lasting 60 s and rest epochs lasting 120 s.

The behavioral data analysis revealed that mean reaction times (RTs) were consistently longer for associative opposed to freely selected responses. This RT difference reflected the difference between both tasks in terms of movement selection. Subjects could decide on the next button press during the pause between two visual stimuli when freely selecting the key presses. In the associative task, no movement preparation was possible before the presentation of the visual cue, resulting in longer RTs. However, the interaction between TMS intensity and task was not significant. Accordingly, pairwise comparisons of mean RTs revealed no effect of TMS intensity in both tasks. The intensity of TMS had also no effect on mean error rates during associative key presses.

The main effect of key presses (pooled across both tasks) versus passive viewing, irrespective of TMS intensity, showed significant rCBF increases in the sensorimotor system, including right (contralateral to the site of stimulation) M1/S1, bilateral cingulate and CMA/SMA as well as bilateral dorsal and ventral premotor areas (PMv, PMd). Task related decreases in

rCBF were observed bilaterally in the superior frontal gyri (SFG), the middle frontal gyri (MFG), the paracingulate gyri, the posterior CMA, the inferior parietal lobe (IPL) and the precuneous.

Several areas exhibited higher rCBF increases with freely selected movements compared to movements based on visuomotor associations. Regional rCBF increases with free selection were found in SFG, MFG and IPL bilaterally, left posterior CMA, as well as right posterior SMA. These increases in regional activity with free movement selection were located mainly outside the brain regions showing common increases in rCBF with both motor tasks, indicating that the free selection task recruited additional cortical areas outside the core executive motor network that subserved both motor tasks. No brain region within the field of view exhibited stronger rCBF increases with associative movement selection relative to free selection at this threshold level.

The interaction between TMS intensity and type of motor task revealed that the modulatory effects of TMS depended on the mode of movement selection (Fig. 9a). Several precentral and mesial cortical motor areas showed a stronger TMS-related increase in rCBF with associative but not with free movement selection, resulting in a significant interaction between TMS intensity and task ($[TMS_{HIGH} - TMS_{LOW}]_{AK} - [TMS_{HIGH} - TMS_{LOW}]_{FK}$). The cortical regions showing a stronger activation for associative movement selection when effective TMS was given to left PMd were primarily located in the right hemisphere, including the right M1, right PMd and adjacent parts of right PMv and the caudal part of right BA9 as well as the right anterior insula. Additional clusters were found in mesial premotor areas, including clusters in posterior SMA and anterior CMA. In mesial regions, TMS-related differences in motor activation were expressed bilaterally, yet activity changes were more pronounced in the right hemisphere. We also tested for brain areas exhibiting TMS-related rCBF increases during associative key presses compared to passive viewing ($[TMS_{HIGH} - TMS_{LOW}]_{AK} - [TMS_{HIGH} - TMS_{LOW}]_{PV}$). Again, mesial and right-hemispheric cortical areas showed stronger TMS-related increases in rCBF with associative movement selection relative to the non-motor control task (green and blue regions in Fig. 9b). Distinct clusters in the right M1, PMd, BA9 and CMA showed TMS-induced rCBF increases for associative movement selection compared to both, free selection and passive viewing (blue areas in Fig. 9b).

No TMS-related increases in rCBF were observed during freely selected movements relative to associative movement selection. The cuneus was the only region where TMS enhanced rCBF with free movement selection compared to passive viewing ($[TMS_{HIGH} - TMS_{LOW}]_{FK} - [TMS_{HIGH} - TMS_{LOW}]_{PV}$).

Our results up to now showed that both motor tasks evoked similar activation levels in a common network of parieto-premotor regions including the stimulated left PMd. In fact, freely selected responses engaged additional prefrontal regions. However, effective TMS caused specific rCBF increases in medial and right motor regions only when a prelearned associative visuomotor mapping had to be used, but not for freely selected responses and passive viewing.

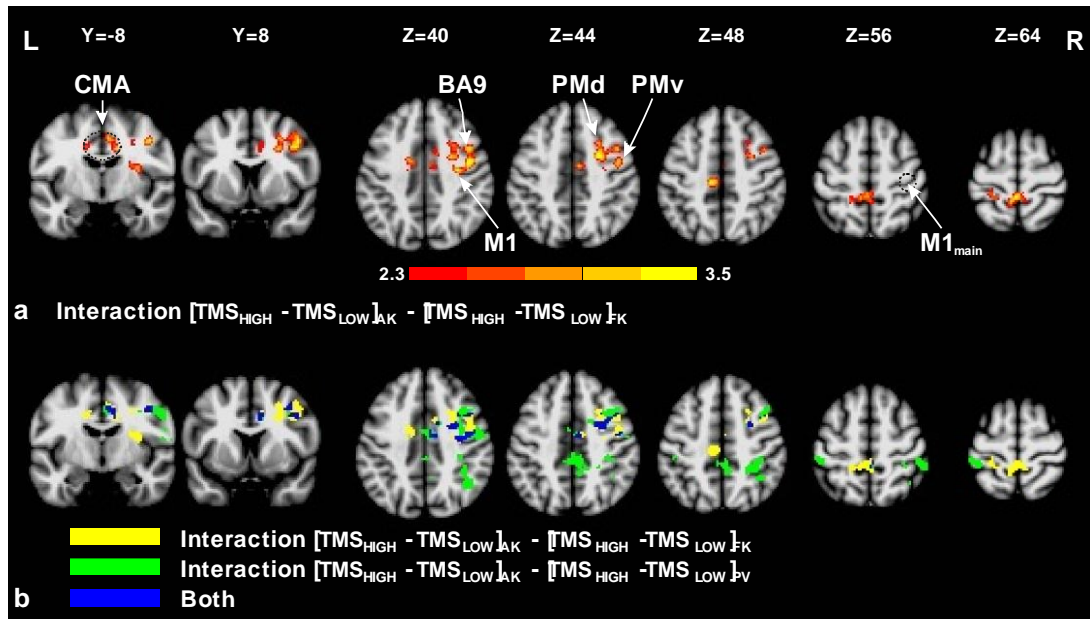


Fig. 9 a) Interaction between motor task and TMS intensity ($[TMS_{HIGH} - TMS_{LOW}]_{AK} - [TMS_{HIGH} - TMS_{LOW}]_{FK}$). b) Overlap of the results depicted in (a) with the interaction between associative key presses vs. passive viewing and TMS intensity ($[TMS_{HIGH} - TMS_{LOW}]_{AK} - [TMS_{HIGH} - TMS_{LOW}]_{PV}$).

In addition to a standard GLM analysis we used psychophysiological interaction (PPI) analyses (Friston et al. 1997) to investigate how the functional connectivity between the stimulated left PMd and the other motor areas changed across motor task. The first PPI was used to test for regions showing a change in functional coupling with the left PMd during the associative compared to passive viewing condition. The second PPI analysis was conducted to compare the associative task with the freely selective task. A range of areas (right M1, right PMd, right BA9, left secondary somatosensory motor cortex, bilateral CMA and SMA) exhibited increased functional coupling for the associative task compared to passive viewing (blue and green regions in Fig. 10a). The second PPI analysis revealed an enhanced coupling between the left PMd and a subgroup of these regions (right M1, right BA9 and bilateral CMA) when comparing associative with freely selected responses, using a threshold of $Z=1.96$ at the voxel level and a cluster extent threshold of 35 voxel (yellow and blue regions in Fig. 10a). The areas identified in this second PPI overlapped with those determined when testing the interaction between TMS intensity and task (blue regions in Fig. 10b), thus confirming the specificity of the TMS effects for AK as observed in the previous analysis.

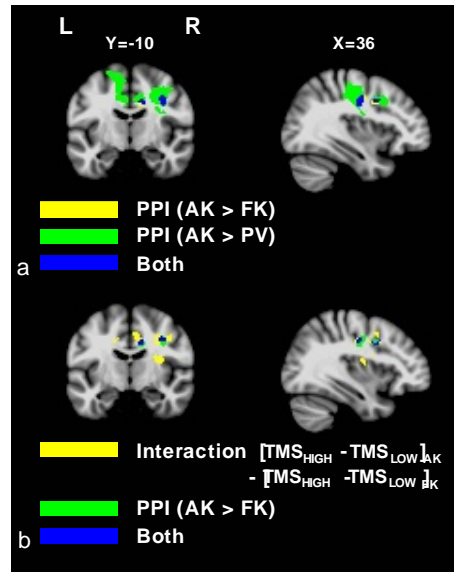


Fig. 10 Task-dependent changes in the functional coupling between the left PMd and other motor areas, assessed using PPI analyses. a) Overlap between the PPI results indicating increased coupling for associative vs. freely selected movements and the PPI results indicating stronger coupling for associative responses compared to passive viewing. b) Overlap between the PPI results indicating increased coupling for associative versus freely selected movements and the interaction between associative versus freely selected key presses and TMS intensity (as depicted in Fig. 9a).

4. Discussion

New Coil Positioning Method for Interleaved TMS/fMRI and Validation of our Overall Setup

A novel method for TMS coil placement in interleaved TMS/fMRI studies that allows the exchange of coil positions between a neuronavigation system and a MR-compatible holding device was developed. The spatial accuracy (2.9 ± 1.3 mm) of this method is in the range reported for neuronavigation systems used in normal TMS studies (Schönfeldt-Lecuona et al., 2005). This method was motivated by Bohning et al. (Bohning et al., 2003) and therefore shares some similarities with their approach. However, our method incorporates several important advantages. It provides an easy way to repeatedly position the TMS coil at pre-recorded stimulation sites, without the need to manually identify brain structures in structural 2D images before each new experiment. In addition, it allows us to easily determine the amount of coil displacement due to subject movement in the course of an experiment. Finally, the automatic calculation of the EPI slice tilts to minimize the susceptibility artifacts reduces the required setup time. We demonstrated that the interleaved TMS-fMRI setup is safe to use and the quality measurements showed that we can acquire EPI images at a good quality. In particular, the static signal dropouts in the EPI images of the agar phantom were moderate and were not visible in the images of the subjects' brains. Also, the moderate distortions visible in the EPIs of the phantom were absent in the brain images, making it unnecessary to use distortion correction based on field mapping. The SFNR images did not reveal any additional noise induced by the TMS stimuli or the stimulator itself. The results of the motor cortex stimulation study are in concordance with previous findings (Bohning et al., 2000; Bestmann et al., 2004) and together with the quality assurance measurements demonstrate the viability of our overall setup.

After the implementation, the feasibility of the interleaved TMS/CASL setup was tested. The results of the phantom quality measurements are in concordance with the results of our first quality test (Moisa et al., 2009) and show that we can achieve ASL images at a good quality. The analysis of the phase maps measurements revealed that the maximum voxel shifts occur at the rim of the brain and in general only few voxels exhibited shifts greater than 1 or smaller than -1, which should be acceptable for most applications.

Comparison of the Effects of Two Stimulation Protocols: Continuous 2Hz rTMS and Short 10Hz rTMS Trains

The effects of two stimulation protocols (2 Hz continuous rTMS and short 10 Hz rTMS trains) on rCBF were investigated using interleaved TMS/CASL. We found robust rCBF changes in response to rTMS stimulation, measured by simultaneous ASL imaging, thereby demonstrating the feasibility of this new combination. The observed spatial activation patterns are in concordance with the results of previous motor cortex studies (Bestmann et al., 2004; Bohning et al., 2000; Fox et al., 1997; Siebner et al., 2001b), showing significant rCBF increases due to rTMS in motor and premotor areas. Additionally, the positive rCBF activation clusters overlap well with the positive BOLD activation as well as with the rCBF

increases due to volitional movement. The activation clusters due to volitional movement were generally smaller than those due to rTMS and did not involve regions in the right hemisphere. This was probably caused by the employed behavioral task (simple finger tapping instead of, e.g. sequential finger movements).

For continuous 2 Hz rTMS, significant rCBF increases with increasing stimulation intensity were mainly restricted to the stimulated M1/S1, ipsilateral PMd, and small parts of CMA/SMA, but did not extend to regions contralateral to the coil. This is in concordance with the findings of previous combined TMS-PET (Fox et al., 2006; Speer et al., 2003) and interleaved TMS-fMRI studies (Bestmann et al., 2004). The MEP time courses show a trend towards increased amplitudes at the end of the stimulation blocks for continuous 2 Hz rTMS. This seems to be mirrored by similar tendencies in the rCBF time courses in some of the areas (e.g., CMA, lateral part of PMd ipsilateral to coil). Importantly, however, the time courses for rCBF and MEPs, respectively, do not show a comparable dissociation for continuous 2 Hz rTMS as for the 10 Hz trains.

For the stimulation with 10 Hz rTMS trains, the linear increases in rCBF with increasing number of trains are in contrast to previous PET results (Paus et al., 1998). In fact, Paus and colleagues (1998) observed negative rCBF in M1/S1 when spacing the trains at 2 s intervals, while this condition yielded the highest rCBF values in our case. This discrepancy probably arises from the fact that we used supra- rather than sub-MT stimulation and applied shorter stimulation periods (24 s instead of 60 s). We did, however, observe a significant decrease in rCBF amplitude in the second part of the stimulation in many regions, consistently across all stimulations with 10Hz trains. As the MEP amplitudes for 10Hz trains did not show a similar decrease, this particular change in rCBF cannot be explained by changes in sensory feedback and might therefore hint towards the slow build-up of a cortical inhibitory component. Since the PET results reported by Paus and colleagues (1998) are based on the summation of rTMS effects across 60 s, it might be that the inhibitory overcomes the excitatory effect for extended stimulation periods. This might lead to an overall negative net effect, in particular in the absence of activity related to sensory feedback. Support for this hypothesis comes from a study in which short high-frequency trains (6 Hz, 10 s inter-train interval) were applied to the primary visual cortex of the cat while recording from single cells in the dorsal lateral geniculate nucleus (de Labra et al., 2007). The repeated TMS trains led to a successive reduction of both the spontaneous spiking activity and the responses to visual stimulation, and this effect remained for a few minutes even after TMS stopped. Interestingly, mainly tonic activity but not spike bursts was affected by TMS. This might explain why in our case dissociations between MEPs (which are elicited by rather short-term bursts of activity) and rCBF (averaging across both bursts and the tonic activity in the inter-train intervals) were observed. Clearly, this interpretation has to be considered with caution, as the study of de Labra et al. (2007) was conducted in anaesthetized animals, thereby targeting a different brain area than done here.

State Dependence of rTMS Effects on the Dorsal Premotor Cortex

Finally, interleaved TMS/CASL was used in order to test the effects of TMS bursts delivered to the left PMd on remote brain activity during two different motor tasks performed with the ipsilateral hand and during passive viewing as additional control. We demonstrated that effective TMS caused specific rCBF increases in a network of regions consisting of right PMd, an adjacent area in right BA9, right M1 and right CMA only when a prelearned associative visuomotor mapping had to be used, but not for freely selected responses and passive viewing (blue areas in Fig. 9b). These results were further confirmed by PPI analyses revealing an enhanced functional coupling between the left, stimulated PMd and similar right and mesial motor regions that occurred specifically for the associative responses compared to freely selected key presses and passive viewing (blue areas in Fig. 10a). Importantly, the missing TMS effects on error rates and reaction times preclude the possibility that our findings were affected by behavioral confounds.

The subjects responded generally faster for freely selected compared to associative responses. Deiber and colleagues (1991) already pointed out that this difference is expected as, when making internal selections, the subjects can determine the next key press during the time period between two visual stimuli that set the pace of the responses. In contrast, when using a prelearned visuomotor mapping, they have to wait for the next stimulus to come up in order to select the appropriate response. Importantly, however, the activation levels in a common parietal-premotor network were roughly matched between the two tasks in our case. In fact, compared to both associative responses and passive viewing, freely selected responses engaged additional parietal and prefrontal structures including the right dorsolateral prefrontal cortex.

Both motor tasks used matched visual input and relied on the preparation and execution of non-stereotyped key press sequences of similar complexity. The specific difference was in the usage of a prelearned visuomotor association for motor selection compared to free selection. Our results concord with the view obtained from lesion studies in humans and monkeys that PMd is critically involved in conditional sensorimotor mappings (Halsband and Passingham, 1982; Petrides, 1986; Halsband and Freund, 1990; Petrides, 1997) despite the fact that functional imaging studies in humans did observe learning-related activity changes only in other premotor areas (Sakai et al., 1999; Toni et al., 2001; Eliassen et al., 2003; Bédard and Sanes, 2009). Our findings support the hypothesis that PMd is predominantly involved in the execution and maintenance of already learned rules (Bédard and Sanes, 2009). In that respect, they significantly extend and complement the results of two prior studies combining TMS with fMRI to study the role of PMd in visuomotor control (O'Shea et al., 2007; Bestmann et al., 2008). These studies used passive viewing (Bestmann et al. 2008) or a simple motor execution task (O'Shea et al. 2007) as control conditions. O'Shea and colleagues (2007) temporally lesioned the left PMd using 1 Hz rTMS and showed subsequent compensatory activity increases in mesial and right premotor areas for a conditional visuomotor task performed with the right hand. Here, we demonstrated immediate rCBF increases in response to TMS hinting towards on-the-flight compensation in a very similar

network of regions. In addition, this compensatory pattern occurred for key presses performed with the left hand, consistent with the generalized role suggested for the left PMd in controlling both contra- and ipsilateral movements (Chen et al., 1997b; Schluter et al., 1998; Johansen-Berg et al., 2002; Rushworth et al., 2003).

By revealing immediate compensatory effects to rTMS trains delivered repeatedly during the 1 min task periods, our study bridges the temporal gap between the offline effects studied by o'Shea et al. (2007) and the study of Bestmann et al. (2008) in which event-related TMS was used to look at functional effective connectivity. Bestmann et al. used a task involving visual feedback for the online control of the grip force of the left hand. They demonstrated specific activity increases in right PMd and right M1 in response to the stimulation of left PMd only when the subjects performed the task, but not during rest. We extend this finding by showing that right-hemispheric compensation generalizes beyond grip control. Importantly, a similar response pattern for internally guided movements was absent in our case. This suggests that, for both the associative tasks used in our study and by o'Shea et al. and the online-control task employed by Bestmann et al., the common functional role of the left PMd was the maintenance of a specific sensorimotor mapping.

To conclude, this study demonstrated context-dependent effects of left PMd stimulation on a specific remote network of medial and right motor regions. Effective TMS increased rCBF in this network only for key presses relying on a prelearned associative visuomotor mapping, but not for freely selected responses and passive viewing. The absence of behavioral TMS effects suggests that these increases reflect compensatory activity in response to the disturbed left PMd. Despite the occurrence of longer reaction times for associative compared to freely selected key presses, both motor tasks evoked similar activation levels in a common network of parieto-premotor regions including the stimulated left PMd. Furthermore, freely selected responses recruited additional prefrontal regions. This makes it unlikely that the observed differences in the impact of TMS on remote activity simply stem from differences in task complexity. Rather, our results strengthen the view that the execution and maintenance of a specific sensorimotor mapping is a critical function of PMd.

Methodological considerations of interleaved TMS/CASL

In contrast to combining TMS with PET, interleaved TMS/CASL offers a better temporal and spatial resolution and does not utilize radiation. ASL is insensitive to low-frequency fluctuations and exhibits a reduced inter-subject and inter-session variability compared to BOLD imaging, possibly reflecting a more direct link between rCBF and neural activity (Aguirre et al. 2002; Tjandra et al. 2005; Liu and Brown 2007). As a consequence, we were able to carry out normal random-effects group analyses at acceptable significance levels despite the reduced sensitivity of ASL compared to BOLD fMRI on the single subject level. In particular, the good inter-session reproducibility proved to be beneficial, e.g. for comparing the impact of TMS over left PMd on different motor tasks. Disadvantages of the ASL approach were the limited field of view that only partially covered subcortical structures and did not extend to the cerebellum as well as the reduced temporal resolution stemming from the alternating acquisition of tag and control images. However, these disadvantages are

offset by the possibility to study rCBF changes across longer time periods (Wang et al., 2003; Wang et al., 2005a).

5. Summary

The objectives of this dissertation were to develop new methodological improvements in combining TMS with fMRI. First, a setup for interleaved TMS/fMRI was implemented. Phantom quality measurements helped to demonstrate that we can acquire EPI images with good quality. A new positioning method was developed which allows placing the TMS coil inside the MR scanner, with good spatial accuracy, over cortical sites previously determined with a neuronavigation system. The first motor cortex study validated our overall interleaved TMS/fMRI setup and demonstrated that it is safe to use.

Our setup was then extended in order to be able to interleave TMS with CASL. The feasibility of this novel combination was demonstrated both by phantom quality measurements and a study targeting the human motor cortex. In particular, it was shown that interleaved TMS/CASL can be used to investigate the effects on rCBF of different rTMS protocols, offering a better temporal resolution than PET and preventing the subjects' exposure to radiation. Different rCBF time courses could be distinguished for different rTMS protocols, namely for continuous 2Hz rTMS and short 10Hz trains. Finally, it was further demonstrated that interleaved TMS/CASL is also suitable for cognitive neuroscience research. We showed that CASL is able to detect task-dependent rTMS effects on rCBF across interconnected brain regions when targeting the left PMd. Importantly, behavior was not disrupted by TMS, ruling out confounding effects of, e.g. reaction times on the brain activation pattern. Most notably, the stimulation of left PMd resulted in an increased rCBF in a specific remote network of medial and right motor regions only during a conditional response task relying on a prelearned associative visuomotor mapping, but not for freely selected responses or passive viewing. This strengthens the view that the left PMd is a key node maintaining an already learned conditional rule. The rCBF increases in functionally related medial and right motor areas hint towards an immediate (on-the-flight) compensatory reorganization, in turn maintaining behavioral performance.

6. Outlook

One interesting aspect which could be investigated in future studies using interleaved TMS/ASL is the rCBF responses to sub-threshold rTMS intensities. This seems feasible since we have already demonstrated that the CASL method is sensitive enough to detect rCBF changes at relatively low TMS intensities of 100% rMT (i.e., just eliciting finger twitches when left M1 was stimulated during rest). By stimulating with sub-threshold intensities, direct rCBF changes due to rTMS stimulation could be investigated without confounding indirect activity changes due to the afferent sensory feedback caused by the muscles responses.

ASL imaging offers the possibility to study rCBF changes across longer time periods (Wang et al., 2003; Wang et al., 2005a). In this respect, ASL imaging should be particularly well suited for studying the impact of fully-fledged rTMS protocols. Furthermore, ASL could be implied not only to investigate new stimulation paradigms but also other stimulation techniques such as transcranial direct current stimulation (tDCS) (Paulus 2003). Moreover, the combination of ASL and TMS also has the potential to determine neural correlates of compensatory plasticity both in healthy volunteers and in patients. It is important to know whether stimulation protocols that are effective in healthy subjects are equally effective or suitable to patients. This may lead to the development of more efficient protocols for basic research and therapeutic TMS applications.

Different studies have shown that neuroactive drugs can change the cortical excitability and thereby the effectiveness of TMS (Ziemann 2004). The direct quantitative measure of rCBF provided by ASL is less susceptible to drug administration compared to BOLD signal. Thus, combined TMS/ASL could be implied to investigate drug-related rCBF changes that accompany the modulation of the TMS effects on the peripheral electrophysiological level. In particular, this approach could offer insights into the question whether the changed effectiveness is caused by local or rather by network-effects of the drug.

We showed that interleaved TMS/CASL can be applied to study TMS effects on baseline rCBF as well as task-dependent TMS effects. Since little work has been done so far in this respect, this novel combination could also offer important insights into how focal TMS disrupts neuronal processing during a task, causing a “virtual lesion” (Pascual-Leone et al., 1999; Pascual-Leone et al., 2000). In this respect, ASL imaging could be used as a complement to BOLD EPI imaging to topographically monitor the brain activity changes due to a transient, non-invasive, TMS-induced behavioral perturbation. The measured rCBF signal comes primarily from small vessels and surrounding tissue while the BOLD signal derives primarily from larger arteries and veins. In particular, it has been hypothesized that the functional rCBF signal may be more localized to the sites of neuronal activation than the BOLD signal. However, whether ASL imaging helps to gain more useful insights in this respect compared to BOLD imaging remains to be seen.

One future direction of investigation involves the comparison of the functional connectivity assessed using interleaved TMS/ASL with the structural connectivity revealed by diffusion tensor imaging (DTI) (Behrens et al., 2005). Because brain regions that are connected functionally are also likely to be connected anatomically, areas of functional connectivity may show direct or indirect connectivity pathways on DTI images. In this sense, the DTI technique can be used for determining the structural connectivity between the stimulated cortical area and the direct connected areas in the brain, thus excluding the regions showing non-specific coactivations. A comprehensive description of the TMS effect on interconnected brain areas could be achieved by determining the degree of correlation between functional and structural connectivity. Due to its better spatial specificity compared to BOLD, ASL could be implied to compare the network of regions modulated by rTMS with structural connectivity pattern of the target area assessed with DTI while BOLD EPI could be used to investigate the immediate impact of TMS on brain connectivity.

In order to better understand the TMS effects on brain activity, model-based analyses of the impact of TMS on effective connectivity could be applied using, e.g. dynamic causal modeling (DCM) (Friston, 2003). This approach could help to obtain hypotheses on the question how causal interregional influences in response to TMS are mediated across brain regions. For example, using DCM and Bayesian model selection one could test if TMS over a targeted region modulates the activity in remote brain regions more likely via a direct connection or via intermediate interconnected areas. However, whether model-based analysis is more suitable for TMS-ASL studies compared with TMS-BOLD fMRI studies remains to be seen. In this respect, TMS combined with ASL could be used for experimental designs which are not suitable for BOLD imaging (e.g., designs which implies comparison of data from different experimental sessions or for pre-post designs).

7. References

- Aguirre GK, Detre JA, Zarahn E, Alsop DC. 2002. Experimental design and the relative sensitivity of BOLD and perfusion fMRI. *Neuroimage*. 15: 488-500.
- Barker AT, Jalinous R, Freeston IL. 1985. Non-invasive magnetic stimulation of human motor cortex. *Lancet*. 1: 1106-1107.
- Baudewig J, Paulus W, Frahm J. 2000. Artifacts caused by transcranial magnetic stimulation coils and EEG electrodes in T(2)*-weighted echo-planar imaging. *Magn Reson Imaging*. 18: 479-484.
- Bédard P, Sanes JN. 2009. On a basal ganglia role in learning and rehearsing visual-motor associations. *Neuroimage*. 47: 1701-1710.
- Behrens TE, Johansen-Berg H. 2005. Relating connectional architecture to grey matter function using diffusion imaging. *Philos Trans R Soc Lond B Biol Sci*. 360: 903-911.
- Bestmann S, Baudewig J, Frahm J. 2003. On the synchronization of transcranial magnetic stimulation and functional echo-planar imaging. *J Magn Reson Imaging*. 17: 309-316.
- Bestmann S, Baudewig J, Siebner HR, Rothwell JC, Frahm J. 2004. Functional MRI of the immediate impact of transcranial magnetic stimulation on cortical and subcortical motor circuits. *Eur J Neurosci*. 19: 1950-1962.
- Bestmann S, Baudewig J, Siebner HR, Rothwell JC, Frahm J. 2005. BOLD MRI responses to repetitive TMS over human dorsal premotor cortex. *Neuroimage*. 28: 22-29.
- Bestmann S, Ruff CC, Blankenburg F, Weiskopf N, Driver J, Rothwell JC. 2008. Mapping causal interregional influences with concurrent TMS-fMRI. *Exp Brain Res*. 191: 383-402.
- Bestmann S, Swayne O, Blankenburg F, Ruff CC, Haggard P, Weiskopf N, Josephs O, Driver J, Rothwell JC, Ward NS. 2008. Dorsal premotor cortex exerts state-dependent causal influences on activity in contralateral primary motor and dorsal premotor cortex. *Cereb Cortex*. 18:1281-1291.
- Bohning DE, Denslow S, Bohning PA, Walker JA, George MS. 2003. A TMS coil positioning/holding system for MR image-guided TMS interleaved with fMRI. *Clin Neurophysiol*. 114: 2210-2219.
- Bohning DE, Pecheny AP, Epstein CM, Speer AM, Vincent DJ, Dannels W, George MS. 1997. Mapping transcranial magnetic stimulation (TMS) fields in vivo with MRI. *Neuroreport*. 8: 2535-2538.
- Bohning DE, Shastri A, McGavin L, McConnell KA, Nahas Z, Lorberbaum JP, Roberts DR, George MS. 2000. Motor cortex brain activity induced by 1-Hz transcranial magnetic stimulation is similar in location and level to that for volitional movement. *Invest Radiol*. 35: 676-683.
- Bohning DE, Shastri A, Nahas Z, Lorberbaum JP, Andersen SW, Dannels WR, Haxthausen EU, Vincent DJ, George MS. 1998. Echoplanar BOLD fMRI of brain activation induced by concurrent transcranial magnetic stimulation. *Invest Radiol*. 33: 336-340.

- Chen R, Classen J, Gerloff C, Celnik P, Wassermann EM, Hallett M, Cohen LG. 1997a. Depression of motor cortex excitability by low-frequency transcranial magnetic stimulation. *Neurology*. 48: 1398-1403.
- Chen R, Cohen LG, Hallett M. 1997b. Role of the ipsilateral motor cortex in voluntary movement. *Can J Neurol Sci*. 24: 284-291.
- de Labra C, Rivadulla C, Grieve K, Marino J, Espinosa N, Cudeiro J. 2007. Changes in Visual Responses in the Feline dLGN: Selective Thalamic Suppression Induced by Transcranial Magnetic Stimulation of V1. *Cerebral Cortex*. 17: 1376-1385.
- Deiber MP, Passingham RE, Colebatch JG, Friston KJ, Nixon PD, Frackowiak RS. 1991. Cortical areas and the selection of movement: a study with positron emission tomography. *Exp Brain Res*. 84: 393-402.
- Dimyan MA, Cohen LG. 2009. Contribution of transcranial magnetic stimulation to the understanding of functional recovery mechanisms after stroke. *Neurorehabil Neural Repair*. 24:125-135.
- Eliassen JC, Souza T, Sanes JN. 2003. Experience-dependent activation patterns in human brain during visual-motor associative learning. *J Neurosci*. 23: 10540-10547.
- Fox P, Ingham R, George MS, Mayberg H, Ingham J, Roby J, Martin C, Jerabek P. 1997. Imaging human intra-cerebral connectivity by PET during TMS. *Neuroreport*. 8: 2787-2791.
- Fox P, Narayana S, Tandon N, Fox SP, Sandoval H, Kochunov P, Capaday C, Lancaster JL. 2006. Intensity modulation of TMS-induced cortical excitation: primary motor cortex. *Human Brain Mapping*. 26: 478-487.
- Friedman L, Glover GH. 2006. Report on a multicenter fMRI quality assurance protocol, *J Magn Reson Imaging*. 23 :827-839.
- Friston KJ, Buechel C, Fink GR, Morris J, Rolls E, Dolan RJ. 1997. Psychophysiological and modulatory interactions in neuroimaging. *Neuroimage*. 6:218-229.
- Friston KJ, Harrison L, Penny W. 2003. Dynamic causal modelling. *Neuroimage*. 19: 1273-1302.
- Halsband U, Freund HJ. 1990. Premotor cortex and conditional motor learning in man. *Brain*. 113 (Pt 1): 207-222.
- Halsband U, Passingham R. 1982. The role of premotor and parietal cortex in the direction of action. *Brain Res*. 240: 368-372.
- Huang YZ, Edwards MJ, Rounis E, Bhatia KP, Rothwell JC. 2005. Theta burst stimulation of the human motor cortex. *Neuron*. 45: 201-206.
- Johansen-Berg H, Rushworth MF, Bogdanovic MD, Kischka U, Wimalaratna S, Matthews PM. 2002. The role of ipsilateral premotor cortex in hand movement after stroke. *Proc Natl Acad Sci USA*. 99: 14518-14523.
- Lam RW, Chan P, Wilkins-Ho M, Yatham LN. 2008. Repetitive transcranial magnetic stimulation for treatment-resistant depression: a systematic review and metaanalysis. *Can J Psychiatry*. 53: 621-631.

Lee L, Siebner HR, Rowe JB, Rizzo V, Rothwell JC, Frackowiak RS, Friston KJ. 2003. Acute remapping within the motor system induced by low-frequency repetitive transcranial magnetic stimulation. *J Neurosci.* 23: 5308-5318.

Liu TT, Brown GG. 2007. Measurement of cerebral perfusion with arterial spin labeling: Part 1. *Methods. J Int Neuropsychol Soc.* 13: 517-525.

Moisa, M., Pohmann, R., Ewald, L., Thielscher, A., 2009. New Coil Positioning Method for Interleaved Transcranial Magnetic Stimulation (TMS)/Functional MRI (fMRI) and Its Validation in a Motor Cortex Study. *JMRI* 29, 189-197.

Mushiakhe H, Inase M, Tanji J. 1991. Neuronal activity in the primate premotor, supplementary, and precentral motor cortex during visually guided and internally determined sequential movements. *J Neurophysiol.* 66: 705-718.

Nahas Z, Lomarev M, Roberts DR, Shastri A, Lorberbaum JP, Teneback C, McConnell K, Vincent DJ, Li X, George MS, Bohning DE. 2001. Unilateral left prefrontal transcranial magnetic stimulation (TMS) produces intensity-dependent bilateral effects as measured by interleaved BOLD fMRI. *Biol Psychiatry.* 50: 712-720.

Nowak DA, Bösl K, Podubeckà J, Carey JR. 2010. Noninvasive brain stimulation and motor recovery after stroke. *Restor Neurol Neurosci.* 28: 531-544.

O'Shea J, Johansen-Berg H, Trief D, Göbel S, Rushworth MF. 2007. Functionally specific reorganization in human premotor cortex. *Neuron.* 54:479-490.

Pascual-Leone A, Bartres-Faz D, Keenan JP. 1999. Transcranial magnetic stimulation: studying the brain-behaviour relationship by induction of 'virtual lesions'. *Philos Trans R Soc Lond B Biol Sci.* 354: 1229-1238.

Pascual-Leone A, Valls-Solé J, Wassermann EM, Hallett M. 1994. Responses to rapid-rate transcranial magnetic stimulation of the human motor cortex. *Brain.* 117: 847-858.

Pascual-Leone A, Walsh V, Rothwell J. 2000. Transcranial magnetic stimulation in cognitive neuroscience--virtual lesion, chronometry, and functional connectivity. *Curr Opin Neurobiol.* 10: 232-237.

Passingham RE, Ramnani N, Rowe JB. 2004. The Motor System. In: Frackowiak RSJ, Friston KJ, Frith CD, Dolan RJ, Price CJ, Zeki S, Ashburner J, Penny W, eds. *Human Brain Function* 2nd ed. Elsevier p 5-32.

Paulus W. 2003. Transcranial direct current stimulation (tDCS). *Suppl Clin Neurophysiol.* 56: 249-254.

Paus T, Jech R, Thompson CJ, Comeau R, Peters T, Evans AC, 1997. Transcranial magnetic stimulation during positron emission tomography: a new method for studying connectivity of the human cerebral cortex. *J Neurosci.* 17: 3178-3184.

Petrides M. 1986. The effect of periarculate lesions in the monkey on the performance of symmetrically and asymmetrically reinforced visual and auditory go, no-go tasks. *J Neurosci.* 6: 2054-2063.

- Petrides M. 1997. Visuo-motor conditional associative learning after frontal and temporal lesions in the human brain. *Neuropsychologia*. 35: 989-997.
- Ruff CC, Blankenburg F, Bjoertomt O, Bestmann S, Freeman E, Haynes JD, Rees G, Josephs O, Deichmann R, Driver J. 2006. Concurrent TMS-fMRI and psychophysics reveal frontal influences on human retinotopic visual cortex. *Curr Biol*. 16: 1479-1488.
- Rushworth MF, Johansen-Berg H, Göbel SM, Devlin JT. 2003. The left parietal and premotor cortices: motor attention and selection. *Neuroimage*. 20(Suppl 1):S89-S100.
- Sack AT, Cohen Kadosh R, Schuhmann T, Moerel M, Walsh V, Goebel R. 2009. Optimizing functional accuracy of TMS in cognitive studies: a comparison of methods. *J Cogn Neurosci*. 21: 207-221.
- Sack AT, Kohler A, Bestmann S, Linden DE, Dechent P, Goebel R, Baudewig J. 2007. Imaging the brain activity changes underlying impaired visuospatial judgments: simultaneous FMRI, TMS, and behavioral studies. *Cereb Cortex*. 17: 2841-2852.
- Sakai K, Hikosaka O, Miyauchi S, Sasaki Y, Fujimaki N, Putz B. 1999. Presupplementary motor area activation during sequence learning reflects visuo-motor association. *J Neurosci*. 19: RC1.
- Schluter ND, Rushworth MF, Passingham RE, Mills KR. 1998. Temporary interference in human lateral premotor cortex suggests dominance for the selection of movements. A study using transcranial magnetic stimulation. *Brain*. 121: 785-799.
- Schönfeldt-Lecuona C, Thielscher A, Freudenmann RW, Kron M, Spitzer M, Herwig U. 2005. Accuracy of stereotaxic positioning of transcranial magnetic stimulation. *Brain Topogr*. 17: 253-259.
- Schutter DJ. 2009. Antidepressant efficacy of high-frequency transcranial magnetic stimulation over the left dorsolateral prefrontal cortex in double-blind sham-controlled designs: a meta-analysis. *Psychol Med*. 39: 65-75.
- Siebner HR, Filipovic SR, Rowe JB, Cordivari C, Gerschlager W, Rothwell JC, Frackowiak RS, Bhatia KP. 2003. Patients with focal arm dystonia have increased sensitivity to slow-frequency repetitive TMS of the dorsal premotor cortex. *Brain*. 126:2710-2725.
- Siebner HR, Peller M, Bartenstein P, Willoch F, Rossmair C, Schwaiger M, Conrad B. 2001b. Activation of frontal premotor areas during suprathreshold transcranial magnetic stimulation of the left primary sensorimotor cortex: a glucose metabolic PET study. *Human Brain Mapping*. 12: 157-167.
- Siebner HR, Peller M, Takano B, Conrad B. 2001a. New insights into brain function by combination of transcranial magnetic stimulation and functional brain mapping. *Nervenarzt*. 72: 320-326.
- Siebner HR, Takano B, Peinemann A, Schwaiger M, Conrad B, Drzezga A, 2001c. Continuous transcranial magnetic stimulation during positron emission tomography: a suitable tool for imaging regional excitability of the human cortex. *Neuroimage*. 14: 883-890.
- Siebner HR, Willoch F, Peller M, Auer C, Boecker H, Conrad B, Bartenstein P, 1998. Imaging brain activation induced by long trains of repetitive transcranial magnetic stimulation. *NeuroReport*. 9: 943-948.

Speer AM, Kimbrell TA, Wassermann EM, D Repella J, Willis MW, Herscovitch P, Post RM. 2000. Opposite effects of high and low frequency rTMS on regional brain activity in depressed patients. *Biol Psychiatry*. 48: 1133-1141.

Speer AM, Willis MW, Herscovitch P, Daube-Witherspoon M, Shelton JR, Benson BE, Post RM, Wassermann EM. 2003. Intensity-dependent regional cerebral blood flow during 1-Hz repetitive transcranial magnetic stimulation (rTMS) in healthy volunteers studied with H215O positron emission tomography: I. Effects of primary motor cortex rTMS. *Biol Psychiatry*. 54: 818-825.

Tjandra T, Brooks JC, Figueiredo P, Wise R, Matthews PM, Tracey I. 2005. Quantitative assessment of the reproducibility of functional activation measured with BOLD and MR perfusion imaging: implications for clinical trial design. *Neuroimage*. 27: 393-401.

Toni I, Ramnani N, Josephs O, Ashburner J, Passingham RE. 2001. Learning arbitrary visuomotor associations: temporal dynamic of brain activity. *Neuroimage*. 14: 1048-1057.

Wang J, Aguirre GK, Kimberg DY, Roc AC, Li L, Detre JA. 2003. Arterial spin labeling perfusion fMRI with very low task frequency. *Magn Reson Med*. 49: 796-802.

Wang J, Rao H, Wetmore GS, Furlan PM, Korczykowski M, Dinges DF, Detre JA. 2005a. Perfusion functional MRI reveals cerebral blood flow pattern under psychological stress. *Proc Natl Acad Sci U S A*. 102: 17804-17809.

Zaharchuk G, Ledden PJ, Kwong KK, Reese TG, Rosen BR, Wald LL. 1999. Multislice perfusion and perfusion territory imaging in humans with separate label and image coils. *Magn Reson Med*. 41: 1093-1098.

Ziemann U. 2004. TMS induced plasticity in human cortex. *Rev Neurosci*. 15: 253-266.

Abbreviations

AK	Associative key presses
AMT	Active motor threshold
APB	Abductor pollicis brevis
ASL	Arterial spin labeling
BA9	Brodmann area 9
BOLD	Blood oxygenation level dependent
CASL	Continuous Arterial spin labeling
CMA	Cingulate motor areas
DCM	Dynamic causal modeling
DTI	Diffusion tensor imaging
EPI	Echo planar imaging
FBIRN	Functional biomedical informatics research network
FK	Freely selected key presses
FMRI	Functional magnetic resonance imaging
IPL	Inferior parietal lobe
M1	Primary motor cortex
MEP	Motor evoked potentials
MFG	Middle frontal gyri
MR	Magnetic resonance
MRI	Magnetic resonance imaging
PET	Positron emission tomography
PMd	Dorsal premotor cortex
PMv	Ventral premotor cortex
PPI	Psychophysiological interaction
PV	Passive viewing
RCBF	Regional cerebral blood flow
RCMRglc	Regional cerebral metabolic rate of glucose consumption
RF	Radio frequency
RMT	Resting motor threshold
ROI	Region of interest
RT	Reaction time
RTMS	Repetitive transcranial magnetic stimulation
S1	Primary somatosensory cortex
SFG	Superior frontal gyri
SMA	Supplementary motor areas
SNR	Signal to noise ratio
SFNR	Signal-to-fluctuation-noise ratio
TDCS	Transcranial direct current stimulation
TMS	Transcranial magnetic stimulation
TR	Repetition time

Acknowledgements

First and foremost I would like to thank my supervisor, Dr. Axel Thielscher, for his guidance, patience and tremendous support. I consider myself very fortunate for being his PhD student and for benefitting from his extensive knowledge and expertise. I learned a lot from him and I am convinced that this knowledge will help me in the future.

I am very grateful to Dr. Rolf Pohmann for his help in establishing the CASL setup and for adapting the imaging sequences to our specific needs. I would also like to thank Prof. Dr. Hartwig Siebner and Dr. Kamil Uludag for bringing their expertise into my projects.

I'm indebted to Prof. Dr. Uwe Klose and to Prof. Dr. Klaus Scheffler for agreeing to be part of my review committee and for their valuable comments. I would also like to express my gratitude to Prof. Dr. Wolfgang Grodd, Prof. Dr. Fritz Schick and Prof. Dr. Hartwig Siebner for agreeing to be members of my thesis committee.

I would also like to acknowledge Max Planck Society for the financial support that made my doctorate studies at the Max Planck Institute for Biological Cybernetics possible.

Last but not least, I would like to thank my parents, Iulia and Viorel, my grandma Elena, and my brother Mihai, for their unconditional support. Their love and encouragement were always motivating me.

Personal Contributions to the Publications

M1. New Coil Positioning Method for Interleaved Transcranial Magnetic Stimulation (TMS)/Functional MRI (fMRI) and Its Validation in a Motor Cortex Study.

Authors: **Marius Moisă**, Rolf Pohmann, Lars Ewald, Axel Thielscher.

Journal: Journal of Magnetic Resonance Imaging, 29(1), 189-197, 2009.

Own contribution: I programmed the software for positioning the TMS coil inside the scanner with help of Dr. Axel Thielscher. I conducted the experiments and I analyzed the data. I wrote the first draft of the manuscript.

M2. Interleaved TMS/CASL: Comparison of different rTMS protocols.

Authors: **Marius Moisă**, Rolf Pohmann, Kâmil Uludağ, Axel Thielscher.

Journal: Neuroimage, 49(1), 612-620, 2010.

Own contribution: I implemented the interleaved TMS/CASL setup together with Dr. Axel Thielscher and Dr. Rolf Pohmann. I designed the study together with Dr. Axel Thielscher. I conducted the experiments and I analyzed the data. I wrote the first draft of the manuscript.

M3. Remote Motor Cortical Areas Acutely Compensate for a Transient Lesion of Left Dorsal Premotor Cortex during Arbitrary Visuomotor Mapping.

Authors: **Marius Moisă**, Hartwig R. Siebner, Rolf Pohmann, Axel Thielscher.

Journal: submitted

Own contribution: I designed the study together with Dr. Axel Thielscher and Prof. Dr. Hartwig Siebner. I conducted the experiments and I analyzed the data. I wrote the first draft of the manuscript.

Manuscripts

- M1.** New Coil Positioning Method for Interleaved Transcranial Magnetic Stimulation (TMS)/Functional MRI (fMRI) and Its Validation in a Motor Cortex Study.
Authors: **Marius Moisă**, Rolf Pohmann, Lars Ewald, Axel Thielscher.
Journal: Journal of Magnetic Resonance Imaging, 29(1), 189-197, 2009.

Technical Note

New Coil Positioning Method for Interleaved Transcranial Magnetic Stimulation (TMS)/Functional MRI (fMRI) and Its Validation in a Motor Cortex Study

Marius Moisa, MS,¹ Rolf Pohmann, PhD,¹ Lars Ewald, MS,² and Axel Thielscher, PhD^{1*}

Purpose: To develop and test a novel method for coil placement in interleaved transcranial magnetic stimulation (TMS)/functional MRI (fMRI) studies.

Materials and Methods: Initially, a desired TMS coil position at the subject's head is recorded using a neuronavigation system. Subsequently, a custom-made holding device is used for coil placement inside the MR scanner. The parameters of the device corresponding to the prerecorded position are automatically determined from a fast structural image acquired directly before the experiment. The spatial accuracy of our method was verified on a phantom. Finally, in a study on five subjects, the coil was placed above the cortical representation of a hand muscle in M1 and the blood oxygenation level-dependent (BOLD) responses to short repetitive TMS (rTMS) trains were assessed using echo-planar imaging (EPI) recordings.

Results: The spatial accuracy of our method is in the range of 2.9 ± 1.3 (SD) mm. Motor cortex stimulation resulted in robust BOLD activations in motor- and auditory-related brain areas, with the activation in M1 being localized in the hand knob.

Conclusion: We present a user-friendly method for TMS coil positioning in the MR scanner that exhibits good spatial accuracy and speeds up the setup of the experiment. The motor-cortex study proves the viability of the approach and validates our interleaved TMS/fMRI setup.

Key Words: interleaved TMS/fMRI; motor cortex; neuronavigation; coil positioning; image quality

J. Magn. Reson. Imaging 2009;29:189–197.

© 2008 Wiley-Liss, Inc.

INTERLEAVING TRANSCRANIAL MAGNETIC STIMULATION (TMS) with functional MRI (fMRI) is a promising approach to study the functional connectivity between brain areas in humans. For example, fMRI can be used to measure the blood oxygenation level-dependent (BOLD) activity induced by TMS to demonstrate the connectivity between the stimulated area and coactivated areas (1,2). Alternatively, in the so-called “virtual lesion approach,” TMS disturbs task-related activity in a targeted brain region and fMRI monitors the effect on local and remote BOLD activations (3).

A major practical problem is the positioning of the TMS coil at the subject's head inside the MR scanner to precisely target a desired brain area. Neuronavigation systems have become the advanced standard in TMS to achieve high spatial accuracy of coil placement (4,5). However, these systems cannot be used inside the MR cabin. Here, we present a positioning method for interleaved TMS/fMRI that for the first time allows the exchange of TMS coil positions between a neuronavigation system and an MR-compatible holding device. This allows easy and precise TMS coil placement inside the MR scanner using preplanned positions that were previously recorded using the neuronavigation system. First, our method is introduced and its spatial accuracy is validated. Subsequently, its viability is demonstrated in a pilot study on five subjects, in which it is used to target the representation of a hand muscle in M1.

MATERIALS AND METHODS

Coil Positioning Method: General Outline

Our method is based on a custom-built mechanical coil-holding device with 6 degrees of freedom (DoF) (Fig. 1a and e). It consists of MR-compatible materials and fits into the cylindrical radiofrequency (RF) head coil with an inner diameter of 29 cm. The mechanical design of the device was inspired by one previously described (6).

Initially, a high-resolution structural image is acquired once for each subject (magnetization-prepared rapid gradient echo [MPRAGE], 192 sagittal slices, matrix size = 256×256 , voxel size = 1 mm^3 , TR/TE/TI =

¹High-Field Magnetic Resonance Center, Max Planck Institute (MPI) for Biological Cybernetics, Tübingen, Germany.

²MagVenture, Farum, Denmark.

Contract grant sponsor: Max-Planck Society; Contract grant sponsor: German Research Foundation; Contract grant number: TH1330/2-1.

*Address reprint requests to: A.T., Max Planck Institute for Biological Cybernetics, Spemannstraße 41, D-72076 Tübingen, Germany.

E-mail: axel.thielscher@tuebingen.mpg.de

Additional Supporting Information may be found in the online version of this article.

Received April 14, 2008; Accepted August 27, 2008.

DOI 10.1002/jmri.21611

Published online in Wiley InterScience (www.interscience.wiley.com).

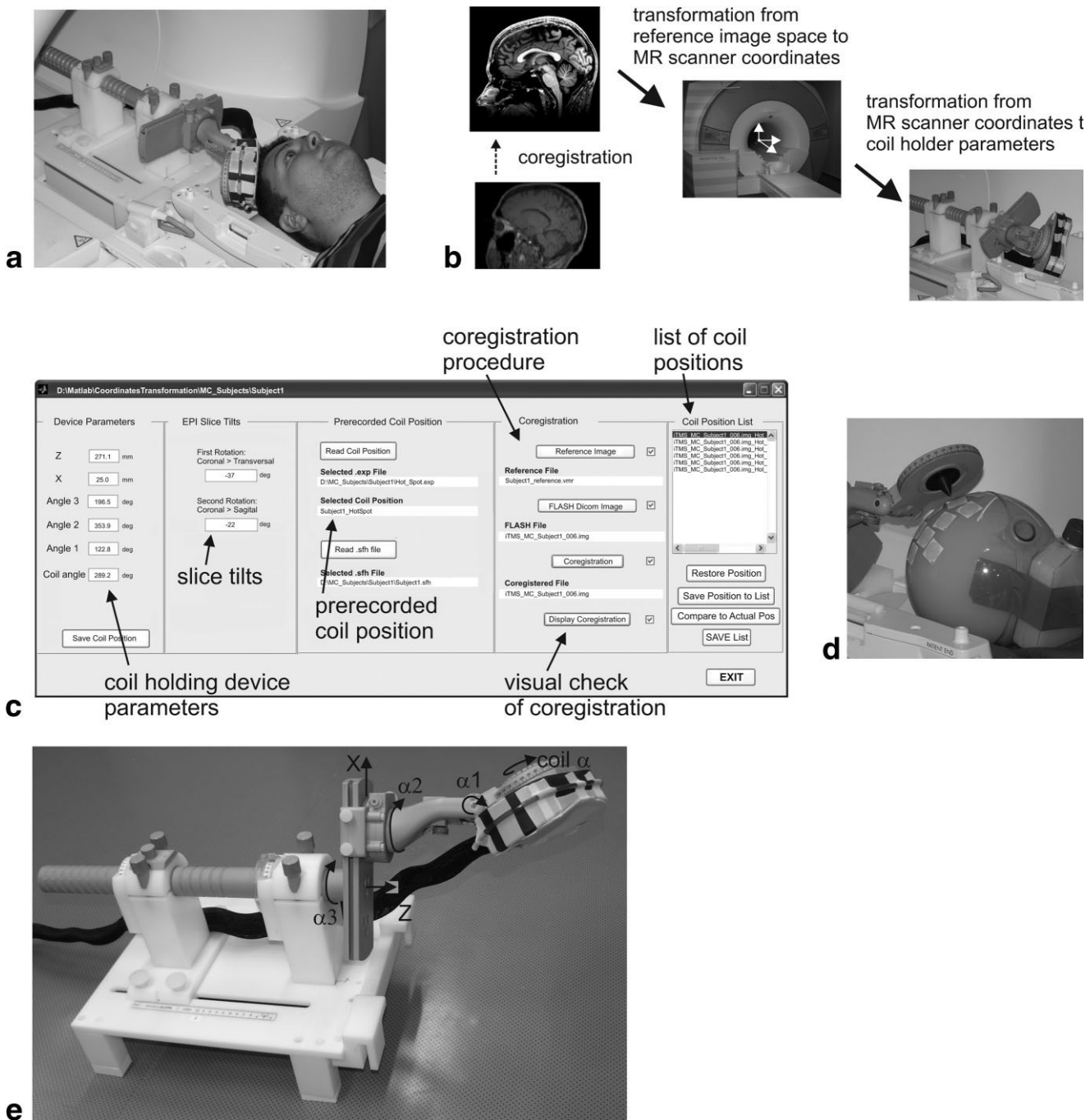


Figure 1. **a:** The TMS coil and the coil-holding device mounted in the scanner. **b:** Transformation steps performed by the software to compute the coil-holding parameters from a prerecorded coil position. **c:** GUI of the positioning software. **d:** Validation measurements: markers were placed on an agar phantom (a 250-mL plastic bottle attached to a 17-cm sphere). The TMS coil was replaced by a pointer. The average distance between the tip of the pointer and the positions indicated by the markers determines the spatial accuracy of our positioning method. **e:** Coil holder with the different translation and rotation axes indicated by arrows.

1900/2.26/900 msec, 12-channel head coil, 3T Siemens TIM Trio, Erlangen, Germany). The image is loaded into a neuronavigation system (BrainView, Fraunhofer IPA, Stuttgart, Germany) (7) that tracks the TMS coil position in real time and visualizes it in respect to the subject's individual brain anatomy.

Prior to an interleaved TMS/fMRI experiment, the neuronavigation system is used to record the desired

coil positions, which are saved with respect to the high-resolution image. This step can be done at any time before the experiment, which reduces the time to set up the subject in the scanner.

At the beginning of an experiment, the position of the subject's head inside the RF head coil is determined by a fast structural image (fast low-angle shot [FLASH], 60 horizontal slices, matrix size = 128×128 , voxel size =

$2 \times 2 \times 3$ mm, TR/TE = 339/2.46 msec, one-channel transmit/receive (Tx/Rx) head coil, PN 2414895; USA Instruments, Aurora, CO, USA) within 54 seconds. The image is loaded into our custom-written positioning software (based on MATLAB, The MathWorks, Natick, MA, USA) and automatically coregistered to the high-resolution reference image by means of SPM5 functions (Wellcome Trust Centre for Neuroimaging, University College London [UCL], London, UK). This step is used to determine the coordinate transformation from the high-resolution reference image to the scanner coordinate system relative to the isocenter (Fig. 1b). The pre-planned coil positions can then be loaded into the positioning software and transformed into real-world scanner coordinates. The latter values are used in a second transformation step to determine the translation and rotation parameters of the coil-holding device, similar to the method described by Bohning et al (6). Once a coil position has been recorded using the neuronavigation system, the parameters for the holding device are automatically determined by our software based on a fast FLASH image of the subject's head. Additional software features are as follows (Fig. 1c):

- The high-resolution structural image is displayed together with the coregistered FLASH image to visually verify the coregistration result.
- A list of coil positions is provided. The user has the possibility to add a position, to restore it, and to save the overall list as MATLAB file.
- Head movements in the course of an experiment displace the originally targeted cortical area with respect to the fixed TMS coil. The amount of displacement can be monitored by regularly acquiring FLASH images. For each new image, the software computes an updated coil position and compares it with the positions in the list, so that the (apparent) change of coil position indicates the amount of displacement.
- A set of coil-holding parameters can be transformed back into a coil position for usage in the neuronavigation system, or in a further interleaved TMS/fMRI session.
- The echo-planar imaging (EPI) slice tilts that are necessary to minimize the susceptibility artifacts induced by the TMS coil (8) are automatically determined. It should be noted that the tilts minimizing the image artifacts underneath the coil might unfavorably affect susceptibility-related signal loss in brain regions such as the orbitofrontal cortices (9). Consequently, depending on the experimental question under study, a compromise will sometimes be necessary.

Coil Positioning Method: Calibration and Validation

The precision of our method depends on the two successive coordinate transformations from the high-resolution reference image to the MR scanner space, and further on from these coordinates into the parameter space of the holding device (Fig. 1b). The accuracy of the first step is determined by the coregistration procedure of the FLASH image onto the reference image, which is

ensured by regular visual inspection of the coregistration results. Additionally, for two subjects, the accuracy was checked post hoc using five FLASH images from different experimental sessions. The coregistered and resliced FLASH images were coregistered among each other (i.e., the first onto the second, third, fourth, and fifth; the second onto the first, third, fourth, and fifth, etc.). If the initial coregistrations of the FLASH images onto the reference image were perfect, the coregistered FLASH images would overlap perfectly and the subsequent mutual coregistrations would yield identity transformation matrices. In other words, the deviations of the transformation matrices from the identity matrix were used to quantify the stability of the first transformation step across different sessions.

To adjust the second transformation step from the MR scanner space to holding device parameters, the coil was replaced by three small MR-visible spheres placed on a small plate and FLASH images for 20 parameter sets of the coil-holding device were taken, thereby approximately covering the space corresponding to frontal, parietal, and temporal brain regions. The sphere centers were manually localized in the FLASH images and compared with their theoretical positions calculated from the parameter sets. Subsequently, in a numerical search procedure (a trust-region interior-reflective Newton method provided by the Optimization Toolbox of MATLAB), offsets were added to the coil parameters and the set of offset values was determined that minimized the average deviation between the theoretical and measured values across all 20 parameter sets. The robustness of the search procedure was ensured by randomly jittering the initial values of the search and refitting the data. The estimated values were saved and used as constant offsets in the subsequent calculations. After one week, the coil-holding device was remounted in the scanner and 20 additional measurements were performed. The average deviation between the theoretical and measured values was determined to validate the optimized second transformation step.

The accuracy of the *overall* procedure from the recording of a position using the neuronavigation system to the calculation of the holding device parameters was validated using the agar phantom shown in Fig. 1d. To ensure mathematically unambiguous results of the coregistration procedure, the overall phantom was made asymmetric by gluing a small box-like phantom to a spherical phantom. Twenty-six points were marked on the surface of the sphere and their positions were recorded with the neuronavigation system, again covering the space corresponding to frontal, parietal, and temporal brain regions. As markers we used paper labels with one central dot indicating the target position, surrounded by concentric rings having millimeter spacing. After placing the phantom in the MR scanner and taking a FLASH image, the holding device parameters corresponding to the 26 coil positions were computed. The positions indicated by the holding device were then visually compared with the target points on the phantom using the concentric rings on the marker and a small ruler to determine their spatial deviation. This procedure was conducted two times in sessions one

week apart to assess the stability of the overall positioning method. It should be noted that only five of six DoFs are tested in this way. The pointing device (Fig. 1d) replacing the TMS coil in these measurements represents an axis that is perpendicular to the coil plane and runs through the midpoint of the coil. It corresponds to the peak of the induced electric field (10). The accuracy of coil rotations around this axis was not tested.

Coil Positioning Method: Technical Details on the Coil Holder

Figure 1e shows the coil holder with the TMS coil attached to it. Its basis (material: Delrin) is stably attached to the patient table of the MR scanner by two clamps at the front side of the holder so that its position relative to the RF head coil stays fixed when the patient table moves. The main axis of the holder (indicated by Z in Fig. 1e) is oriented parallel to the z-axis of the scanner. Its height was chosen to coincide with the center of the RF head coil. The main axis and the frontal parts are made from polyetheretherylketone (PEEK) to increase their mechanical stability. The holder has two translation (X, Z) and four rotation DoFs (coil α , $\alpha 1$, $\alpha 2$, and $\alpha 3$). Axis $\alpha 1$ is displaced from a position directly above the TMS coil in order to reduce the thickness of the part of the holder that is attached at the back of the TMS coil. This in turn helps to maximize the available space inside the RF head coil. Axis $\alpha 1$ (material: bronze) is indirectly driven by a worm drive (bronze) that operates toothed rings (aluminum) by means of a tooth belt (internally enforced using aramid fibers rather than metal wires). Axis $\alpha 2$ is directly driven by a worm drive (bronze). The scale of axis $\alpha 1$ has a resolution of 3° , and can be read with an accuracy of $\sim 1.5^\circ$. The scales of the other axes have a resolution of 1 mm and 1° , respectively. A computer-aided design (CAD) model of the frontal holder parts (starting with the plate corresponding to the X-axis) is available in STEP (ISO 10303) format and may be obtained from the corresponding author.

Coil Positioning Method: Software Details

The positioning software (graphical user interface [GUI] shown in Fig. 1c) and the BrainView navigation system (Fraunhofer IPA, Stuttgart, Germany) use the BrainVoyager (Brain Innovation, The Netherlands) data formats and coordinate systems for the structural reference image and the coil positions. Coil positions are saved in a head coordinate system that was originally developed to store electroencephalograph (EEG) electrode positions in BrainVoyager and uses the left and right ears and the nasion as anatomical landmarks. The reference image is stored as a structural volume file (*.vnr). Additionally, the transformation matrix from the head coordinate system to the structural image space is stored in a separate file (*.sfh). These two files have to be loaded into the positioning software prior to loading coil positions. Coil positions can either be pre-recorded using the neuronavigation system, or planned offline by using the coordinates of a desired target position as shown by BrainVoyager.

The FLASH images have to be exported in digital imaging and communications in medicine (DICOM) format from the scanner console to a target directory on the computer running the positioning software. The software imports the FLASH images from this directory and coregisters them on the structural image using SPM5 functions. Up to now, only Siemens DICOM files have been tested. However, as our software uses the SPM5 import function, its usage should also be possible with other MR scanner brands. After coregistration, the software computes the translation and rotation parameters of the holding device, which then have to be manually adjusted. The overall process of FLASH image acquisition (54 seconds), transfer and import into the positioning software (about one minute), coregistration (three minutes), and manual adjustment (three minutes) takes around eight minutes. The MATLAB code of the software may be obtained by contacting the corresponding author.

Tests on Safety and Subject Comfort

Prior to the motor study, the safety of the interleaved TMS/fMRI setup and the EPI data quality during TMS stimulation were assessed. The voltages induced in the TMS coil by the MR gradients were measured using the approach described in (15). To test for torque reactions, the TMS coil was manually held in the scanner bore at several different orientations and fired at 100% output intensity. The coil windings are embedded in dampening material that is placed between the wires and the outer coil casing, which effectively reduces the vibration and noise levels when applying TMS pulses in the scanner bore. This was tested in one subject by stimulating occipital, frontal, central, and parietal areas in the MR scanner at 100% output. The mechanical stability of the coil was ensured in a stress test. The coil plane was consecutively oriented orthogonal and parallel to the orientation of the static B₀ field. The output level of the stimulator was set to 100% biphasic "Powermode," in which the capacitors of the stimulator and the MagOption extension are operated in parallel so that the peak currents reach $\sim 140\%$ of the peak currents for normal biphasic stimulation. Continuous repetitive stimulation at 10 Hz was applied until the coil reached the temperature limit (42°C) and the stimulator switched off automatically. This was repeated twice for each of the two coil orientations tested.

Motor Cortex Study: General Procedure

Five healthy subjects gave informed written consent to participate in the study, which was approved by the local ethics committee. In an initial "Hot Spot" search, the TMS coil position that caused the strongest twitching of a particular finger muscle (abductor pollicis brevis) was determined and its position was saved using the neuronavigation system. In the MR scanner, the TMS coil was placed on the "Hot Spot" using our positioning method. As a side note, an earlier version of the holding device than described in this work was used in the motor study. Parts of it were mechanically less stable, resulting in a slightly lower accuracy (~ 1 mm) of

the overall positioning method. However, we do not think that this had a major impact on the outcome of the study.

After coil placement, the lowest stimulation intensity resulting in an activation of the muscle (the “motor threshold” [MT]) was determined using electromyographic recordings. The interleaved TMS/fMRI setup consisted of a MagPro X100 stimulator with MagOption (MagVenture, Farum, Denmark) and an MR-compatible figure-8 coil (MRi-B88). To prevent the MR images from being affected by RF noise, the stimulator was placed outside the MR cabin and the coil was connected through a high-current filter (E-LMF-4071; ETS-Lindgren, St. Louis, MO, USA) attached to the copper shielding of the cabin (11). The TMS stimulation was interleaved with the MRI acquisition using custom-written software. Pauses of 68 msec were introduced after every 133 msec in the gradient echo (GE) EPI sequence, i.e., after every second slice (204 volumes, 24 slices parallel to the coil plane, voxel size = $3 \times 3 \times 4 \text{ mm}^3$, 0.5 mm gap, matrix size = 64×64 , TR/TE = 2410/30 msec, bandwidth (BW) = 2232 Hz/pixel, one-channel Tx/Rx head coil). The pauses were used to interleave the EPI sequence with trains of 10 biphasic TMS pulses applied every 200 msec for two seconds at 110% MT, followed by rest periods of 17.2 seconds (Fig. 3a). This was repeated 25 times. Two runs with TMS stimulation at 110% MT were acquired. In one additional run, the TMS intensity was set to 50% MT and the subjects performed volitional thumb movements, acoustically triggered by the TMS coil clicks. After each run a FLASH image was acquired to check for coil displacements due to head movements.

Motor Cortex Study: Data Analysis

After careful visual inspection of the EPI volumes for putative TMS-related artifacts, the data were analyzed using FSL3.3 (FMRIB, Oxford University, Oxford, UK). Motion and slice time correction was applied to the EPI time series, followed by brain extraction, temporal high-pass filtering (50-second cutoff) and Gaussian spatial smoothing (5-mm full-width at half-maximum [FWHM]). The statistical model was constructed by convolving a stick function that indicated the times of TMS stimulation with a gamma function modeling the standard hemodynamic response. After estimation of the general linear model (FSL FILM), the resulting statistical maps were registered onto the Montreal Neurological Institute (MNI) template. The single statistical results for the runs of an individual subject were first combined in a fixed-effects analysis. An FSL FLAME mixed-effects analysis was then used to obtain group results (threshold: $z = 2.3$ at voxel level and $P = 0.05$ corrected at cluster level).

Time courses were obtained for eight structural regions of interest (ROIs) corresponding to the motor system (M1/S1, cingulate motor area [CMA]/supplementary motor area [SMA], posterior bilateral putamen), the auditory system (bilateral auditory cortex, inferior colliculi) and a control region in white matter (centered at $x = 24$, $y = -28$, $z = 33$, MNI space). For each subject, the ROIs were manually determined in the high-resolu-

tion structural image. They were intersected with the individual statistical maps (threshold: $P = 0.05$ uncorrected at voxel level) to determine the subregions exhibiting task-related activity. The mean signal change of the voxels in the subregions was averaged across trials, using the mean of the two volumes prior to trial onset as baseline. Additionally, the variability of the observed BOLD signals was assessed by calculating the standard error across trials.

EPI Image Quality

A spherical agar phantom and the procedures outlined in the Function Biomedical Informatics Research Network (fBIRN) protocol (16) were used to assess the EPI data quality during TMS stimulation. Three EPI runs were performed and their results compared 1) without the TMS coil, 2) with the coil attached to the phantom but not connected to the stimulator, and 3) with TMS stimulation at 80% of the maximal output intensity (thereby exceeding the maximal intensity used for motor cortex stimulation). The EPI parameters were identical to those used in the motor cortex study. For each EPI slice, the mean across volumes was determined to check for static signal dropout and distortions. Additionally, the signal-to-fluctuation-noise ratio (SFNR) was determined by dividing the mean by the SD across volumes. Low SFNR values signal a high temporal variability of the EPI signal, hinting, e.g., toward an unwanted impact of the TMS pulses on the EPI measurements.

In order to quantify the amount of distortions in the EPI brain images, phase maps were recorded for two subjects using the standard Siemens GE field map sequence, with and without the TMS coil being positioned over the motor cortex. The raw maps were phase-unwrapped, converted to radians/second, and used to estimate the pixel shifts in the EPI images (using FSL PRELUDE and FUGUE).

RF Noise Measurements

The effectiveness of the high-current filter in eliminating the RF noise caused by the stimulator was tested using the Siemens RF noise service sequence. During the sequence, the MR gradients and RF excitation are kept switched off while the RF receiver scans for RF noise in a range of ± 250 kHz relative to the center frequency. The setup was identical to that used for the EPI data quality measurements. In a further test, the amplitudes of the RF excitation pulses of the EPI images were set to 0V while keeping the other EPI parameters unchanged from those used in the motor cortex study, and the three conditions previously tested with the fBIRN protocol were repeated. Additionally, one run was acquired with the TMS coil connected to the stimulator, which was set to 100% output intensity but was not firing. For each of the runs, the SD across volumes was calculated to determine the amount by which the RF noise contributes to the noise in the SFNR measurements.

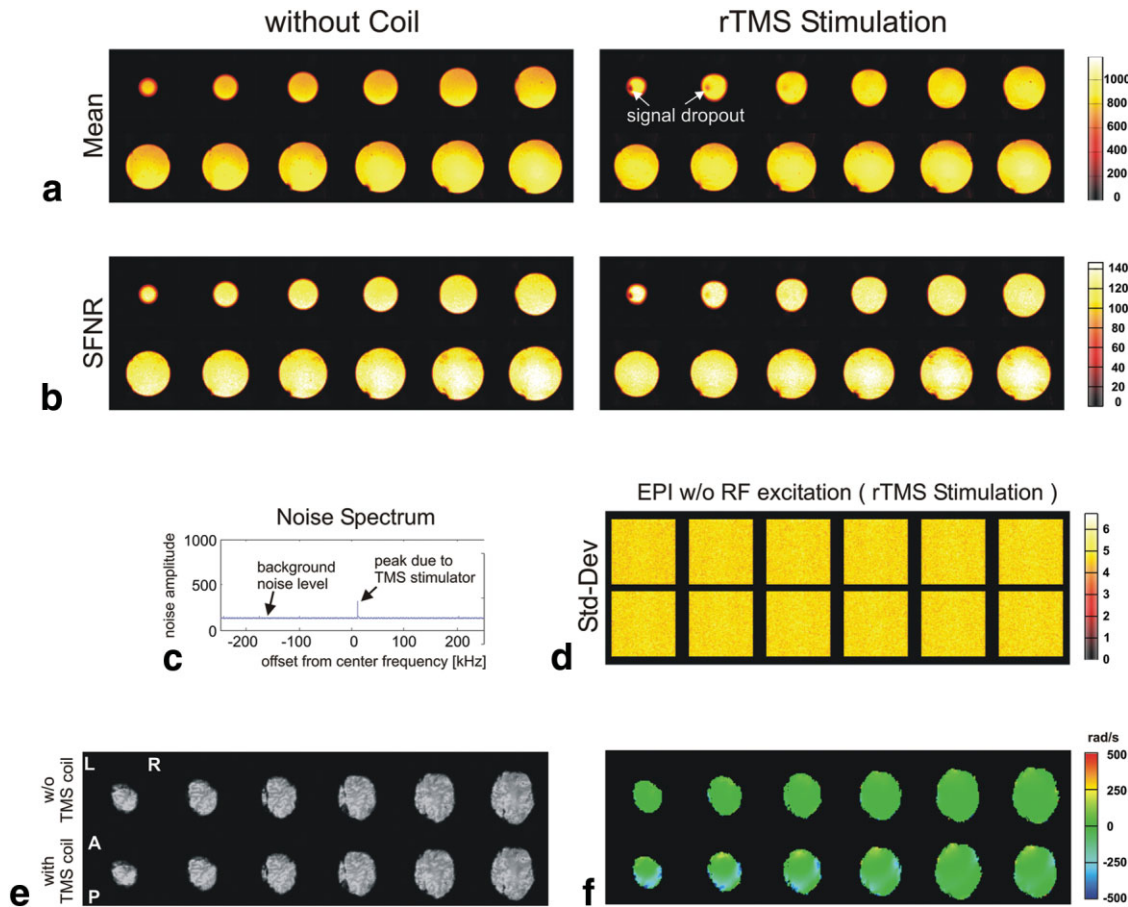


Figure 2. **a:** Mean images of the 12 EPI slices closest to the TMS coil for the EPI measurements without coil and with rTMS stimulation. The TMS coil is placed directly above the first slice. **b:** SFNR images without the coil and with rTMS stimulation. With ~ 130 , the SFNR values in both the control run and the measurement with TMS fall below the limit of 200 for good EPI quality given in the fBIRN protocol (16). This was caused by choosing a higher BW than defined by fBIRN. The normal SFNR values of the scanner exceed 220 when using the standard fBIRN parameters. **c:** Noise spectrum for the TMS coil connected to the enabled stimulator. The noise amplitude is scaled in arbitrary units (range, 0–4096). **d:** SD images for the EPI measurements without RF excitation pulse. Shown are the results for rTMS stimulation. The same slices as in image a are selected. **e:** EPI images for one exemplary subject, with and without the TMS coil placed above the first slice. The slice orientation was chosen to be parallel to the TMS coil placed above the motor cortex. **f:** Phase maps for the images shown in e. [Color figure can be viewed in the online issue, which is available at www.interscience.wiley.com.]

RESULTS

Coil Positioning Method: Validation Results

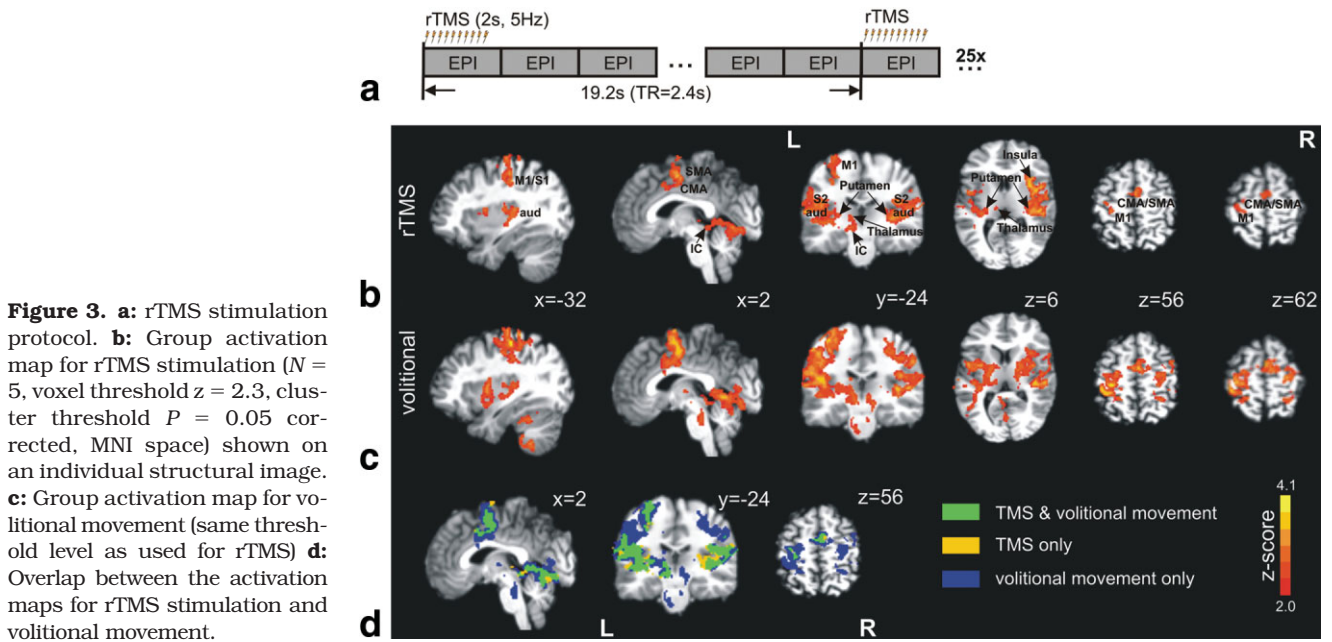
The mutual coreregistrations of the resliced FLASH images resulted in negligible rotation angles and mean deviations (\pm SD) of 0.55 ± 0.09 mm and 0.69 ± 0.14 mm for the two subjects tested. This indicates that the first transformation step of the FLASH images onto the high-resolution image yields stable results across different sessions. Additionally, we checked whether the presence of the skull in the FLASH images affected the registration results. In two subjects, the brains were extracted in the reference and the FLASH images using the BET tool of FSL3.3. The FLASH images with and without skull were subsequently registered to the reference image. The results differed only marginally (<0.5 mm), so that subsequently the original FLASH images with skull were used for coregistration.

After calibration, the accuracy of the second transformation step from MR scanner coordinates to the pa-

rameter space of the coil holder was in the range of 1.9 ± 0.8 mm (mean \pm SD) for the 20 positions used in the validation measurements. The average deviations in the x-, y-, and z-directions (in scanner coordinates) were 1.0 ± 0.8 mm, 1.2 ± 0.8 mm, and 0.7 ± 0.4 mm, respectively. The accuracy of the overall procedure was tested twice in separate sessions by comparing the 20 markers on the phantom with their corresponding positions indicated by the holding device (Fig. 1d). The average deviations were 2.9 ± 1.3 mm (maximum offset: 6.0 mm) and 2.6 ± 0.9 mm (maximum offset: 4.5 mm), respectively.

Safety and Subject Comfort

The maximal peak-to-peak voltage induced in the TMS coil by the MR gradients was $<4V$, which is low enough to not affect the stimulator. We could not detect any torque reactions when firing the coil inside the scanner. Using an additional thin (~ 2 mm) layer of foam plastic



was sufficient to reduce the coil vibrations to a subjectively comfortable level, even at 100% stimulator output. Noise levels could be reduced to subjectively comfortable levels by ear plugs. The stress test did not reveal any mechanical or electrical damage of the coil, indicating that it is safe to use the coil up 100% biphasic output level at 3T.

EPI Image Quality

The TMS coil caused signal dropouts in the three EPI slices closest to it and spatially more extended but moderate distortions (Fig. 2a). As expected, these effects were static and were also visible when assessing the effects of the coil without stimulation (data not shown). The SFNR images did not reveal any additional temporal EPI signal fluctuations due to the repetitive TMS (rTMS) trains (Fig. 2b). The EPI images of the subjects' brains contained no visible dropouts, probably because the coil-cortex distance was larger than the distance between the first three slices in Fig. 2 and the coil (< 14 mm). The field maps acquired for two subjects revealed moderate distortions that were mainly restricted to the first four slices underneath the coil (Fig. 2e and f show the results for one of the subjects). In both subjects, the estimated maximal pixel shifts for the corresponding EPI slices were 1.4 and -1.8 voxels, respectively. Importantly, the central brain region directly underneath the TMS coil (corresponding to the stimulated M1/S1) exhibited hardly any distortions.

RF Noise

Figure 2c shows the RF noise spectrum for TMS coil placed in the scanner and connected to the enabled TMS stimulator. The high-current filter effectively prevents RF noise from entering the MR cabin, except for one small peak close to the center frequency. The frequency and amplitude (230% of the background noise) of the peak stays constant within and between sessions. The

peak stays when the stimulator is left on, but is disabled (which prevents the power unit from recharging the capacitor). This makes it unlikely that the peak is generated in the high-voltage section of the stimulator.

In order to determine the impact of the RF noise peak on EPI image quality, EPI measurements without initial RF excitation were acquired. In this case, no signal from the phantom is acquired, so only RF noise contributes to the images. Visual inspection of the mean and SD images did not reveal any patterns like bright dots or stripes that usually hint of RF noise in any of the conditions tested (Fig. 2d). However, when the TMS coil was connected to the stimulator, the average SD was generally slightly enhanced throughout the whole image (4.6 compared to 4.4 for baseline). No difference was observed between the conditions with rTMS stimulation and with connected coil but without stimulation. Given the intensities and noise levels of the EPI acquisitions shown in Fig. 2a, increasing the SD by 0.2 corresponds to decreasing the SFNR by approximately 3 units. In consequence, the impact of the RF noise peak on the EPI image quality is negligible.

Motor Cortex Stimulation

Significant BOLD responses were observed in the motor system (stimulated left M1/S1, SMA/CMA, thalamus ipsilateral to stimulated M1, bilateral putamen, and bilateral cerebellum), in the bilateral auditory cortices, the ipsilateral inferior colliculus, and the bilateral insula (Fig. 3b). Volitional movement resulted in stronger BOLD effects, but in a similar spatial activation pattern (Fig. 3c and d). In contrast to rTMS stimulation, volitional movement led to a positive BOLD activation in M1 contralateral to the TMS coil. The numbers of activated voxels in the ROIs are presented in Table 1. The cluster sizes for rTMS stimulation are on average lower, but in the same range as for volitional movement. In all

Table 1
Average size (\pm SE) of the ROIs in Cubic Millimeters for the Two Experimental Conditions

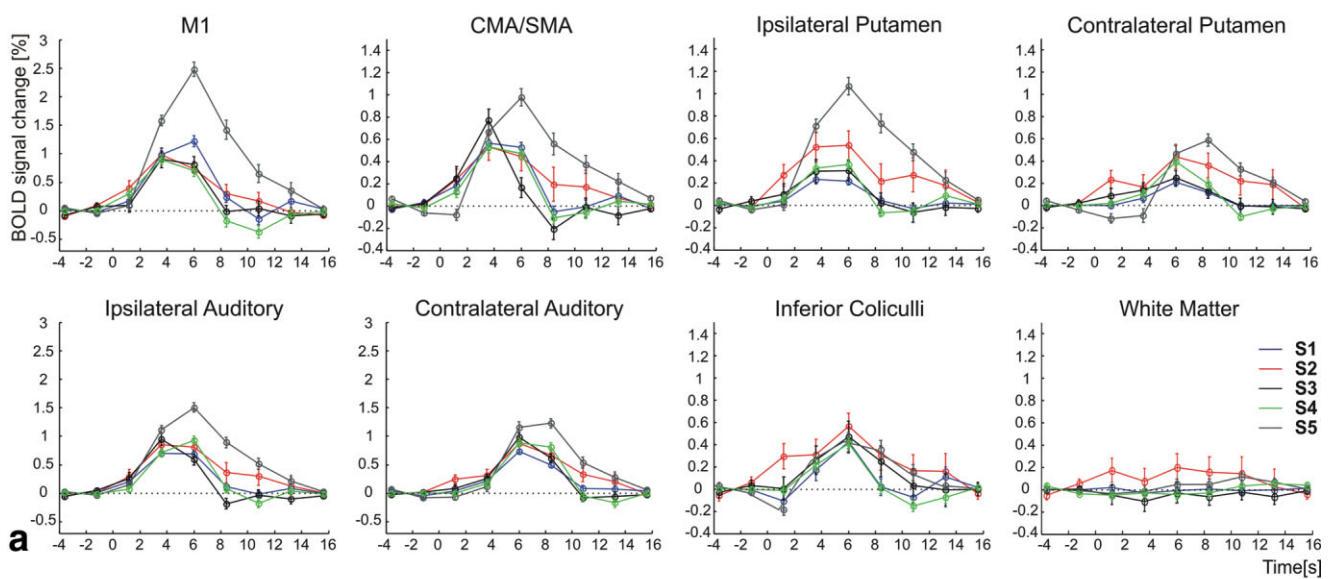
Condition	M1/S1	CMA/SMA	Ipsilateral putamen	Contralateral putamen	Ipsilateral auditory	Contralateral auditory	Inferior colliculi	White matter
rTMS	439 \pm 63	644 \pm 113	405 \pm 60	343 \pm 75	1300 \pm 166	1259 \pm 200	102 \pm 15	96
Volitional	484 \pm 87	810 \pm 166	481 \pm 32	393 \pm 47	1290 \pm 161	1253 \pm 194	123 \pm 18	96

subjects, rTMS stimulation results in robust BOLD curves for all ROIs tested, except for the control region in white matter (Fig. 4a). Averaged across subjects, the-BOLD effect strength for rTMS stimulation is comparable to that caused by volitional movements (Fig. 4b).

DISCUSSION

We present a novel method for TMS coil placement in interleaved TMS/fMRI studies that allows the exchange of coil positions between a neuronavigation system

rTMS Stimulation



Volitional Movement vs. rTMS

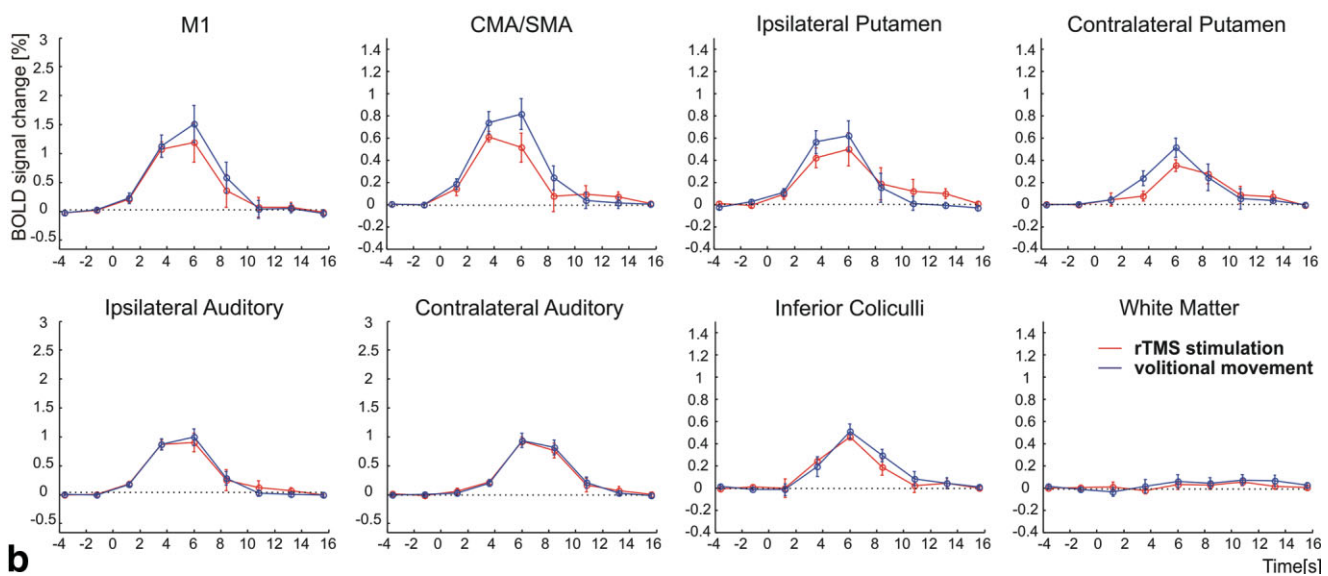


Figure 4. a: Individual ROI time courses for rTMS stimulation. **b:** Time courses for rTMS stimulation and volitional movement, averaged across subjects. Shown is the mean signal change \pm standard error (SE). [Color figure can be viewed in the online issue, which is available at www.interscience.wiley.com.]

and an MR-compatible holding device. The method was validated in a motor cortex study on five subjects. The spatial accuracy (2.9 ± 1.3 and 2.6 ± 0.9 mm, respectively) of our method is in the range reported for neuronavigation systems used in normal TMS studies (5). With one exception, the observed deviations were below 5 mm. The maximally observed deviation was 6.0 mm, which still compares favorably to, e.g., coil placement according to the EEG 10-20 system (12) or relative to the motor representation of finger muscles (13). However, it will depend upon the experimental question if this amount of accuracy is sufficient or not.

Our method was motivated by Bohning et al (6) and therefore shares some similarities with their approach. However, our method incorporates several important advantages. It provides an easy way to repeatedly position the TMS coil at prerecorded stimulation sites, without the need to manually identify brain structures in structural 2D images before each new experiment. In addition, it allows us to easily determine the amount by which the originally targeted area is displaced from the TMS coil due to subject movement in the course of an experiment. Finally, the automatic calculation of the EPI slice tilts to minimize the susceptibility artifacts reduces the required setup time. However, our approach is limited concerning the brain areas that can be reached. While coil positioning over the frontal, parietal, and parts of the temporal areas is feasible, the coil cannot be positioned over the occipital poles and surrounding brain areas.

The presented interleaved TMS-fMRI setup is safe to use and enables us to acquire EPI images of good quality. In particular, the static signal dropouts in the EPI images of the agar phantom were moderate and were not visible in the images of the subjects' brains. EPI images of both the phantom and the subjects' brains exhibited moderate distortions. In the brain images, the distortions were restricted mainly to the first four EPI slices and did not affect the stimulated M1/S1 region. Consequently, it is very unlikely that the spatial localization of the observed BOLD activations was strongly affected by them. Still, we plan to use field maps for distortion correction in future studies. The SFNR images and RF noise measurements demonstrated that the noise induced by the TMS stimuli or the stimulator itself was negligible.

In concordance with previous findings (1,2), the brain regions activated by rTMS stimulation belong mainly to the motor or the auditory system. They exhibit a robust spatial overlap with those obtained for volitional movement. The signals in the ROIs show the expected BOLD time course. Taken together, these findings and the results of the quality assurance (QA) measurement demonstrate a good EPI signal quality and validate our overall setup. The rTMS-induced activation in M1 is localized to the hand knob (14), i.e., to the part of M1 containing the representation of the hand muscles (Fig.

3b, $z = 56$ and 62). This, in turn, validates the spatial accuracy of our positioning method.

ACKNOWLEDGMENTS

We thank two anonymous reviewers for their insightful comments, which helped to significantly improve the manuscript. We thank Nikolaus Weiskopf (UCL, London, UK) for pointing out the possibility of acquiring EPI without RF excitation for RF noise measurement. A.T. was supported in part by the German Research Foundation (grant TH1330/2-1).

REFERENCES

- Bestmann S, Baudewig J, Siebner HR, Rothwell JC, Frahm J. Functional MRI of the immediate impact of transcranial magnetic stimulation on cortical and subcortical motor circuits. *Eur J Neurosci* 2004;19:1950–1962.
- Bohning DE, Shastri A, Lomarev MP, Lorberbaum JP, Nahas Z, George MS. BOLD-fMRI response vs. transcranial magnetic stimulation (TMS) pulse-train length: testing for linearity. *J Magn Reson Imaging* 2003;17:279–290.
- Sack AT, Kohler A, Bestmann S, et al. Imaging the brain activity changes underlying impaired visuospatial judgments: simultaneous fMRI, TMS, and behavioral studies. *Cerebral Cortex* 2007;17:2841–2852.
- Ettinger GJ, Leventon ME, Grimson WE, et al. Experimentation with a transcranial magnetic stimulation system for functional brain mapping. *Med Image Anal* 1998;2:133–142.
- Schönfeldt-Lecuona C, Thielscher A, Freudenmann R, Kron M, Spitzer M, Herwig U. Accuracy of stereotaxic positioning of transcranial magnetic stimulation. *Brain Topogr* 2005;17:253–259.
- Bohning DE, Denslow S, Bohning PA, Walker JA, George MS. A TMS coil positioning/holding system for MR image-guided TMS interleaved with fMRI. *Clin Neurophysiol* 2003;114:2210–2219.
- Kammer T, Vorwerk M, Herrnberger B. Anisotropy in the visual cortex investigated by neuronavigated transcranial magnetic stimulation. *Neuroimage* 2007;36:313–321.
- Baudewig J, Paulus W, Frahm J. Artifacts caused by transcranial magnetic stimulation coils and EEG electrodes in T*-weighted echo-planar imaging. *Magn Reson Imaging* 2000;18:479–484.
- Weiskopf N, Hutton C, Josephs O, Deichmann R. Optimal EPI parameters for reduction of susceptibility-induced BOLD sensitivity losses: a whole-brain analysis at 3 T and 1.5 T. *Neuroimage* 2006;33:493–504.
- Thielscher A, Kammer T. Electric field properties of two commercial figure-8 coils in TMS: calculation of focality and efficiency. *Clin Neurophysiol* 2004;115:1697–1708.
- Bohning DE, Denslow S, Bohning PA, Lomarev MP, George MS. Interleaving fMRI and rTMS. *Suppl Clin Neurophysiol* 2003;56:42–54.
- Herwig U, Satrapi P, Schönfeldt-Lecuona C. Using the international 10-20 EEG system for positioning of transcranial magnetic stimulation. *Brain Topogr* 2003;16:95–99.
- Herwig U, Padberg F, Unger J, Spitzer M, Schönfeldt-Lecuona C. Transcranial magnetic stimulation in therapy studies: examination of the reliability of “standard” coil positioning by neuronavigation. *Biol Psychiatry* 2001;50:58–61.
- Yousry TA, Schmid UD, Alkadhi H, et al. Localization of the motor hand area to a knob on the precentral gyrus—a new landmark. *Brain* 1997;120:141–157.
- Bohning DE, Shastri A, Nahas Z, et al. Echoplanar BOLD fMRI of brain activation induced by concurrent transcranial magnetic stimulation. *Invest Radiol* 1998;33:336–340.
- Friedman L, Glover GH. Report on a multicenter fMRI quality assurance protocol. *J Magn Reson Imaging* 2006;23:827–839.

- M2.** Interleaved TMS/CASL: Comparison of different rTMS protocols.
Authors: **Marius Moisă**, Rolf Pohmann, Kâmil Uludağ, Axel Thielscher.
Journal: *Neuroimage*, 49(1), 612-620, 2010.

Contents lists available at [ScienceDirect](http://www.sciencedirect.com)

NeuroImage

journal homepage: www.elsevier.com/locate/ynimg

Interleaved TMS/CASL: Comparison of different rTMS protocols

Marius Moisa, Rolf Pohmann, Kamil Uludağ, Axel Thielscher*

High-Field Magnetic Resonance Center, MPI for Biological Cybernetics, Tübingen, Germany

ARTICLE INFO

Article history:
Received 16 April 2009
Revised 29 June 2009
Accepted 3 July 2009
Available online 14 July 2009

ABSTRACT

Continuous Arterial Spin Labeling (CASL) offers the possibility to quantitatively measure the regional cerebral blood flow (rCBF). We demonstrate, for the first time, the feasibility of interleaving Transcranial Magnetic Stimulation (TMS) with CASL at 3 T. Two different repetitive TMS (rTMS) protocols were applied to the motor cortex in 10 subjects and the effect on rCBF was measured using a CASL sequence with separate RF coils for labeling the inflowing blood. Each subject was investigated, using a block design, under 7 different conditions: continuous 2 Hz rTMS (3 intensities: 100%, 110% and 120% resting motor threshold [MT]), short 10 Hz rTMS trains at 110% MT (8 pulses per train; 3 different numbers of trains per block with 2, 4 and 12 s intervals between trains) and volitional movement (acoustically triggered by 50% MT stimuli). We show robust rCBF increases in motor and premotor areas due to rTMS, even at the lowest stimulation intensity of 100% MT. rCBF exhibited a linear positive dependency on stimulation intensity (for continuous 2 Hz rTMS) and the number of 10 Hz trains in the stimulated M1/S1 as well as in premotor and supplementary motor areas. Interestingly, the 2 different rTMS protocols yielded markedly different rCBF activation time courses, which did not correlate with the electromyographic recordings of the muscle responses. In future, this novel combination of TMS with ASL will offer the possibility to investigate the immediate and after-effects of rTMS stimulation on rCBF, which previously was only possible using PET.

© 2009 Elsevier Inc. All rights reserved.

Introduction

Up to now, two different imaging techniques have been used for assessing the effect of Transcranial Magnetic Stimulation (TMS) on brain metabolism in the stimulated cortex and in connected areas. The first approach combines TMS with positron emission tomography (PET) to measure changes in regional cerebral blood flow (rCBF using $H_2^{15}O$ PET; Paus et al., 1997; Siebner et al., 2001b; Speer et al., 2003) or regional cerebral metabolic rate of glucose (rCMRglc, [^{18}F]deoxyglucose PET; Siebner et al., 2001a, 1998) in order to characterize the immediate and after-effects of repetitive TMS (rTMS) protocols. PET offers high sensitivity and specificity and provides absolute measurements, allowing for direct comparisons between different scanning sessions and the assessment of longer lasting effects. However, PET imaging has low temporal resolution, limiting the experiments to block designs. Another major disadvantage of PET imaging is the subjects' exposure to radiation, which limits the number of measurements per subject.

The second technique combines TMS with blood oxygenation level-dependent echo planar imaging (BOLD EPI; Bestmann et al., 2004; Bohning et al., 2000), offering a better spatial and temporal resolution. However, the baseline value of the BOLD signal depends on scanning parameters (such as coil sensitivity, amplifier linearity, etc.)

that vary between experiments. As a consequence, the assessment of slow BOLD signal changes hinting towards modulatory rTMS effects and the comparison of absolute values in pre-post designs are not possible. As an alternative to BOLD imaging, TMS can be combined with arterial spin labeling (ASL) imaging. ASL provides a direct quantitative measure of perfusion (i.e., rCBF), thereby complementing the information offered by BOLD imaging in characterizing the brain responses to TMS stimulation. For example, this could help to remove the confounding effects of baseline perfusion changes on BOLD activity after different drug administrations. In ASL imaging, rCBF is assessed based on the subtraction of tag images in which an RF pulse is used to tag the inflowing blood from unaltered control images. Both types of images are acquired in an alternating sequence, so that image variations caused by scanner instabilities like field drifts or a subject motion effectively cancel out after subtraction, allowing the acquisition of quantitative and constant signals during long-term measurements and even different sessions. This allows us to determine baseline perfusion values and measure rCBF quantitatively and, in turn, opens the possibility to assess both the immediate and the more long-term effects of rTMS stimulation on brain baseline state and activation. In contrast to PET imaging, the subjects are not exposed to radiation and the spatial and temporal resolutions are in the range of normal fMRI experiments.

The aim of the present study was to demonstrate, for the first time, the technical feasibility to interleave TMS with multi slice continuous ASL (CASL) imaging. Combined TMS–PET studies have previously shown that periods of continuous rTMS and periods of short successive

* Corresponding author. Max Planck Institute for Biological Cybernetics, Spemannstraße 41 D-72076 Tübingen, Germany. Fax: +49 7071 601702.

E-mail address: axel.thielscher@tuebingen.mpg.de (A. Thielscher).

rTMS trains act differently onto rCBF in motor and premotor regions: rCBF was positively correlated with stimulation intensity for continuous 1 Hz rTMS (Speer et al., 2003), while it was negatively correlated with the number of 10 Hz rTMS trains (Paus et al., 1998). Here, two different rTMS protocols (continuous 2 Hz rTMS and 10 Hz trains) were applied to the motor cortex in 10 subjects while acquiring CASL images. We directly compared the rCBF time courses in response to these protocols, thereby capitalizing on the higher temporal resolution of CASL compared to PET imaging. We show that the sensitivity of CASL is high enough to robustly detect rCBF increases due to rTMS stimulation in motor and premotor areas, even at a moderate stimulation intensity of 100% motor threshold (MT). In contrast to the findings of Paus et al. (1998), rCBF in these areas correlated positively both with stimulation intensity (continuous 2 Hz rTMS) and the number of 10 Hz trains. Interestingly, the two rTMS protocols yielded markedly different rCBF time courses, which did not correlate with the amplitudes of the peripheral muscle responses. In future studies, the novel combination of TMS with ASL proves to be a promising tool for investigating the effects of rTMS on rCBF, in particular for longer rTMS protocols, which was previously only possible using PET.

Methods

General procedures

Ten right-handed healthy subjects (5 females; mean age \pm SD: 26.3 \pm 3.0 years) with no history of neurological disorders were included in the study. Informed written consent was obtained for each subject prior to the first experiment. The study was approved by the local ethics committee of the Medical Faculty of the University of Tübingen.

A high-resolution structural image was acquired once for each subject which was used for subsequent neuronavigation (MPRAGE, 192 sagittal slices, matrix size = 256 \times 256, voxel size = 1 mm³, TR/TE/TI = 1900/2.26/900 ms, 12-channel head coil, 3T Siemens TIM Trio). Each subject then participated in a session outside the MR scanner in which the optimal TMS coil position (“Hot Spot”) to stimulate a particular finger muscle (right abductor pollicis brevis; APB) was determined and saved using a neuronavigation system (BrainView, Fraunhofer IPA, Stuttgart, Germany). Subsequently, two sessions of interleaved TMS/CASL imaging were performed. In the MR scanner, the TMS coil was positioned over the “Hot Spot” using a method previously described (Moisa et al., 2009) and the motor threshold (MT) was determined using electromyographical (EMG) recordings (details are given in the next section). As outlined below, two different rTMS protocols were then tested in several experimental runs. In a final session, again outside the scanner, the time courses of the motor evoked potentials in response to the different rTMS protocols were recorded.

Interleaved TMS/CASL: data acquisition

Scanning was performed on a 3T Siemens TIM Trio (Siemens AG, Erlangen, Germany) with a one-channel RF transmit/receive head coil (model PN 2414895; USA Instruments, Aurora, CO, USA). The subjects were told to keep their eyes open and their right hand relaxed throughout the experiment. After positioning the TMS coil over the “Hot Spot”, the motor threshold was determined using muscle evoked potentials (MEP) recorded from the right APB inside the MRI scanner by means of a MR-compatible EEG amplifier (BrainAmp MR plus, Brain Products, Germany) and 3 Ag/AgCl pin electrodes. MEP responses were assessed as peak-to-peak amplitudes in time windows from 15 to 40 ms after the magnetic pulses. The resting motor threshold (MT) determined as the lowest TMS intensity eliciting MEP responses of >50 μ V in at least 5 out of 10 trials. Movements of the electrodes within the B₀-field of the scanner due to the TMS-induced muscle twitches resulted in signal variations similar to ballistocardiogram artifacts seen in EEG recordings. These artifacts were generally small

at lower stimulation intensities close to MT and delayed in time compared to the MEP response, allowing us to assess reliable peak-to-peak amplitudes. While using EMG recordings for assessing the MT, we decided not to apply them during the interleaved TMS/CASL measurements as the latter would have required additional methodological development.

In the interleaved TMS/CASL experiments, three different experimental conditions were tested: Continuous 2 Hz rTMS, short 10 Hz rTMS trains and volitional movement. In total, 16 experimental runs were conducted in 2 sessions. The order of conditions was counter-balanced between sessions and between subjects. Each run consisted of 8 blocks of rTMS stimulation, each block consisting of 24 s of rTMS followed by 52 s of rest. Continuous 2 Hz rTMS was tested at three different stimulation intensities, corresponding to 100%, 110% and 120% MT (2 runs per intensity). The 10 Hz rTMS trains consisted of 8 pulses which were separated by 100 ms and delivered at 110% MT. Three different inter-train intervals were investigated: 2, 4 and 12 s corresponding to 12, 6 and 2 trains, respectively, per stimulation block. Two runs were acquired per inter-train interval. Finally, 4 experimental runs (2 in each session) were performed with volitional movement which was acoustically triggered by TMS coil clicks at an intensity of 50% MT, using the protocol for continuous 2 Hz stimulation. Biphasic magnetic stimuli were delivered by a MagPro X100 stimulator (MagVenture, Denmark) with an MR-compatible figure-8 coil (MRI-B88).

An in-house written CASL sequence with EPI readout (2D gradient-echo echo planar imaging) and separate RF coils placed on the subject neck for labeling the inflowing blood in the right and left carotid was used (Zaharchuk et al., 1999; Zhang et al., 1995). Each experimental run contained 158 volumes (79 pairs of control – tag images; imaging parameters: matrix size = 64 \times 64, voxel size = 3 \times 3 \times 4 mm³, 0.5 mm gap, TR/TE = 4000/20 ms, bandwidth = 2442 Hz/pixel, tag duration/delay = 2689/810 ms for 2 Hz stimulation and volitional movement, 2737/820 ms for 10 Hz trains, tag gradient strength 2.0 mT/m). One volume consisted of 8 slices covering the motor and premotor areas and was acquired in ascending order, parallel to the inferior border of rostral and splenial parts of the corpus callosum. In this way, the slice orientation was roughly aligned across subjects to minimize the spatial information loss in the group analysis. Before each functional scan, a control magnitude image used for the rCBF quantification was acquired (6 volumes; TR = 8 s; no labeling and saturation pulses were used, all other parameters were kept the same as for the functional images). Additionally, in the first session, a whole-brain EPI was acquired once that was used for image registration during post-processing (32 slices, matrix size = 64 \times 64, voxel size = 3 \times 3 \times 4 mm³, 0.5 mm gap, TR/TE = 1600/20 ms, bandwidth = 2442 Hz/pixel).

TMS was interleaved with the CASL imaging by applying the magnetic pulses during the tag delay (leaving pauses of at least 100 ms to the next EPI readout; Bestmann et al., 2003a) or directly after the EPI readout before CASL tagging started again. Additionally, short temporal gaps of 20 ms were introduced during the tagging to apply further TMS pulses. These gaps were kept throughout the experimental run to keep the tagging identical between stimulation blocks and rest periods. The temporal distribution of TMS with respect to the acquisition of a CASL volume is shown in Figs. 1B and C for continuous 2 Hz rTMS and 10 Hz rTMS trains, respectively. A schematic diagram of the setup used for interleaving the TMS pulses with the CASL imaging is depicted in Fig. 1A. The MR scanner controlled the timing of the CASL tagging phases and sent triggers indicating the start of a volume to an additional control computer. Custom-written software on this computer triggered the TMS pulses and inhibited the CASL tagging in temporal windows (5 ms pre to 15 ms post) around the pulses. More details on the interleaved TMS/CASL setup, including a quantification of the field distortions by the TMS coil and tests of the image quality based on an agar phantom, can be found in the [Supplementary material](#).

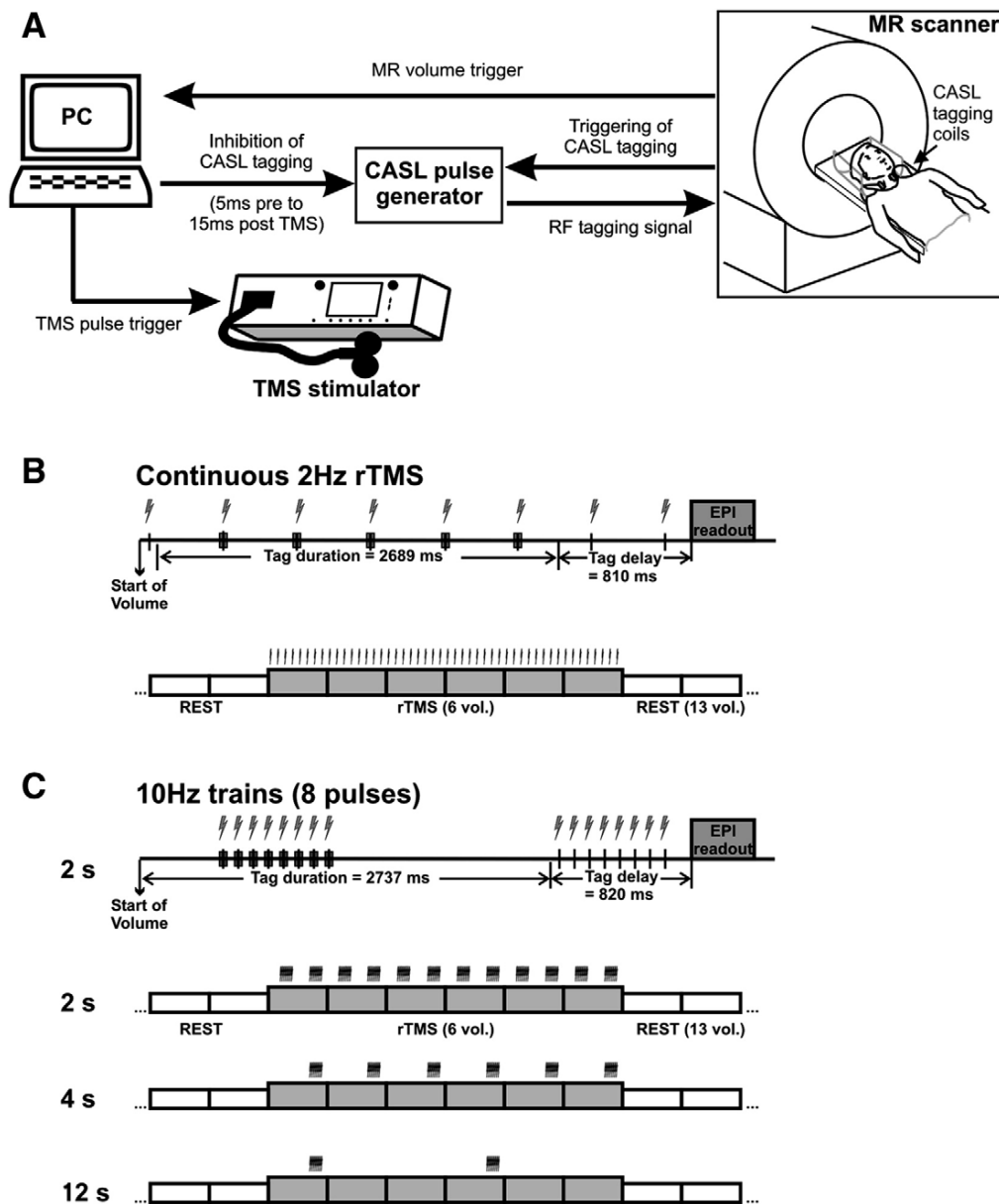


Fig. 1. (A) Schematic diagram of the combined TMS/CASL setup. (B) Relative timing of interleaved 2 Hz rTMS stimulation and CASL volume acquisition. The upper row shows how TMS was interleaved with the acquisition of a single image volume. The second row depicts the temporal distribution of the TMS stimuli within a stimulation block of 6 volumes. (C) Relative timing for interleaving CASL volume acquisition with 10 Hz rTMS trains. The top row shows the distribution of the TMS stimuli within one image volume for an interval of 2 s between rTMS trains. In the next three rows, the distribution of the rTMS trains in a stimulation block of 6 volumes is visualized for the different inter-train intervals. For 10 Hz trains at 4 s intervals (third row), the first train of 8 pulses was skipped so that no gaps had to be introduced during RF tagging. For 10 Hz trains at 12 s intervals (fourth row), one volume containing an rTMS train was followed by two volumes without TMS.

Interleaved TMS/CASL: data analysis

Data preprocessing and analysis were carried out using FSL4.0 (FMRIB, Oxford University, Oxford, UK). The first two volumes of each run were excluded to allow brain tissue to reach steady state magnetization. After visual inspection of the raw images for putative TMS-related artifacts, they were motion corrected, registered to the whole-brain EPI, temporally high-pass filtered (152 s cut-off) and spatially smoothed (Gaussian with 5 mm full-width at half-maximum). For each run, the combined perfusion and BOLD signal was modeled using three regressors (see www.fmrib.ox.ac.uk/fsl/feat5/perfusion.html for details): An alternating intensity variation of constant height between control and tag images was used to model

the perfusion baseline. BOLD activation was modeled as the convolution of the block design pattern (24 s stimulation – 52 s rest, repeated 8 times) with a standard hemodynamic response function (HRF; blue curve in Fig. 2B). Perfusion activation was modeled as the multiplication of the regressors for the baseline and the BOLD signal, thereby implicitly assuming that the stimulus-related perfusion changes have a similar time course as the BOLD signal. The condition using 10 Hz rTMS trains with 12 s gaps in-between was analyzed twice with two different regressor shapes: First, in order to assess the regions activated by this condition, an optimal regressor modeling the two rTMS trains at the beginning and in the middle of the stimulation block with a 12 s gap in-between was used (red curve in Fig. 2A). Second, the original regressor (blue curve in Fig. 2B) that equally

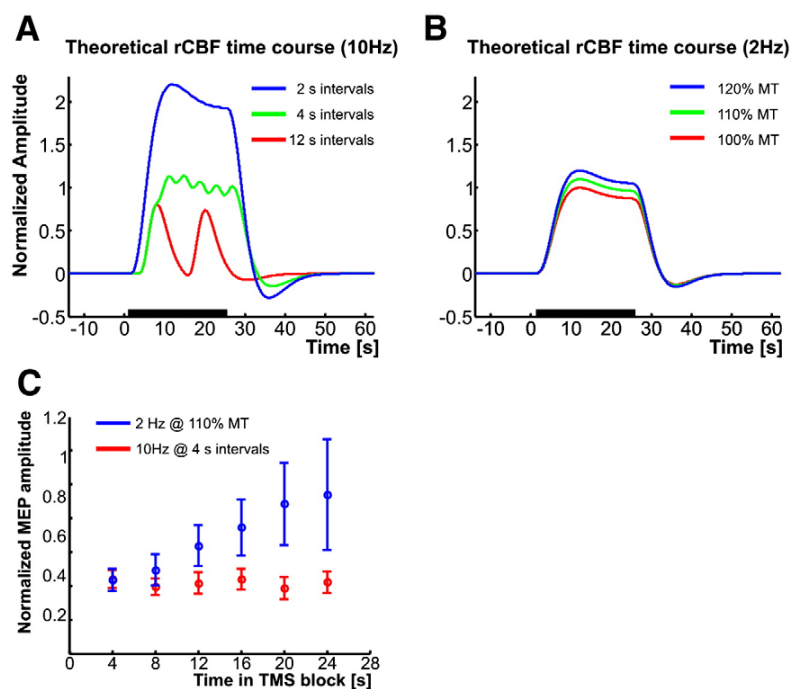


Fig. 2. Theoretical rCBF time courses for stimulation with 10 Hz trains (A) and continuous 2 Hz (B). The signals were normalized to the maximum of the time course for 2 Hz stimulation at 100% MT. The time courses were created by convolution of a stick function indicating the time points of the TMS pulses with a canonical HRF response. They indicate how rCBF would behave if it scaled perfectly linearly with the number of pulses and stimulation intensity. The horizontal black bars on the x-axes indicate the stimulation period. (C) Variation of the MEP amplitude along the stimulation period. The amplitudes were normalized to the mean of all TMS test pulses applied before, after and in between the stimulation blocks and averaged across successive 4 s intervals (corresponding to the TR of one CASL volume).

weighted the 24 s of stimulation was applied to be able to compare the average rCBF change during the stimulation period with the changes caused by other conditions. While the results of the first analysis were used when compiling group activation maps, the results of the second analysis were used for a linear regression analysis to compare the rCBF changes across rTMS conditions (see below).

Analysis started by estimating separate general linear models for each experimental run in every subject. The two runs corresponding to the same rTMS condition (and the four runs for volitional movement) were then combined in each subject using a fixed-effects analysis. At this stage, data from two subjects were excluded from further analysis due to low signal-to-noise ratios of the rCBF values (both for rCBF baseline and activation), possibly caused by poor labeling of the inflowing blood by the two RF tagging coils. In order to create group results, the maps of the individual parameter estimates of the remaining 8 subjects were normalized to MNI space by first registering the whole-brain EPI to the T1-weighted anatomical image and then the anatomical image to the MNI template. The normalized individual maps of parameter estimates were fed into a second-level mixed-effects analysis with experimental conditions and subjects as fixed and random factors, respectively. An F -test pooling across all six rTMS conditions was applied to identify regions exhibiting robust TMS-related rCBF changes ($z=2.3$ at voxel level and $p=0.05$ corrected at cluster level). This initial analysis was used to constrain the search space in the subsequent analysis to voxels showing robust rCBF increases in response to rTMS and thus address the multiple-comparisons problem. Further general F -tests were applied to estimate rTMS-related BOLD activations ($z=3.1$ at voxel level and $p=0.05$ corrected at cluster level) and group rCBF changes due to volitional movement (same threshold level as used for rTMS-related rCBF changes).

In order to identify regions exhibiting parametrical changes in rCBF with increasing stimulation intensity (continuous 2 Hz rTMS) and increasing number of trains (10 Hz rTMS), respectively, two linear regression analyses were conducted on the group level. The resulting

maps were thresholded at $p=0.05$ uncorrected and intersected with the general rCBF activation as determined by the initial F -test.

Further analyses were conducted for 2 of the conditions, namely continuous 2 Hz rTMS and 10 Hz rTMS trains with 4 s intervals, both at 110% MT. Since the stimulation intensity and the number of pulses were matched between both conditions, we wanted to determine the amount of similarity in the rCBF changes. The rCBF activations were compared using a paired T -test on the group level ($p=0.05$ uncorrected). Additionally, in order to determine whether the two rTMS protocols affected rCBF differently during the first versus the second half of the stimulation period, the analysis was repeated using first-level models with separate regressors for the two halves of the stimulation block (regressors for the first and last 12 s, respectively, both convolved with a standard HRF). For each of the two rTMS protocols, the rCBF increases were compared between two halves of the stimulation block using paired T -tests on the group level ($p=0.05$ uncorrected). Additionally, we tested for differences in rCBF activation between the two rTMS protocols, for each of the two halves of the stimulation block separately (paired T -tests; $p=0.05$ uncorrected).

rCBF time courses

The perfusion time courses elicited by the different stimulation conditions were compared in eight regions of interest (ROIs) corresponding to motor and premotor areas. In each subject, the ROIs were first defined based on the individual anatomy. The primary sensorimotor areas (MI/SI) were defined as the parts of the anterior and posterior bank of the central sulcus located around the hand knob (Yousry et al., 1997). The medial portions of the dorsal premotor areas (PMd) were determined using the junction of the superior precentral sulcus with the superior frontal sulcus, and the more lateral parts of the superior precentral sulcus were defined as lateral PMd (Tomassini et al., 2007). The supplementary motor area (SMA) was defined as being located medially between the medial portions of the superior frontal gyri,

anterior to the precentral gyrus (comprising the pre-SMA and SMA subdivisions; Picard and Strick, 2001). The cingulate motor area (CMA) was defined as the region inferior to the SMA lying within the cingulate sulcus (Picard and Strick, 2001). We were specifically interested whether the rCBF time courses differed between continuous 2 Hz rTMS and 10 Hz rTMS trains, thereby only considering those parts of the ROIs that generally responded to rTMS stimulation. Therefore, secondly, an individual rCBF activation map was derived for the complete image volume using an *F*-test pooling across all rTMS conditions ($p=0.05$ uncorrected, fixed-effects analysis) and the anatomical ROIs were intersected with the individual CBF activation map to restrict the ROIs to voxels exhibiting significant rCBF changes due to rTMS stimulation. For ROIs in which none of the voxels was significant on the single-subject level, the rTMS group activation map was used for intersection. As exception, the ROIs for the M1/S1 region contralateral to the stimulation site were solely based on anatomy as, when pooling across all rTMS conditions, this region did not exhibit significant rCBF changes, neither on the single-subject nor on the group level. For each subject, the mean rCBF signal change was averaged across all significant voxels in the defined ROIs and across stimulation blocks. The mean of the last four time points before the rTMS period was used as baseline. Finally, the time courses were averaged across subjects.

Quantification of rCBF

In order to test whether the absolute values of the measured rCBF were in the expected range, quantification of the baseline blood flow was performed for the eight ROIs defined above. The following

equation from Wang et al. (2005) was used that assumes that the labeled blood spins remain primarily in the vasculature rather than exchanging completely with tissue water:

$$rCBF = \lambda R_{1a} \frac{\Delta M}{M_{con} F} \tag{1}$$

with $F = 2\alpha\{exp(-wR_{1a}) - exp[-(\tau + w)R_{1a}]\}$

Constant $\lambda = 0.9$ mL/g is the blood/tissue water partition coefficient and $R_{1a} = 0.67$ s⁻¹ is the longitudinal relaxation rate of blood. ΔM stands for the mean CASL perfusion image and was computed by pairwise subtraction of the control and labeled images and averaging across the last four time points before each rTMS stimulation period. M_{con} is the average control image intensity and was obtained by averaging the 6 EPI volumes acquired with a TR of 8 s before each functional run. The term w is the post labeling delay time and consists of a constant delay between the end of RF labeling and the start of the EPI readout (810 ms for continuous 2 Hz rTMS; 820 ms for 10 Hz trains; Figs. 1B and C) plus the time between EPI onset and the slice acquisition (0–306 ms for the 1st to 8th slices). w was adjusted for each ROI by using the slice acquisition time of the middle slice of the ROI. Constant τ stands for the duration of the labeling pulse. It is 2689 ms and 2737 ms for continuous 2 Hz and 10 Hz trains, respectively, when not taking the tagging gaps introduced for the TMS pulses into account. For continuous 2 Hz rTMS and 10 Hz rTMS with 2 s intervals between trains (Figs. 1B and C), the 20 ms gaps divided the original continuous tagging period in several successive short phases. We

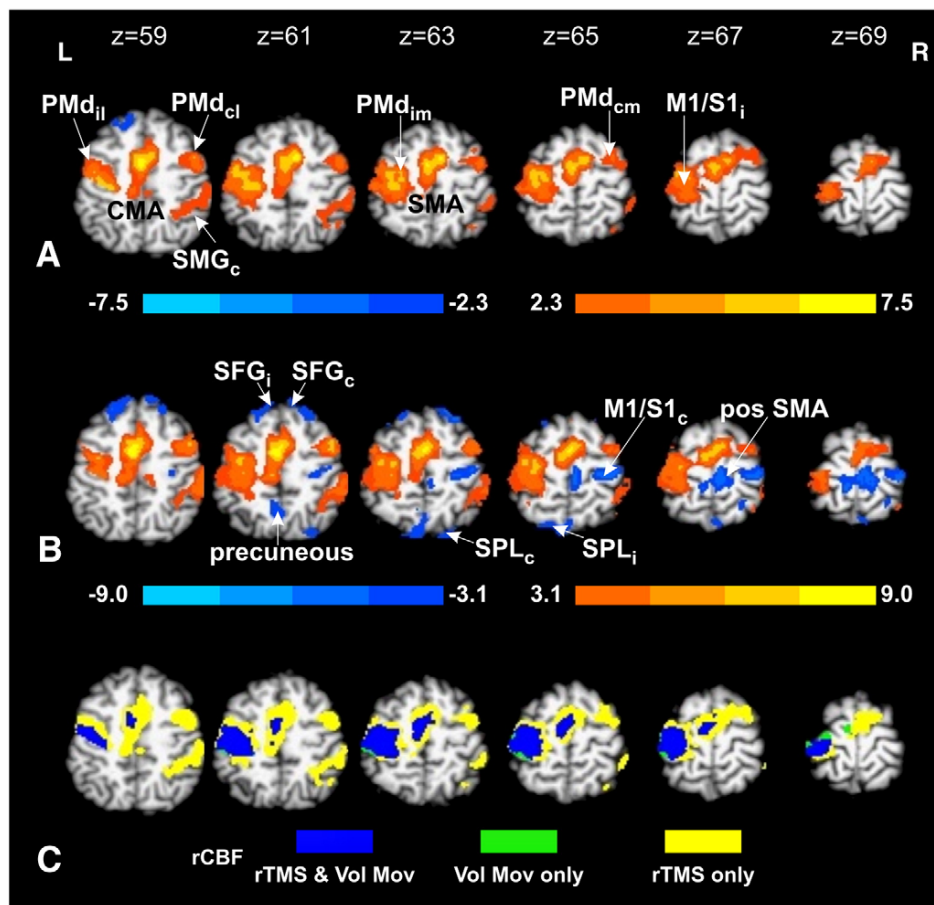


Fig. 3. Group activation maps for rCBF (A) and BOLD (B), pooled across all rTMS conditions and overlaid over an individual high-resolution anatomical image. (C) Overlap between the positive rCBF group activations for rTMS stimulation and volitional movement.

took this into account by replacing the original factor F in Eq. (1) by the sum

$$F = 2\alpha\{ \exp(-wR_{1d}) - \exp[-(w + d_n - 15 \text{ ms})R_{1d}] + \sum_{i=2}^n \{ \exp[-(w + d_i + 5 \text{ ms})R_{1d}] - \exp[-(w + d_{i-1} - 15 \text{ ms})R_{1d}] \} + \exp[-(w + d_1 + 5 \text{ ms})R_{1d}] - \exp[-(\tau + w)R_{1d}] \} \quad (2)$$

where n is the number of stimuli applied in the tagging phase ($n = 5$ for 2 Hz rTMS and $n = 8$ for 10 Hz trains with 2 s intervals) and d_i are the delays of the TMS pulses with respect to the end of the tagging phase. The labeling efficiency α quantifies the inversion of the magnetization of the inflowing blood. Since the inversion process is less efficient at the beginning and the end of RF labeling pulses, the 20 ms gaps during labeling might result in a reduced overall efficiency (i.e., a smaller α) and have to be taken account of when calculating α . For this, the adiabatic inversion process was simulated by Bloch-equation simulations: Using the realistic parameters of the experiment, the inversion was modeled using 50 μs steps (Pohmann et al., 2009). The computation was performed for continuous labeling, as well as including the gaps for continuous 2 Hz rTMS and 10 Hz rTMS with 2 s intervals between trains. The resulting α was then used when calculating factor F in Eq. (2). Comparison of the inverse $1/F$ between CASL acquisitions with and without gaps allowed us to determine the amount by which the gaps affect the quantification.

For each individual experimental run, the absolute baseline rCBF was computed in each of the previously defined 8 ROIs. In order to restrict the calculation to gray matter voxels, the individual map of the

baseline perfusion activation was thresholded and used as mask ($Z = 12$ in 6 subjects; $Z = 9$ in 2 subjects). Subsequently, for each ROI the absolute baseline rCBF was averaged across all runs and subjects.

EMG data recording and analysis

In the TMS lab, the time courses of the motor evoked potentials (MEPs) were investigated for two of the rTMS protocols, namely continuous 2 Hz rTMS and 10 Hz rTMS trains with 4 s intervals (both at 110% MT; same protocol as used inside the scanner). Twenty test pulses were applied before the first stimulation block and again after the last block (pulse interval: 8 s). Additionally, six test pulses (8 s spacing) were applied between each two successive stimulation blocks, resulting in altogether 82 test pulses. MEPs were recorded from the right APB muscle and quantified as peak-to-peak amplitudes. The MEP amplitudes were first normalized to the mean of the 82 test pulses. Subsequently, in order to compare the MEPs with the rCBF time courses, the rTMS blocks were divided in 4 s time intervals (corresponding to the TR of one CASL volume) and the amplitudes were averaged across these intervals. Finally, averaging across blocks and across subjects was performed.

Results

Imaging results

The rTMS stimulation elicited robust rCBF (Fig. 3A) and BOLD signal (Fig. 3B) increases in motor and premotor areas: stimulated primary sensorimotor area (M1/S1₁), cingulate and supplementary motor areas

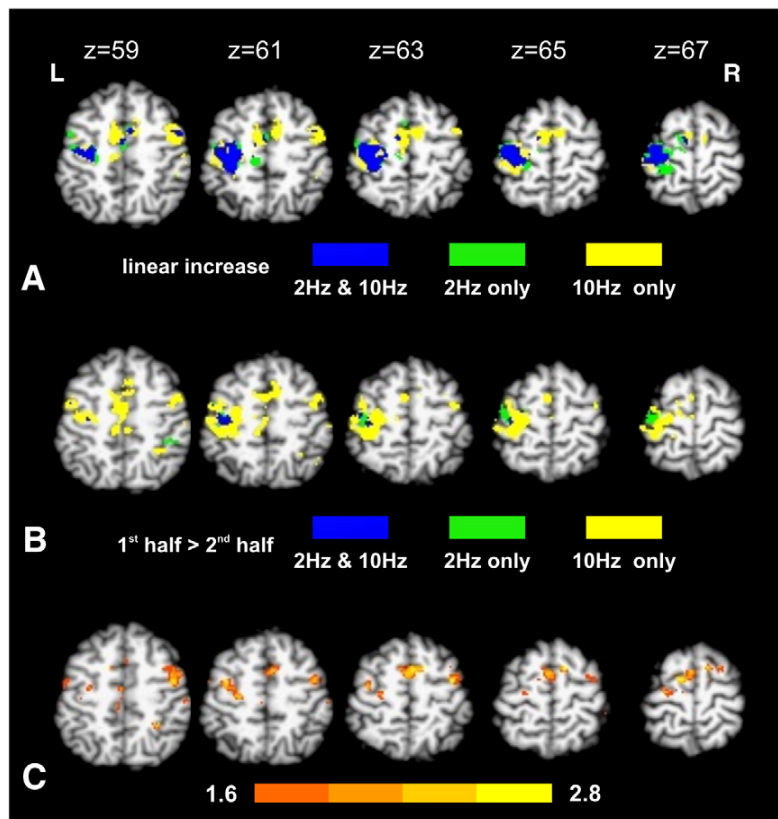


Fig. 4. (A) Regions exhibiting increasing rCBF with increasing stimulation intensity for continuous 2 Hz rTMS (green), with increasing number of trains for 10 Hz rTMS (yellow), and overlap between both (blue). (B) Regions with higher rCBF in the first half compared to the second half of stimulation for 2 Hz rTMS at 110% MT (green), for 10 Hz trains with 4 s intervals (yellow), and overlap between both (blue). (C) Analysis of the second half of stimulation for continuous 2 Hz rTMS and for 10 Hz trains at 4 s intervals (both at 110% MT). The shown regions exhibit higher rCBF for 2 Hz rTMS than for 10 Hz trains.

(CMA, SMA), as well as medial (PMd_{im}, PMd_{cm}) and lateral (PMd_{il}, PMd_{cl}) parts of the bilateral dorsal premotor areas. As can be seen from Figs. 3A and B, the positive group rCBF and BOLD activations largely

overlap. The overlap between the rCBF increases due to rTMS stimulation and volitional movement, respectively, is shown in Fig. 3C. The activation clusters for volitional movement overlap well

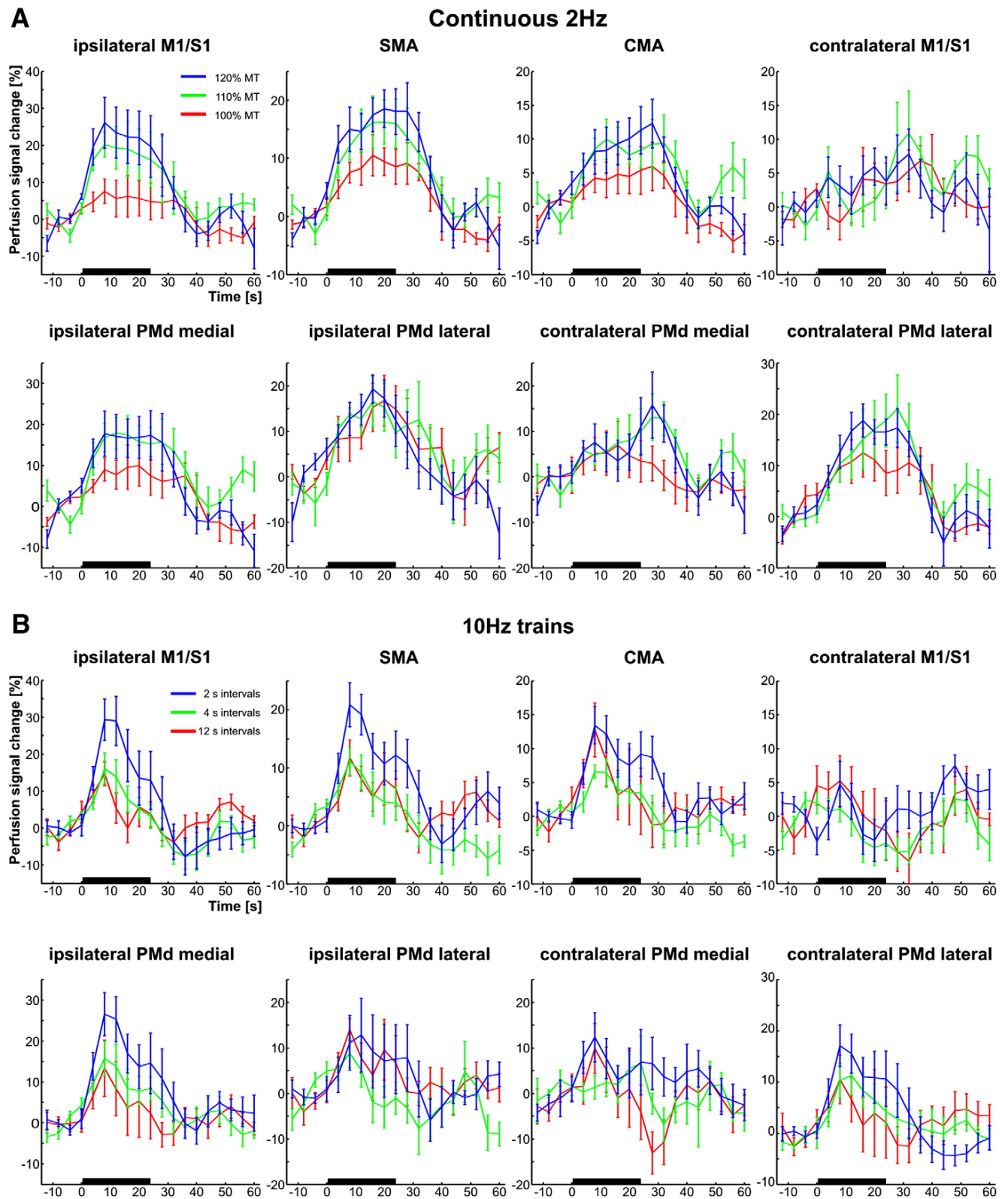


Fig. 5. Mean perfusion time courses (\pm SE) in 8 ROIs for continuous 2 Hz rTMS (A) and for 10 Hz rTMS trains (B). The time courses were normalized to the baseline rCBF determined from the last four volumes before the TMS stimulation period.

Table 1

	CMA	SMA	M1/S1 contra	PM _{dm} contra	PM _{d1} contra	PM _{d1} ipsi	PM _{dm} ipsi	M1/S1 ipsi
Mean ± SE (mL/100 g/min)	76.286 ± 3.297	73.742 ± 3.869	65.964 ± 2.504	69.704 ± 4.530	72.366 ± 2.917	69.558 ± 4.387	63.524 ± 3.357	62.149 ± 3.061

Absolute baseline rCBF values (± SE) in the 8 ROIs.

with those due to rTMS stimulation, but are smaller in extent and are restricted to the ipsilateral M1/S1, ipsilateral PMd, CMA and SMA.

A significant rCBF decrease was observed in the superior frontal gyrus ipsilateral to the TMS coil (SFG_i in Fig. 3A), while BOLD signal decreases occurred in a more widespread network (Fig. 3B; M1/S1 contralateral to coil, posterior SMA, bilateral SFG, posterior part of bilateral superior parietal lobe, precuneus). Inspection of the BOLD signal time courses for the regions being at the rim of the brain (bilateral SFG and SPL) revealed smooth time courses without any hints towards the deactivations being, e.g. driven by putative motion artifacts. For some of the rTMS conditions considered in isolation, an rCBF decrease in the contralateral M1/S1 as well as in other areas exhibiting BOLD signal decreases could be observed (Fig. S.2 in the Supplementary material).

Fig. 4A shows regions exhibiting increasing rCBF with increasing number of trains (10 Hz rTMS; yellow and blue areas) and increasing stimulation intensity (continuous 2 Hz rTMS; green and blue areas), respectively. A positive relationship between the number of 10 Hz trains and rCBF was observed in most of the areas that showed general rCBF activations due to rTMS stimulation (see Fig. 3A). For 2 Hz stimulation, increasing rCBF with increasing stimulation intensity occurred only in the stimulated M1/S1 and, to a lesser extent, in CMA, the medial part of the ipsilateral PMd and the lateral part of the contralateral PMd.

The relative rCBF signal change obtained from 8 ROIs is illustrated in Figs. 5A and B for all six stimulation conditions. For 10 Hz rTMS trains, the time courses consistently show a clear-cut peak at the beginning of the stimulation period and then fall off. In contrast, the rCBF increase is rather constant during continuous 2 Hz stimulation (see Fig. S.3 for the BOLD time courses determined from a subset of the ROIs). This difference was formerly tested for two of the stimulation protocols, namely continuous 2 Hz rTMS and 10 Hz rTMS trains with 4 s intervals, both at 110% MT. The data was reanalyzed using separate regressors for the first and second halves of the stimulation and the two halves compared on the group level (Fig. 4B). For 10 Hz trains, most of the affected motor and premotor regions were more strongly activated during the first half compared to the second half of stimulation (yellow and blue areas in Fig. 4B). In contrast, for 2 Hz rTMS, higher rCBF values during the first half were almost completely restricted to the directly stimulated M1/S1 (blue and green areas). None of the regions exhibited the opposite effect, i.e. stronger activation during the second rather the first half of stimulation. When directly comparing the second halves of stimulation between both rTMS protocols, many regions were more active during continuous 2 Hz stimulation than for 10 Hz trains (Fig. 4C), despite the same number of stimuli applied at the same intensity. No significant differences in rCBF activation strength could be observed for the first halves.

rCBF quantification

The simulations indicate that the labeling efficiency α (see Eq. 1) was only negligibly affected by the 20 ms gaps introduced in the tagging phases: α is 0.937 for conditions without gaps (i.e., 10 Hz trains with 4 and 12 s intervals) and is reduced to 0.925 and 0.919 when introducing 5 gaps for 2 Hz stimulation and 8 gaps for 10 Hz trains at 2 s intervals, respectively. The inverse $1/F$ that describes the dependency of absolute rCBF on both tagging duration and labeling efficiency, was mildly reduced from 0.90 to 0.86 (2 Hz condition) and 0.85 (10 Hz trains at 2 s intervals), respectively. In other words, ignoring the gaps during quantification would have resulted in a relative error of around 6%. The mean baseline perfusion values in the 8 ROIs are summarized in Table 1.

MEP time courses

The mean MEP amplitudes, averaged across successive 4 s intervals of the stimulation block, are shown in Fig. 2C for continuous 2 Hz stimulation (blue lines) and 10 Hz trains with 4 s intervals (red lines), respectively, both at 110% MT. The MEPs for 2 Hz stimulation show an increasing trend ($p = 0.165$, paired *T*-test across subjects between the first 4 s and the last 4 s in the stimulation block) while the MEPs in response to 10 Hz trains were constant throughout the stimulation period.

Discussion

We found robust rCBF changes in response to rTMS stimulation, measured by simultaneous ASL imaging, thereby demonstrating the feasibility of this new combination. The observed spatial activation patterns are in concordance with the results of previous motor cortex studies (Bestmann et al., 2004; Bohning et al., 2003; Fox et al., 1997; Siebner et al., 2001a), showing significant rCBF increases due to rTMS in motor and premotor areas. Additionally, the positive rCBF activation clusters overlap well with the positive BOLD activation as well as with the rCBF increases due to volitional movement. The activation clusters due to volitional movement were generally smaller than those due to rTMS and did not involve regions in the right hemisphere. This was probably caused by the employed behavioral task (simple finger tapping instead of, e.g. sequential finger movements). The absolute values for the baseline rCBF are in the same range as previously reported values (Calamante et al., 1999; Yang et al., 2000; Yongbi et al., 2002), serving as further validation of our novel TMS-CASL combination. As a side note, the gaps introduced during tagging affected the quantification results only mildly. Ignoring them in order to simplify the quantification procedure would therefore cause only small deviations around 6% in the absolute rCBF values.

The regions exhibiting BOLD signal decreases in response to rTMS correspond with previously reported areas showing rCBF and BOLD signal decreases in response to magnetic stimulation (Bestmann et al., 2003b, 2004; Speer et al., 2003). While in our case only one region (SFG_i in Fig. 3A) showed significant rCBF decreases when pooling across all rTMS conditions, additional regions (in particular M1/S1 contralateral to the coil) could be observed for some of the conditions considered in isolation (Fig. S.2 in the Supplementary material). The higher number of regions with deactivations only in the BOLD map but not in the rCBF map was therefore probably caused by the lower SNR of the rCBF measurements.

For continuous 2 Hz rTMS, significant rCBF increases with increasing stimulation intensity were mainly restricted to the stimulated M1/S1, ipsilateral PMd, and small parts of CMA/SMA, but did not extend to regions contralateral to the coil. This is in concordance with the findings of previous combined TMS-PET (Fox et al., 2006; Speer et al., 2003) and interleaved TMS-fMRI studies (Bestmann et al., 2004). This might in part be due to the SNR of PET and CASL being too low to detect moderate rCBF increases in the other areas. When assuming that rCBF depends linearly on the number of pulses and stimulation intensity, then the theoretical rCBF increase due to higher TMS intensities is rather moderate compared to, e.g. the effect of doubling the number of pulses (Figs. 2A and B). Changing the number of TMS pulses might therefore be more powerful to induce clear-cut parametric changes in rCBF. The MEP time courses show a trend towards increased amplitudes at the end of the stimulation blocks for continuous 2 Hz rTMS. This seems to be mirrored by similar tendencies in the rCBF time courses in some of the areas (e.g., CMA, lateral part of PMd ipsilateral to coil; Fig. 5A). Importantly, however,

the time courses for rCBF and MEPs, respectively, do not show such a dissociation for continuous 2 Hz rTMS than for 10 Hz trains.

In contrast to previous PET results (Paus et al., 1998), we found linear increases in rCBF with increasing number of trains for the stimulation with 10 Hz rTMS trains. In fact, Paus et al. (1998) observed negative rCBF in M1/S1 when spacing the trains at 2 s intervals, while this condition yielded the highest rCBF values in our case. This discrepancy probably arises from the fact that we used supra- rather than sub-MT stimulation and applied shorter stimulation periods (24 s instead of 60 s). In particular, supra-MT stimulation induces sensory feedback due to muscle twitches which is likely to increase rather than decrease rCBF in motor and premotor areas. In case of M1, this is possibly also due to the partial voluming of this area with the somatosensory cortex. Thus, in our case, enhancing the number of rTMS trains might have enhanced rCBF in these areas by inducing additional sensory feedback. We did, however, observe a significant decrease in rCBF amplitude in the second part of the stimulation in many regions, consistently across all stimulations with 10 Hz trains (Fig. 4C). As the MEP amplitudes for 10 Hz trains did not show a similar decrease, this particular change in rCBF cannot be explained by changes in sensory feedback and might therefore hint towards the slow build-up of a cortical inhibitory component. Since the PET results reported by Paus et al. (1998) are based on the summation of rTMS effects across 60 s, it might be that the inhibitory overcomes the excitatory effect for extended stimulation periods. This might lead to an overall negative net effect, in particular in the absence of activity related to sensory feedback. Support for this hypothesis comes from a study in which short high-frequency trains (6 Hz, 10 s inter-train interval) were applied to the primary visual cortex of the cat while recording from single cells in the dorsal lateral geniculate nucleus (de Labra et al., 2007). The repeated TMS trains led to a successive reduction of both the spontaneous spiking activity and the responses to visual stimulation, and this effect remained for a few minutes even after TMS stopped. Interestingly, mainly tonic activity but not spike bursts was affected by TMS. This might explain why in our case dissociations between MEPs (which are elicited by rather short-term bursts of activity) and rCBF (averaging across both bursts and the tonic activity in the inter-train intervals) were observed. Clearly, this interpretation has to be considered with caution, as the study of de Labra et al. (2007) was conducted in anaesthetized animals, thereby targeting a different brain area than done here.

To summarize, we present the first study showing the feasibility of interleaving rTMS stimulation with CASL imaging. In contrast to combining TMS with PET, this novel combination offers a better temporal and spatial resolution and does not utilize radiation. Given the lower SNR of ASL compared to PET, we were rather cautious concerning the lowest stimulation intensity tested and the length of the employed rTMS blocks. However, our results demonstrate that the sensitivity of the employed CASL method was good enough to detect rCBF changes already at relatively low TMS intensities of 100% motor threshold (i.e., just eliciting finger twitches). This opens the possibility to investigate rCBF responses to sub-threshold rTMS and longer stimulation periods, respectively, in future studies. In particular, as ASL allows the investigation of slow modulations of rCBF, this novel combination might become an interesting complement to interleaving TMS with normal BOLD EPI.

Acknowledgments

The authors would like to thank the Max Planck Society for financial support; AT was supported in part by the German Research Foundation (grant TH1330/2-1).

Appendix A. Supplementary data

Supplementary data associated with this article can be found, in the online version, at doi:10.1016/j.neuroimage.2009.07.010.

References

- Bestmann, S., Baudewig, J., Frahm, J., 2003a. On the synchronization of Transcranial Magnetic Stimulation and functional echo-planar imaging. *J. Magn. Reson. Imaging* 17, 309–316.
- Bestmann, S., Baudewig, J., Siebner, H.R., Rothwell, J.C., Frahm, J., 2003b. Subthreshold high-frequency TMS of human primary motor cortex modulates interconnected frontal motor areas as detected by interleaved fMRI-TMS. *NeuroImage* 20, 1685–1696.
- Bestmann, S., Baudewig, J., Siebner, H.R., Rothwell, J.C., Frahm, J., 2004. Functional MRI of the immediate impact of Transcranial Magnetic Stimulation on cortical and subcortical motor circuits. *Eur. J. Neurosci.* 19, 1950–1962.
- Bohning, D.E., Shastri, A., McGavin, L., McConnell, K.A., Nahas, Z., Lorberbaum, J.P., Roberts, D.R., George, M.S., 2000. Motor cortex brain activity induced by 1-Hz Transcranial Magnetic Stimulation is similar in location and level to that for volitional movement. *Invest. Radiol.* 35, 676–683.
- Bohning, D.E., Shastri, A., Lomarev, M.P., Lorberbaum, J.P., Nahas, Z., George, M.S., 2003. BOLD-fMRI response vs. Transcranial Magnetic Stimulation (TMS) pulse-train length: testing for linearity. *J. Magn. Reson. Imaging* 17, 279–290.
- Calamante, F., Thomas, D.L., Pell, G.S., Wiersma, J., Turner, R., 1999. Measuring cerebral blood flow using magnetic resonance imaging techniques. *J. Cereb. Blood Flow Metab.* 19, 701–735.
- de Labra, C., Rivadulla, C., Grieve, K., Marino, J., Espinosa, N., Cudeiro, J., 2007. Changes in visual responses in the feline dLGN: selective thalamic suppression induced by transcranial magnetic stimulation of V1. *Cereb. Cortex* 17, 1376–1385.
- Fox, P., Ingham, R., George, M.S., Mayberg, H., Ingham, J., Roby, J., Martin, C., Jerabek, P., 1997. Imaging human intra-cerebral connectivity by PET during TMS. *NeuroReport* 8, 2787–2791.
- Fox, P., Narayana, S., Tandon, N., Fox, S.P., Sandoval, H., Kochunov, P., Capaday, C., Lancaster, J.L., 2006. Intensity modulation of TMS-induced cortical excitation: primary motor cortex. *Hum. Brain Mapp.* 26, 478–487.
- Moisa, M., Pohmann, R., Ewald, L., Thielscher, A., 2009. New coil positioning method for interleaved Transcranial Magnetic Stimulation (TMS)/functional MRI (fMRI) and its validation in a motor cortex study. *JMRI* 29, 189–197.
- Paus, T., Jech, R., Thompson, C.J., Comeau, R., Peters, T., Evans, A.C., 1997. Transcranial Magnetic Stimulation during positron emission tomography: a new method for studying connectivity of the human cerebral cortex. *J. Neurosci.* 17, 3178–3184.
- Paus, T., Jech, R., Thompson, C.J., Comeau, R., Peters, T., Evans, A.C., 1998. Dose-dependent reduction of cerebral blood flow during rapid-rate transcranial magnetic stimulation of the human sensorimotor cortex. *J. Neurophysiol.* 79, 1102–1107.
- Picard, N., Strick, P.L., 2001. Imaging the premotor areas. *Curr. Opin. Neurobiol.* 11, 663–672.
- Pohmann, R., Budde, J., Auerbach, E., Adriany, G., Uğurbil, K., 2009. Theoretical and Experimental Comparison of Different Techniques for Continuous Arterial Spin Labeling. *ISMRM 2009*, Honolulu, Hawaii, p. #1515.
- Siebner, H.R., Willloch, F., Peller, M., Auer, C., Boecker, H., Conrad, B., Bartenstein, P., 1998. Imaging brain activation induced by long trains of repetitive Transcranial Magnetic Stimulation. *NeuroReport* 9, 943–948.
- Siebner, H.R., Peller, M., Bartenstein, P., Willloch, F., Rossmair, C., Schwaiger, M., Conrad, B., 2001a. Activation of frontal premotor areas during supratherreshold Transcranial Magnetic Stimulation of the left primary sensorimotor cortex: a glucose metabolic PET study. *Hum. Brain Mapp.* 12, 157–167.
- Siebner, H.R., Takano, B., Peinemann, A., Schwaiger, M., Conrad, B., Drzezga, A., 2001b. Continuous Transcranial Magnetic Stimulation during positron emission tomography: a suitable tool for imaging regional excitability of the human cortex. *NeuroImage* 14, 883–890.
- Speer, A.M., Willis, M.W., Herscovitch, P., Daube-Witherspoon, M., Shelton, J.R., Benson, B.E., Post, R.M., Wassermann, E.M., 2003. Intensity-dependent regional cerebral blood flow during 1-Hz repetitive Transcranial Magnetic Stimulation (rTMS) in healthy volunteers studied with H215O positron emission tomography: I. Effects of primary motor cortex rTMS. *Biol. Psychiatry* 54, 818–825.
- Tomassini, V., Jbabdi, S., Klein, J., Behrens, T., Pozzilli, C., Matthews, P., Rushworth, M., Johansen-Berg, H., 2007. Diffusion-weighted imaging tractography-based parcellation of the human lateral premotor cortex identifies dorsal and ventral subregions with anatomical and functional specializations. *J. Neurosci.* 27, 10259–10269.
- Wang, J., Zhang, Y., Wolf, R.L., Roc, A.C., Alsop, D.C., Detre, J.A., 2005. Amplitude-modulated continuous arterial spin-labeling 3.0-T perfusion MR imaging with a single coil: feasibility study. *Radiology* 235, 218–228.
- Yang, Y., Engelien, W., Xu, S., Gu, H., Silbersweig, D.A., Stern, E., 2000. Transit time, trailing time, and cerebral blood flow during brain activation: measurement using multislice, pulsed spin-labeling perfusion imaging. *Magn. Reson. Med.* 44, 680–685.
- Yongbi, M.N., Fera, F., Yang, Y., Frank, J.A., Duyn, J.H., 2002. Pulsed arterial spin labeling: comparison of multislice baseline and functional MR imaging perfusion signal at 1.5 and 3.0 T: initial results in six subjects. *Radiology* 222, 569–575.
- Yousry, T.A., Schmid, U.D., Alkadhi, H., Schmidt, D., Peraud, A., Buettner, A., Winkler, P., 1997. Localization of the motor hand area to a knob on the precentral gyrus – a new landmark. *Brain* 120, 141–157.
- Zaharchuk, G., Ledden, P.J., Kwong, K.K., Reese, T.G., Rosen, B.R., Wald, L.L., 1999. Multislice perfusion and perfusion territory imaging in humans with separate label and image coils. *Magn. Reson. Med.* 41, 1093–1098.
- Zhang, W., Sliva, A.C., Williams, D.S., Koretsky, A.P., 1995. NMR measurement of perfusion using arterial spin labeling without saturation of macromolecular spins. *Magn. Reson. Imaging* 33, 370–376.

Moisa et al.

Interleaved TMS/CASL: Comparison of different rTMS protocols Supplementary Material

The interleaved TMS/fMRI setup consisted of a MagPro X100 stimulator with MagOption (MagVenture, Farum, Denmark) and an MR-compatible figure-8 coil (MRi-B88). To prevent the MR images from being affected by RF noise, the stimulator was placed outside the MR cabin and the coil was connected through a high-current filter (E-LMF-4071; ETS Lindgren, St. Louis, MO, USA) attached to the copper shielding of the cabin (Bohning et al., 2003). The effectiveness of the high-current filter in eliminating the RF noise caused by the stimulator was tested using the Siemens RF noise service sequence. The reliable positioning of the TMS coil over the motor cortex was achieved using a special coil-holding device in combination with in-house written software (Moisa et al., 2009).

Phantom Tests on CASL Image Quality

Measurements using a spherical phantom filled with agar gel were performed in order to assess the quality of the CASL images in the presence of TMS stimulation (Friedman and Glover, 2006). Four runs were performed using a procedure previously described (Moisa et al., 2009): without TMS coil, with the coil attached to the phantom but not connected to the stimulator, with continuous 2 Hz rTMS, and with 10Hz rTMS trains (both at 100% stimulator output). The CASL parameters as well as the stimulation protocols were identical to those used in the motor cortex study. For each CASL slice, the mean across volumes was determined to check for static signal dropout and distortions. The mean images showed no signal drop out and only moderate distortions in the first 3 slices at the rim of the phantom. This effect was static, caused by the abrupt susceptibility changes due to the presence of the TMS coil, and was also visible when assessing the effects of the coil without stimulation. Additionally, the signal-to-fluctuation-noise ratio (SFNR) was determined in order to check for putative temporal fluctuations in the EPI readout induced by the TMS stimulation. The SFNR values remained unchanged during rTMS (Fig. S.1E).

Leakage current inhibition

When switched on, TMS stimulators constantly induce very small leakage currents on the coil cable. In case of the MagPro X100, a current flow of 0.8 mA occurs between TMS pulses when it is set to 100% intensity. Weiskopf and colleagues (2009) showed that the EPI images can be subtly affected by these leakage currents. As the currents scale with output intensity, changing the TMS intensity between different experimental conditions can systematically bias the acquired EPIs. This effect can in turn result in false-negative or false-positive activations. In order to prevent these effects, a circuit to suppress the leakage currents was added to the stimulator by the company (Magventure, Farum, Denmark). In order to test its effectiveness, phantom EPI measurements were performed, with and without leakage current inhibition added to the stimulator (245 volumes, 24 slices, voxel size 3x3x4mm³, 0.5mm gap, matrix 64*64, TR/TE 2410/30ms, bandwidth 2232 Hz/Px, 1ch Tx/Rx head coil). Each of the two test runs consisted of 6 blocks of 96.4 s, with the stimulation intensity alternating between 15% and 100% of the maximal output intensity.

TMS pulses were applied every 19.28 s in temporal gaps introduced between the EPI volumes (5 pulses per block). The alternating phases of 100% and 15% stimulation were modeled as block design (19.28 s ON, 19.28 s OFF; no convolution with a canonical HRF shape).

The top rows of Figure S.1A&B show the statistical map (at $p=0.05$ uncorrected) and the unthresholded parameter estimates, respectively, for the run without leakage current inhibition. As the strength of the leakage currents change between the blocks with 15% and 100% intensity, respectively, some regions exhibit clear-cut signal increases and decreases. The signal time courses for two regions with significant signal modulations are shown as dotted lines in Figure S.1C&D. In contrast, in the bottom rows of Figure S.1 A&B, the results for the modified TMS stimulator with circuit for leakage current inhibition are shown. The previous “active” regions are reduced to a random noise pattern. Accordingly, the time courses in the two ROIs are uncorrelated with the experimental design (continuous lines in Fig. S.1C&D). All measurements described in this paper were assessed with enabled leakage current inhibition.

Field distortions caused by the TMS coil

In two subjects, field maps were acquired in order to quantify the amount of distortions in the CASL images due to the TMS coil. The pixel shifts in the images were estimated using FSL4.0 PRELUDE and FUGUE (FMRIB, Oxford University, Oxford, UK). The maximal amount of shift assessed by means of the field maps was 1.3 and -2.3 voxels, respectively. Importantly, the maximal voxel shifts occurred at some positions at the rim of the brain and did not affect motor or premotor areas. In general, only few voxels exhibited shifts greater than 1 or smaller than -1. Based on these results, we decided not to apply distortion correction to the CASL images.

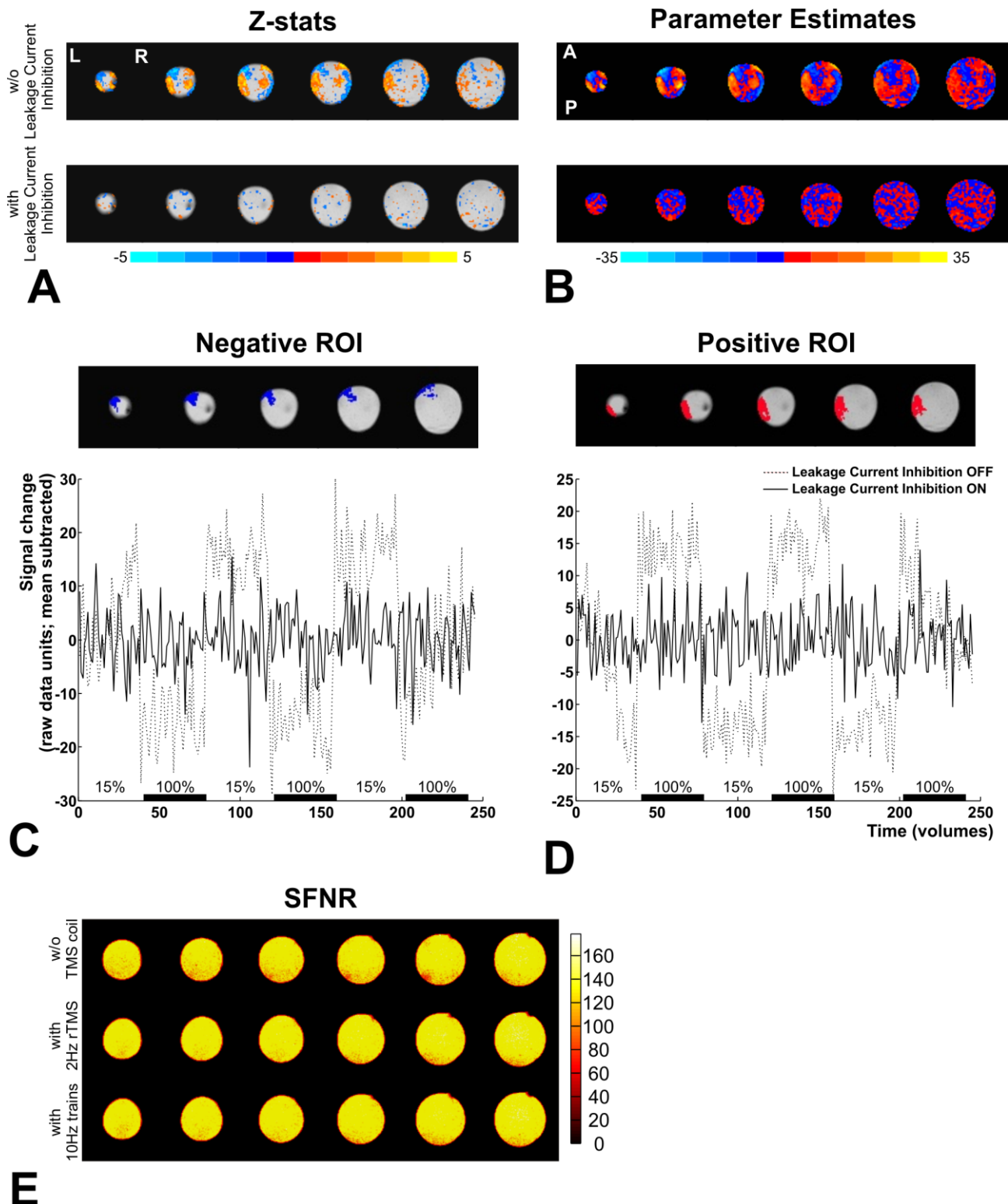


Figure S.1 Statistical maps (thresholded at $p = 0.05$ uncorrected) (A) and parameter estimates (B) when comparing blocks with 100% vs 15% stimulation intensity. The upper and lower rows show the results without and with leakage current inhibition, respectively. (C) Upper row: Visualization of the ROIs based on the positive and negative regions in the statistical map for the condition without leakage current inhibition. Lower row: ROI time courses for the runs with and without leakage current inhibition for the ROIs shown in the upper row. (E) SFNR images of the first six CASL slices (out of eight) for the measurements without coil, with 2Hz continuous rTMS and with 10Hz trains rTMS (both at 100% stimulation intensity).

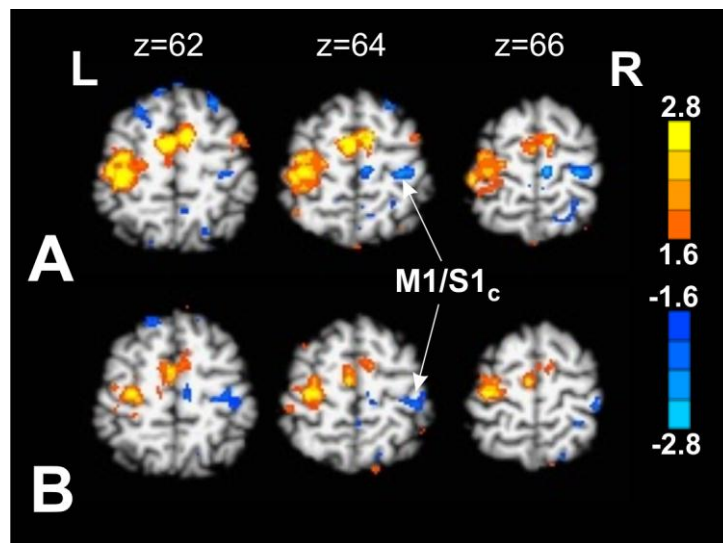


Figure S.2 Group perfusion maps for stimulation with 10Hz trains at 2 s (A) and 4 s (B) intervals, respectively ($p = 0.05$ uncorrected, FSL FLAME mixed effects analysis). In these two conditions, negative activations occurred in M1/S1 contralateral to the TMS coil. Further rCBF decreases were observed the posterior SMA, bilateral SFG, contralateral IPS and precuneus.

References

- Bohning, D.E., Denslow, S., Bohning, P.A., Lomarev, M.P., George, M.S., 2003. Interleaving fMRI and rTMS. *Suppl Clin Neurophysiol* 56, 42-54.
- Friedman, L., Glover, G.H., 2006. Report on a multicenter fMRI quality assurance protocol. *J Magn Reson Imaging* 23, 827-839.
- Moisa, M., Pohmann, R., Ewald, L., Thielscher, A., 2009. New Coil Positioning Method for Interleaved Transcranial Magnetic Stimulation (TMS)/Functional MRI (fMRI) and Its Validation in a Motor Cortex Study. *JMRI* 29, 189-197.
- Weiskopf, N., Josephs, O., Ruff, C.C., Blankenburg, F., Featherstone, E., Thomas, A., Bestmann, S., Driver, J., Deichmann, R., 2009. Image artifacts in concurrent transcranial magnetic stimulation (TMS) and fMRI caused by leakage-currents: modeling and compensation. *JMRI* 29, 1211-1217.

M3. Remote Motor Cortical Areas Acutely Compensate for a Transient Lesion of Left Dorsal Premotor Cortex during Arbitrary Visuomotor Mapping.

Authors: **Marius Moisă**, Hartwig R. Siebner, Rolf Pohmann, Axel Thielscher.

Journal: submitted

Remote motor cortical areas acutely compensate for a transient lesion of left dorsal premotor cortex during arbitrary visuomotor mapping

Moisa, Marius, MS¹; Siebner, Hartwig R., MD²; Pohmann, Rolf, PhD¹; Thielscher, Axel, PhD¹

¹High-Field Magnetic Resonance Center, MPI for Biological Cybernetics, Tübingen, Germany

²Danish Research Centre for Magnetic Resonance, Copenhagen University Hospital Hvidovre, Copenhagen, Denmark

Running title: Acute cortical reorganization during arbitrary visuo-motor mapping

Correspondence should be addressed to:

Dr. Axel Thielscher
Max Planck Institute for Biological Cybernetics
Spemannstraße 41
D-72076 Tübingen
Germany
Tel +49-(0)7071-601907
Fax +49-(0)7071-601702
Email: axel.thielscher@tuebingen.mpg.de

Abstract

The dorsal premotor cortex (PMd) is thought to be involved in movement selection based on external cues. Here we applied transcranial magnetic stimulation (TMS) to the left dorsal premotor cortex (PMd) at low or high intensity while right-handed individuals performed externally paced sequential key presses with their left hand. Movements were cued by abstract visual stimuli, and subjects either freely selected a key press or chose a finger according to a prelearned visuomotor mapping rule. Continuous arterial spin labeling (CASL) was interleaved with TMS to directly assess how stimulation of left PMd modulates task-related brain activity depending on the mode of movement selection. Relative to passive viewing, both tasks activated a similar premotor-parietal core network. High-intensity TMS gave rise to increased activity in medial and right premotor areas compared to low-intensity TMS without affecting task performance. This increase in task-related activity was context-specific because it was only present when movement selection relied on the learned visuomotor associations. We propose that these remote premotor areas were recruited to compensate for disrupted visuomotor mapping in the stimulated left PMd. The present results support the notion that the left PMd plays an important role in mapping external cues onto the appropriate movement.

Keywords: premotor, motor selection, sensory-motor integration, multimodal imaging

Introduction

In humans, it is well established that a fronto-parietal network of brain regions subserves a wide range of different motor behaviors. However, it often proves difficult to determine the specific functional roles of the areas constituting this “cortical motor network” by means of functional neuroimaging, as many of them are commonly activated in most motor tasks. For example, based on studies in non-human primates, a functional distinction between the medial and lateral premotor (PM) areas has been suggested (Mushiake et al. 1991; Passingham et al. 2004). According to this account, medial areas are especially involved in internally generated movements whereas lateral regions, in particular the dorsal premotor cortex (PMd), are preferentially engaged in mapping external cues onto appropriate motor responses. However, neuroimaging studies reported increased activity in both medial premotor areas and PMd for internally triggered compared to externally cued movements (Deiber et al. 1991; Jenkins et al. 2000; Weeks et al. 2001) or even reported a lack of activation in the PMd with externally cued movements (Cunnington et al. 2002). During the learning of arbitrary visuomotor associations, performance-dependent activation changes of medial areas have been reported, while PMd activity stayed mostly unchanged (Sakai et al. 1999; Toni et al. 2001; Eliassen et al. 2003; Bédard and Sanes 2009). Additionally, studies targeting sub-processes such as the preparation or execution of movements reported similar activation time courses in medial premotor areas and PMd (Richter et al. 1997; Cavina-Pratesi et al. 2006; Jankowski et al. 2009). These studies provided converging evidence that the functional specialization of lateral versus medial premotor areas might be gradual rather than absolute.

However, a general limitation of these studies is that the functional involvement of the lateral and mesial premotor areas was probed with correlative measures. Here, the combination of transcranial magnetic stimulation (TMS) with functional neuroimaging adds a causal dimension. TMS can interfere with neuronal processing in a distinct cortical region, and functional neuroimaging can capture the acute effects of the transient TMS-induced focal lesion on the distributed neural activity in the motor network (Siebner et al. 2009). Here, we used functional neuroimaging to assess acute shifts in weighted activity in premotor areas (that is, acute changes in connectivity or short-termed reorganization) during on-line TMS of the left PMd, with the driving idea that the specialization of an area should also be reflected in its connectivity pattern. Interleaved TMS/fMRI offers the possibility to assess the immediate causal influence of single TMS stimuli or short TMS bursts on the activity in remote regions (Bohning et al. 1998; Baudewig et al. 2001; Bestmann et al. 2003a). For example, when a TMS burst was applied to the left PMd, interleaved fMRI revealed a state-dependent change in regional activity in right PMd, showing increased activity during feedback driven grip force control but decreased activity at rest (Bestmann et al. 2008). Alternatively, low-frequency (1Hz) repetitive TMS (rTMS) protocols can be used to temporally reduce the excitability in the stimulated cortical area, with the effects remaining stable for some time after the end of stimulation (Chen et al. 1997a). This evokes compensatory changes in related brain regions which can be mapped “offline” with various neuroimaging methods (O’Shea et al. 2007; Siebner et al. 2003; Ward et al. 2010). For instance, 1Hz rTMS of left PMd increased the blood-oxygen-level-dependent (BOLD) signal

in medial and contralateral premotor areas during a subsequent motor task in which subjects had to apply a complex arbitrary visuomotor mapping rule (O'Shea et al. 2007). This increase in remote premotor activity was associated with a normal level of task performance, again suggesting that the additional recruitment of remote premotor areas helped to compensate for the transient “lesion” that had been induced with 1Hz rTMS in left PMd.

These combined TMS-fMRI studies point to a critical role of the left PMd in visuomotor control of movement that can be compensated by the additional recruitment of remote premotor areas. However, the TMS effects on brain activity became evident relative to less complex motor control tasks (O'Shea et al. 2007) or passive viewing (Bestmann et al. 2008). Therefore it remains unclear whether the observed compensatory network effects were specifically related to the task requirements in terms of visuomotor control or simply reflected a non-specific change in the overall activation levels within the cortical motor network.

To address this question, we repeatedly applied short bursts of high-frequency TMS to left PMd to disrupt neural processing in the left PMd while healthy volunteers produced a sequence of key presses with the fingers of the left hand. The experimental design included two high-level motor conditions which only differed in terms of movement selection: externally guided versus internally determined movements. The acute effects of TMS of left PMd on regional neuronal activity were tested using interleaved CASL (continuous arterial spin labeling) to assess regional cerebral blood flow (rCBF) (Moisa et al. 2010). We hypothesized that TMS of left PMd would trigger a compensatory recruitment of other premotor areas but only during externally guided movements in which movement selection was based on pre-learned visuomotor associations.

Materials and Methods

Subjects

Nine right-handed volunteers with a mean age of 26 years (range 24 - 31) participated in the study after they had given written informed consent. None of them had a history of neurological or psychiatric diseases or was on regular medication. The study was approved by the local ethics committee of the Medical Faculty of the University of Tübingen.

Experimental design

Figure 1A illustrates the experimental design. In a preparatory session we acquired a high-resolution structural image and defined the site for TMS of the left PMd using neuronavigation. After the preparatory session, subjects participated in two experimental sessions in which we interleaved TMS and CASL-based fMRI while subjects performed externally paced sequential key presses with their left non-dominant hand. In one experimental session, each finger movement was determined by an arbitrary non-spatial cue (i.e., associative key presses; AK). In the other experimental session the cue only specified the timing of the movement, but subjects freely selected which finger to move (i.e., freely selected key presses; FK). Additional CASL fMRI runs in which participants only passively viewed (PV) the cues without performing any movement served as baseline condition. We decided not to intermingle the two motor tasks within one session to prevent putative cross-over effects. In particular, we wanted to rule out any interfering effect of task switching on steady-state performance in the associative finger tapping task. Further on, for subjects being tested on freely selected responses in the second session, the temporal separation renders it unlikely that the results were biased by an active suppression of the prelearned response mapping. The two experimental sessions were separated by at least one week and the order of sessions was counterbalanced across subjects.

Each TMS-CASL session consisted of eight runs. Four fMRI runs were acquired while subjects performed one of the two motor tasks (TASK) and four fMRI runs were obtained during passive viewing (CONTROL). In two of the four TASK and CONTROL runs, we applied high-intensity or low-intensity TMS, respectively, with the order of experimental conditions being counterbalanced across subjects. Thus, the experiment had a two-factorial blocked design with the factor TMS intensity (2 levels: TMS_{HIGH} vs. TMS_{LOW}, within-session effect) and motor state (2 levels: freely selected vs. externally determined movements, between-session effect).

Experimental tasks

During task periods, subjects viewed a randomized sequence of 5 geometrical figures presented in the centre of the visual field at a rate of 0.8 Hz. Subjects were required to produce a sequence of key presses with the fingers of their left hand in response to the visual cues. In experimental runs with associative key presses, each figure instructed a response with a specific finger. In experimental runs with freely selected key presses, subjects had to randomly select a new response each time a figure was displayed. Here the cues merely served to pace the movement but were not relevant in terms of which key to press. There were two restrictions to random movement selection. Participants were not allowed to press

the same key twice in a row to ensure a change in motor output from trial to trial. The subjects were also instructed not to perform an ascending or descending key presses sequence. In the control runs, subjects had to passively view the figures without performing any movements.

Prior to CASL-fMRI, participants were trained on the tasks (associative or freely selected key presses) which they were to perform in the MR scanner. In the training session, participants learned the specific associations between each geometrical figure and key press. Subjects practiced the task until they made no errors (3-10 minutes of practice) and were retested again immediately before the first fMRI run.

Using an epoch-related CASL-fMRI design, each run consisted of three alternating epochs of task and rest with task epochs lasting 60 s and rest epochs lasting 120 s. During the rest periods the subjects had to fixate a white cross presented in the central visual field. Visual stimulation and recording of the button presses was done using Cogent (Wellcome Department of Imaging Neuroscience, University College London, www.vislab.ucl.ac.uk/CogentGraphics.html) programmed in MATLAB (The Mathworks, Natick, USA).

Transcranial magnetic stimulation

The site for TMS of the left PMd was identified in the TMS laboratory. We first defined the location of the primary motor hand area (M1-HAND). The M1-HAND site was functionally defined as the site on the skull where a clearly suprathreshold TMS pulse elicited the largest muscle twitch in the relaxed first dorsal interosseous muscle (FDI) of the right hand. The M1-HAND site was then used as anchor point for defining the stimulation site in the left PMd. According to Schluter and colleagues (1998), the PMd site for TMS was located 2 cm anterior and 1 cm medial to the functionally defined M1-HAND site. The exact position of the TMS coil over the left PMd was saved using a neuronavigation system (BrainView, Fraunhofer IPA, Stuttgart, Germany). This enabled us to precisely locate the PMd site with neuronavigated TMS in the following sessions of interleaved TMS-CASL imaging.

A MagPro X100 stimulator (MagVenture, Denmark) with an MR-compatible figure-8 coil (MRi-B88) was used to deliver biphasic magnetic stimuli in the MR environment. The coil was positioned tangentially to the skull, with the induced current orientation being approximately 45 degrees with the subject's body mid-line. Prior to each TMS-CASL session, the left M1-HAND and PMd sites were marked on the subject's skull based on the positions saved by the neuronavigation system. Inside the scanner, the TMS coil was first positioned over the M1-HAND using a custom-built MR-compatible coil holding device (Moisa et al. 2009) and individual resting and active motor thresholds (rMT and aMT) were determined. After threshold measurements, the coil was positioned over the cortical target region, the left PMd.

During the TMS-CASL sessions, we delivered short high-frequency TMS bursts to the left PMd in the MR scanner while measuring changes in regional blood flow with interleaved CASL. TMS bursts were given at a high intensity ($TMS_{HIGH} = 110\%$ of individual resting motor threshold) or low intensity ($TMS_{LOW} = 70\%$ of individual active motor threshold). High-intensity TMS was considered to be effective in modulating PMd activity. In contrast, low-intensity TMS was considered too weak to significantly modulate PMd activity, but

served as a high-level control for the non-specific effects of TMS caused by acoustic and somatosensory stimulation. TMS consisted of high-frequency (10 Hz) bursts consisting of five biphasic pulses with an inter-stimulus interval of 100 ms. These bursts were continuously applied during the task periods of the experimental runs with a 4.0 s gap between two consecutive bursts. The stimulus intensity was kept constant during a task block, but pseudo-randomized among the task blocks of an experimental run.

Interleaved TMS-CASL procedure

Scanning was performed on a 3T Siemens TIM Trio (Siemens AG, Erlangen, Germany). In the preparatory session, we acquired a high-resolution structural MRI of the whole brain (MPRAGE, 192 sagittal slices, matrix size = 256×256, voxel size = 1 mm³, TR/TE/TI= 1900/2.26/900 ms, 12-channel head coil). During the experimental sessions, a one-channel RF transmit/receive head coil (model PN 2414895; USA Instruments, Aurora, CO, USA) was used for interleaved CASL-TMS.

An in-house written CASL sequence with EPI readout (2D gradient-echo echo planar imaging) and separate RF coils placed on the subject neck for labeling the inflowing blood in the right and left carotid was used for imaging (Zhang et al. 1995; Zaharchuk et al. 1999). Each of the 8 experimental runs acquired per session contained 142 volumes (71 pairs of control – tag images; imaging parameters: matrix size = 64*64, voxel size = 3x3x4 mm³, 0.5 mm gap, TR/TE = 4000/20 ms, bandwidth = 2442 Hz/pixel, tag duration/delay = 2343/820 ms, tag gradient strength 2.0 mT/m). One volume consisted of 16 slices covering the motor, premotor, frontal and parietal areas (see Fig. 1B). Before each functional scan, a control magnitude image was acquired (6 volumes; TR = 8 s; no labeling and saturation pulses; all other parameters were identical to those of the functional images). The control magnitude images were used to check for systematic global differences in image intensities between sessions. Additionally, in the first session, a whole-brain EPI was acquired once that was used for image registration during post-processing (32 slices, matrix size = 64*64, voxel size = 3x3x4 mm³, 0.5 mm gap, TR/TE = 1600/20 ms, bandwidth = 2442 Hz/pixel).

The 10Hz rTMS trains were applied during the tagging delay of the CASL sequence (starting directly after the end of tagging; stopping at least 100 ms before the EPI acquisition) to prevent any side effects of the TMS stimulation on the image acquisition (Bestmann et al., 2003b; Moisa et al. 2010). Further details on the interleaved TMS/CASL setup can be found in Moisa et al. 2010.

Data Analysis

Reaction times (RTs) were analyzed using a two-way repeated measures analysis of variance (ANOVA) with TMS intensity (high vs. low) and task (associative vs. freely key presses) as factors. The main effects of TMS intensity and task were assessed, as well as the interaction between both. In addition, uncorrected pairwise comparisons of the RTs corresponding to the two different TMS intensities were performed separately for each of the motor tasks in order to exclude even subtle effects of TMS on task performance. Incorrect responses during associative key presses were discarded during the analysis of RTs. A paired t-test assessed whether the TMS intensity (TMS_{HIGH} vs. TMS_{LOW}) had an impact on the number of incorrect button presses during associative finger tapping.

The functional imaging data were preprocessed and analyzed with FSL4.0 (FMRIB, Oxford University, Oxford, UK). The first two volumes in each experimental run were discarded to allow the brain tissue to reach steady state magnetization. Preprocessing of the functional time series included motion correction, linear registration to the individual whole-brain EPI (6 degrees of freedom), high-pass filtering (360 s cut-off) and spatial smoothing (Gaussian with 5 mm full-width at half-maximum). For each run, the combined perfusion and BOLD signal was modeled using three regressors (see www.fmrib.ox.ac.uk/fsl/feat5/perfusion.html for details). An alternating intensity variation of constant height between control and tag images was used to model the perfusion baseline. BOLD activation was modeled as the convolution of the block design pattern (60 s stimulation – 120 s rest, repeated 3 times) with a standard hemodynamic response function (HRF). Perfusion activation was modeled as the multiplication of the regressors for the rCBF baseline and the BOLD signal, thereby implicitly assuming that the stimulus-related perfusion changes have a similar time course as the BOLD signal.

A general linear model was estimated separately for each experimental run and the runs corresponding to the same experimental condition were subsequently combined for each subject in a fixed effects analysis. At this stage, the analysis of the second session was repeated for two randomly selected subjects to control for putative systematic effects of varying image intensities on the subsequent statistical comparisons across sessions. Generally, the possibility for absolute quantification of rCBF enables robust across-session comparisons in ASL imaging. Here, we use differences in image intensity rather than absolute rCBF values to limit the complexity of the analysis. However, the only parameter of the equation applied for rCBF quantification (Wang et al. 2005b; Moisa et al. 2010) that varied across sessions was the intensity of the control magnitude images (M_{CON}). Therefore, we obtained two mean M_{CON} images by averaging all control magnitude images separately for each session and scaled the raw functional data of the second session voxel-wise by the ratio of the two average M_{CON} images. The results of the GLM analyses were only marginally affected by this scaling, i.e. the effect of global differences in M_{CON} intensities across sessions could be neglected in our study.

To allow for group level inferences, the maps of the individual parameter estimates were normalized to MNI space in a two-step procedure: First, the whole-brain EPI was registered to the individual T1-weighted anatomical image and then the anatomical image was registered to the MNI template. The normalized individual maps of parameter estimates were fed into a second-level mixed-effects analysis with experimental conditions and subjects as fixed and random factors, respectively. In addition to the covariates of interest, the two different scanning sessions were modeled as additional regressors to further control for unwanted across-session effects. Group Z-statistical images were derived using a corrected statistical threshold of $p < 0.05$ at the cluster level. Correction was performed using Monte Carlo simulations (AlphaSim, AFNI, <http://afni.nimh.nih.gov/afni>). The threshold for each voxel within a given cluster being set at an uncorrected $p < 0.01$ (corresponding to $Z = 2.3$) and the extent threshold corresponded to 81 contiguous voxels within a given cluster.

We were specifically interested to learn how the TMS-induced perfusion changes depended on the task, as revealed by the interaction between factors TMS and TASK. The corresponding activation map was used to determine five regions of interest (ROIs) for the visualization of the perfusion changes across conditions. The ROIs were first defined based on anatomy and MNI coordinates. The right primary motor area (M1) was defined as the part of the anterior bank of the central sulcus located around the hand knob (Yousry et al. 1997). The right dorsal premotor area (PMd) was determined using the junction of the superior precentral sulcus with the superior frontal sulcus. Based on MNI coordinates, an adjacent lateral part of the superior precentral sulcus was determined as the dorsal portion of right PMv bordering PMd (Tomassini et al. 2007). The area anterior to the PMv ROI was defined as the caudal part of Brodmann area 9 (BA9). The bilateral cingulate motor areas (CMA) were determined as the regions anterior to the precentral gyri and lying within the cingulate sulci (i.e., inferior to the proper and pre-supplementary motor areas; Picard and Strick 2001). The raw ROIs were subsequently intersected with the group activation map for the interaction TMS x TASK. This procedure revealed the ventral portion of right M1, so that a further control ROI was created for the main part of M1 by intersecting the anatomical ROI with the main effect of both tasks versus passive viewing (thresholded at $z = 8.0$ at voxel level and $p = 0.05$ corrected at cluster level). The ROIs were transformed to the individual low resolution EPIs. Within each ROI, the statistical parameter estimates (PE) were averaged across all voxels. Finally, the PEs were averaged across subjects and plotted for the different conditions.

In addition to a standard GLM analysis as outlined above we used psychophysiological interaction (PPI) analyses (Friston et al. 1997) to investigate how the functional connectivity between the stimulated left PMd and the other motor areas was influenced by the mode of movement selection, TMS intensity, and the interaction between both. The first PPI was used to test for regions showing a change in functional coupling with the left PMd during the associative compared to the free selection task. At the subject level, we first created the input data for the PPI analysis by determining the perfusion subtraction time courses between the control and tagged EPIs for each run. A sinc interpolation was used to create data sets having the same number of volumes as the original input data (see <http://www.fmrib.ox.ac.uk/fsl/feat5/perfusion.html> for details). Subsequently, all runs corresponding to either of the two tasks, irrespective of TMS intensity, were combined into one data set. The statistical model contained three main regressors: the physiological and the psychological time series as effects of no interest; multiplication of both revealed the PPI term as the effect of interest. The psychological regressor was obtained by convolving a boxcar waveform coding the contrast of tasks (1 during associative key presses, -1 during freely selected key presses and 0 during the fixation periods between the task epochs) with a canonical HRF. The physiological regressor was generated by averaging the perfusion time courses across all voxels within a seed region in the targeted left PMd. This region was defined based on the group perfusion activation for factor TMS in the passive viewing condition ($p < .01$ at the voxel level; peak coordinates $x = -20$, $y = -6$, $z = 54$; cluster volume = 128 mm^3 ; see Fig. S2 in the Supplementary Material). Any putative impact of systematic, but unspecific baseline differences between the runs on the PPI results was ruled out by

centering the PMd time courses for each run prior to building the physiological regressor. The final PPI regressor represented the interaction between the psychological and physiological factors. Seven additional regressors of no interest were used to model the time periods of the first seven runs using boxcar functions, thereby (in combination with the constant term) accounting for any unspecific baseline differences between the eight runs. The subject-specific statistical PPI maps were normalized to MNI space and fed into a second-level mixed-effects analysis to identify consistent changes in functional connectivity at the group level. Using the procedure described above, a second PPI analysis was conducted to compare the associative task with the passive viewing condition. A third PPI analysis was used to test for between-session effects. Here we used the passive viewing periods of both sessions to create the psychological regressor.

Results

None of the participants reported any adverse effects during the course of the experiment. Mean stimulus intensity in the TMS_{HIGH} condition was 62.1 ± 4.7 % of maximal stimulator output, while mean intensity was 29.5 ± 1.4 % of maximal stimulator output for the TMS_{LOW} condition.

Task performance

The behavioral data are summarized in Figure 1. Mean RTs were consistently longer for associative opposed to freely selected responses ($F_{1,8} = 137.63$, $p < .001$; Fig. 1C). This RT difference reflected the different mode of movement selection between the two motor tasks. Subjects were able to decide on the next button press during the interval between two consecutive visual stimuli when they freely selected the key presses. In contrast, no movement preparation was possible in the associative task, resulting in longer RTs. This task-specific difference in RT was not modified by the TMS condition because the interaction between TMS intensity and task was not significant. Accordingly, pairwise comparisons of mean RTs revealed no effect of TMS intensity in both tasks (Fig. 1E & 1F). The intensity of TMS had also no effect on mean error rates during associative key presses (Fig 1D).

Task related brain activation

Figure 2A depicts the brain regions that were consistently activated during both tasks relative to passive viewing, irrespective of TMS intensity. Significant rCBF increases were found in the sensorimotor system, including right (contralateral to the site of stimulation) primary sensorimotor area (M1/S1), bilateral cingulate and supplementary motor areas (CMA/SMA) as well as bilateral dorsal and ventral premotor areas (PMv, PMd). Task related decreases in rCBF were observed bilaterally in the superior frontal gyri (SFG), the middle frontal gyri (MFG), the paracingulate gyri, the posterior CMA, the inferior parietal lobe (IPL) and the precuneous.

Several areas exhibited increased rCBF with freely selected movements compared to movements based on visuomotor associations (Fig. 2B). However, this often corresponded to less deactivation when compared to passive viewing rather than real rCBF activations. Regions showing increased rCBF for the associative task compared to both freely selected

movements and passive viewing were found in right MFG, left inferior frontal gyrus (IFG), bilateral SFG, bilateral supramarginal gyri (SMG) and right posterior SMA (Fig. S1 in the Supplementary Material). Increases in regional activity with free movement selection were mainly located outside the brain regions showing common increases in rCBF with both motor tasks (see Fig. 2A). No brain region within the field of view exhibited significantly stronger rCBF increases with associative movement selection relative to free selection.

Effect of transcranial magnetic stimulation

The comparison of high vs. low TMS intensity revealed rCBF increases in the bilateral auditory cortices, the right IPL, the posterior CMA and the cuneus during the TMS_{HIGH} condition (Fig. 2C). TMS_{HIGH} caused no significant decreases in rCBF relative to TMS_{LOW}. Interleaved TMS had no consistent effect on the rCBF in the directly stimulated left PMd during both motor tasks. In the passive viewing condition, a trend towards an increase in rCBF was observed in left PMd (peak coordinates: $x = -20$, $y = -6$, $z = 54$, $Z_{\text{preak}} = 2.8$) at a lowered statistical threshold ($p < .01$ at the voxel level, no cluster threshold; see Fig. S2 in the Supplementary Material). This trend increase in rCBF was not located at the hemispheric surface close to the TMS coil, but rather deep in the superior frontal sulcus.

The modulatory effects of TMS depended on the mode of movement selection (Fig. 3A and Table 1). Several precentral and mesial cortical motor areas showed a stronger TMS-related increase in rCBF with associative but not with free movement selection, resulting in a significant interaction between TMS intensity and task ($[TMS_{\text{HIGH}} - TMS_{\text{LOW}}]_{\text{AK}} - [TMS_{\text{HIGH}} - TMS_{\text{LOW}}]_{\text{FK}}$). The cortical regions showing a stronger activation for associative relative to free movement selection with effective relative to ineffective TMS were primarily located in the right hemisphere, including the right M1, right PMd and adjacent parts of right PMv as well as the caudal part of right dorsolateral prefrontal cortex (dlPFC) as well as the right anterior insula. Additional regions were found in mesial premotor areas, including clusters in posterior SMA and anterior CMA. In these mesial regions, TMS-induced differences in motor activation with associative movement selection were expressed bilaterally, yet activity changes were more pronounced in the right hemisphere. Figure 3C shows the parameter estimates (PE; proportional to the rCBF changes) for both motor tasks in six ROIs. The first five ROIs correspond to the regions revealed by the interaction analysis (Fig. 3A). The PE plots reveal that the interaction was predominantly driven by an increase in activation for TMS_{HIGH} versus TMS_{LOW} during associate movements. The sixth ROI served as control ROI and was positioned around the activation peak in right M1 for the main effect of both tasks compared to passive viewing (Fig. 2A). The PE plot shows a consistent and robust level of rCBF activation for both tasks and both stimulation intensities. In order to rule out the impact of unwanted across-session effects on the results presented above, a control analysis tested the interaction between TMS intensity and the passive viewing periods across sessions ($[TMS_{\text{HIGH}} - TMS_{\text{LOW}}]_{\text{PV1}} - [TMS_{\text{HIGH}} - TMS_{\text{LOW}}]_{\text{PV2}}$). Visual inspection of the results thresholded at a liberal level of $p = .05$ uncorrected revealed some spurious activations that overlapped not at all or only by a few negligible voxels with the regions reported above (data not shown). We also tested for brain areas exhibiting TMS-related rCBF increases during associative key presses compared to passive viewing ($[TMS_{\text{HIGH}} - TMS_{\text{LOW}}]_{\text{AK}} - [TMS_{\text{HIGH}} -$

TMS_{LOW}]PV). Again, mesial and right-hemispheric cortical areas showed stronger TMS-related increases in rCBF with associative movement selection relative to the non-motor control task (green and blue regions in Fig. 3B & Table S1). Distinct clusters in the right M1, PMd, BA9 and CMA showed TMS-induced rCBF increases for associative movement selection compared to both, free selection and passive viewing (blue areas in Fig. 3B & Table 1).

No TMS-related increases in rCBF were observed during freely selected movements relative to associative movement selection. The cuneus was the only region where TMS enhanced rCBF with free movement selection compared to passive viewing ($[TMS_{HIGH} - TMS_{LOW}]_{FK} - [TMS_{HIGH} - TMS_{LOW}]_{PV}$; Fig. S3 in the Supplementary Material).

The PPI analyses revealed task-dependent changes in functional connectivity between the stimulated left PMd (seed region) and other regions within the motor network. A range of areas (right M1, right PMd, right BA9, left secondary somatosensory motor cortex, bilateral CMA and SMA) showed increased functional coupling for the associative task compared to passive viewing (blue and green regions in Fig. 4A; Table S2). In addition, a second PPI analysis revealed enhanced coupling between the left PMd and a subgroup of these regions (right M1, right BA9 and bilateral CMA) when comparing associative with freely selected responses, using a more liberal cluster threshold with a minimum Z-score of 1.96 at the voxel level and a cluster extent threshold of 35 voxel (yellow and blue regions in Fig. 4A). The areas identified in this second PPI overlapped with those determined when testing the interaction between TMS intensity and task (blue regions in Fig. 4B; Table 2). Finally, the control PPI analysis confirmed that no region within the motor network changed its functional coupling with other brain regions in the field of view when comparing the passive viewing conditions across sessions. Here we used a very liberal threshold with an uncorrected $p < 0.05$ at the voxel level to minimize the risk for false negative findings.

Discussion

Our CASL measurements of rCBF revealed that a transient functional impairment of left dorsal premotor cortex induced by online TMS caused an immediate redistribution of neural activity in cortical motor areas when healthy volunteers performed visually paced sequential key presses with the left hand. Online TMS induced increases in rCBF in right-hemispheric premotor and motor areas as well as in bilateral mesial motor regions including the caudal SMA and CMA. Critically, online TMS only increased neuronal activity in these regions when movement selection relied on prelearned arbitrary visuomotor associations, but not during freely selected key presses or passive viewing. In addition, we found a context-specific increase in functional coupling between the stimulated left PMd and remote right-hemispheric and mesial motor regions. Again, this increase in connectivity was only present during arbitrary visuomotor mapping but not during freely selected key presses or passive viewing.

Importantly, online TMS did not affect error rates and reaction times during associative movement selection. The maintenance of normal task performance during online TMS has two implications. First, it is safe to conclude that the observed changes in task-related activity and connectivity were not confounded by TMS induced changes in task performance. Second, we infer that online TMS failed to induce a functional perturbation that was sufficiently strong to deteriorate task performance. Given the fact that the left PMd is an important area for mapping arbitrary cues onto the appropriate actions (O'Shea et al. 2007) it is plausible to assume that other motor regions that are able to compute visuomotor associations effectively compensated for the TMS-induced functional lesion of the left PMd. As the TMS bursts were continuously delivered for 1 min during the task blocks, we propose that the increased activity in non-stimulated motor areas with arbitrary visuomotor mapping reflects an immediate redistribution of neuronal activity in the cortical motor network to effectively cope with the disruption of neuronal processing in left PMd. This hypothesis is supported by the observation that the increases in activation recruited additional sites adjacent to those showing peak activations during the task. For example, a task-specific increase in rCBF was observed in the ventromedial part of right M1 while the dorsally located part of M1 which overall showed stronger task related activation exhibited no significant change in activation during online TMS (Geyer et al. 1996), hinting towards the recruitment of additional motor representations.

For freely selected responses, the only increase in task-related activity during effective TMS relative to passive viewing was located in the cuneus. However, this effect was present during both motor tasks regardless of the mode of movement selection. A similar, though non-significant trend towards higher rCBF with effective TMS was also observed during associative responses (data not shown). This non-specific increase in visual activity during both motor tasks might be induced by a concurrent disruptive effect of TMS on the frontal eye field which is located close to the PMd. Alternatively, it might be attributed to non-specific effects of TMS as the concurrent auditory and somatosensory stimulation during TMS might have increased the attentional demands during the processing of the visual stimuli.

Externally versus internally-guided key presses

Both motor tasks were matched in terms of visual input and motor output. Both tasks required the preparation and execution of non-stereotyped key press sequences of similar complexity. The critical difference was that the associative task required subjects to apply prelearned visuomotor association for motor selection compared to free selection. The subjects responded generally faster for freely selected compared to associative responses (Fig. 1C). Deiber and colleagues (1991) already pointed out that this difference is expected as, when making internal selections, the subjects can determine the next key press during the time period between two visual stimuli that set the pace of the responses. In contrast, when applying prelearned visuomotor mapping rules, participants had to wait for the next stimulus to come up in order to select the appropriate response. Importantly, however, the activation levels in a common parietal-premotor network were roughly matched between the two tasks in our case. In fact, compared to both associative responses and passive viewing, freely selected responses engaged additional parietal and prefrontal structures including the right dorsolateral prefrontal cortex (Figs. 1B & S1). This is in line with previous results on internally guided responses (Deiber et al. 1991; Jenkins et al. 2000; Weeks et al. 2001) and indicates that RT might not be well suited to fully represent the complexity of the decision processes involved in the free selection task in our case.

Our neuroimaging results are in good agreement with the view obtained from lesion studies in humans and monkeys that PMd is critically involved in conditional sensorimotor mappings (Halsband and Passingham 1982; Petrides 1986; Halsband and Freund 1990; Petrides 1997). Previous functional imaging studies in humans observed learning-related activity in other premotor areas when subjects learned arbitrary sensorimotor associations (Sakai et al. 1999; Toni et al. 2001; Eliassen et al. 2003; Bédard and Sanes 2009). This is not in contrast to our findings which suggest that at least in right-handed individuals, the left PMd is predominantly involved in the execution and maintenance of already learned rules (Bédard and Sanes 2009). In this respect, the present study significantly extends and complements the results of two prior studies combining TMS with fMRI to study the role of PMd in visuomotor control of hand actions (O'Shea et al. 2007; Bestmann et al. 2008). These studies used passive viewing (Bestmann et al. 2008) or a simple motor execution task (O'Shea et al. 2007) as control conditions. O'Shea and colleagues (2007) temporally lesioned the left PMd using 1 Hz rTMS and showed subsequent compensatory activity increases in mesial and right premotor areas for a conditional visuomotor task performed with the right hand. Here, we demonstrated immediate rCBF increases in response to TMS hinting towards on-the-flight compensation in a very similar network of regions. In addition, this compensatory pattern occurred for key presses performed with the left hand, consistent with the generalized role suggested for the left PMd in controlling both contra- and ipsilateral movements (Chen et al. 1997b; Schluter et al. 1998; Johansen-Berg et al. 2002; Rushworth et al. 2003).

By revealing immediate compensatory effects to rTMS trains delivered repeatedly during the 1 min task periods, our study bridges the temporal gap between the offline rTMS effects studied by O'Shea et al. (2007) and the online TMS-fMRI study of Bestmann et al. (2008) in which event-related TMS was used to look at functional effective connectivity. Bestmann et al. used a task involving visual feedback for the online control of the grip force of the left hand. They demonstrated specific activity increases in right PMd and right M1 in response to

the stimulation of left PMd only when the subjects performed the task, but not during rest. We extend this finding by showing that right-hemispheric compensation generalizes beyond grip control. Importantly, a similar response pattern for internally guided movements was absent in our case. This suggests that, for the associative tasks used in our study and by O'Shea et al. (2007) as well as for the grip force control task employed by Bestmann et al. (2008), the common functional role of the left PMd was the maintenance of specific prelearned sensorimotor mapping rules.

Bestmann et al. (2008) argue that the different TMS effects observed for active grip versus rest might stem from a different interplay between transcallosal inhibition and excitation depending on the current activation state (Ferber et al. 1992; Chouinard et al. 2003; Marconi et al. 2003; Mochizuki et al. 2004; Bestmann et al. 2005). Here, we show that this explanation likely is too simple, as we observed context-dependent remote effects despite roughly similar activation levels evoked by the two tasks. At any case, our study demonstrates the limitations of surrogate markers such as rCBF or BOLD in unambiguously reflecting the state of the underlying neural activity (as already pointed out by Bestmann et al.) and shows that the combination of TMS with functional neuroimaging can be used to partly overcome this problem.

So far, functional imaging studies which compared the contribution of medial and lateral premotor areas to internally vs. externally guided movements have revealed inconsistent results (Deiber et al. 1991; Larsson et al. 1996; Jenkins et al. 2000; Weeks et al. 2001). By showing that left PMd stimulation did not trigger compensatory activity increases for internally guided movements, the present study supports the notion based on studies in non-human primates (Mushiake et al. 1991; Tanji and Shima 1994; Chen et al. 1995) that internally guided movements are predominantly controlled by medial premotor areas. We hypothesise that the left PMd might be coactivated in human neuroimaging studies on internally guided movements without performing a pivotal functional role, at least if movements are performed with the ipsilateral hand. Given the role of left PMd in controlling movements of both hands in right-handed subjects, it is likely that similar findings also hold for movements with the contralateral right hand. For example, Siebner et al. (2003) reported widespread rCBF decreases after 1 Hz rTMS delivered to the left PMd in healthy individuals and patients with focal hand dystonia. The suppressive effects of TMS on rCBF were similar at rest and during freely selected key presses with the right hand. Consistent with our findings, this indicates that the pattern of movement-related activation did not change during internally guided movements.

Methodological considerations

After having demonstrated the technical feasibility of interleaving TMS with ASL imaging (Moisa et al. 2010), we now show that this novel combination can also be applied to study task-dependent TMS effects rather than just the impact of TMS on baseline rCBF. ASL is insensitive to low-frequency fluctuations and exhibits a reduced inter-subject and inter-session variability compared to BOLD imaging, possibly reflecting a more direct link between rCBF and neural activity (Aguirre et al. 2002; Tjandra et al. 2005; Liu and Brown 2007). As a consequence, we were able to carry out normal random-effects group analyses at acceptable significance levels despite the reduced sensitivity of ASL compared to BOLD

fMRI on the single subject level. In particular, the good inter-session reproducibility proved beneficial for comparing the impact of TMS on the two motor tasks, as confirmed by our several control analyses. Disadvantages of the ASL approach were the limited field of view that only partially covered subcortical structures and did not extend to the cerebellum as well as the reduced temporal resolution stemming from the alternating acquisition of tag and control images. To our view, these disadvantages are offset by the possibility to study rCBF changes across longer time periods (Wang et al. 2003; Wang et al. 2005a). In this respect, the current study further paves the way for studying the impact of fully-fledged repetitive TMS protocols for which ASL imaging should be particularly well suited.

Conclusion

Using interleaved TMS/CASL imaging, this study demonstrated context-dependent effects of left PMd stimulation on motor activity in remote right-hemispheric and mesial cortical regions. Effective TMS increased rCBF in these cortical areas only for key presses relying on a prelearned associative visuomotor mapping, but not for freely selected responses and passive viewing. These changes in activation were associated with a change in functional connectivity between the stimulated left PMd and remote motor cortical areas in the context of arbitrary sensorimotor mappings. These findings show that focal online TMS of a distinct brain region triggers an immediate compensatory redistribution of functional activity at the network level. Mapping this acute reorganization with CASL imaging offers important new insights into the causal dynamics of the functional neuroarchitecture of the intact human brain in health and disease.

Acknowledgments

MM, RP and AT thank the Max Planck Society for financial support. H.R.S. received financial support by a grant of excellence “ContAct” from the Lundbeckfonden.

References

- Aguirre GK, Detre JA, Zarahn E, Alsop DC. 2002. Experimental design and the relative sensitivity of BOLD and perfusion fMRI. *Neuroimage*. 15: 488-500.
- Baudewig J, Siebner H, Bestmann S, Tergau F, Tings T, Paulus W, Frahm J. 2001. Functional MRI of cortical activations induced by transcranial magnetic stimulation (TMS). *NeuroReport*. 12: 3543-3548.
- Bédard P, Sanes JN. 2009. On a basal ganglia role in learning and rehearsing visual-motor associations. *Neuroimage*. 47: 1701-1710.
- Bestmann S, Baudewig J, Siebner HR, Rothwell JC, Frahm J. 2003a. Subthreshold high-frequency TMS of human primary motor cortex modulates interconnected frontal motor areas as detected by interleaved fMRI-TMS. *NeuroImage*. 20: 1685-1696.
- Bestmann S, Baudewig J, Frahm J. 2003b. On the synchronization of transcranial magnetic stimulation and functional echo-planar imaging. *J Magn Reson Imaging*. 17:309-316.
- Bestmann S, Baudewig J, Siebner HR, Rothwell JC, Frahm J. 2005. BOLD MRI responses to repetitive TMS over human dorsal premotor cortex. *Neuroimage*. 28:22-29.
- Bestmann S, Swayne O, Blankenburg F, Ruff CC, Haggard P, Weiskopf N, Josephs O, Driver J, Rothwell JC, Ward NS. 2008. Dorsal premotor cortex exerts state-dependent causal influences on activity in contralateral primary motor and dorsal premotor cortex. *Cereb Cortex*. 18:1281-1291.
- Bohning DE, Shastri A, Nahas Z, Lorberbaum JP, Andersen SW, Dannels WR, Haxthausen EU, Vincent DJ, George MS. 1998. Echoplanar BOLD fMRI of brain activation induced by concurrent transcranial magnetic stimulation. *Invest Radiol*. 33: 336-340.
- Cavina-Pratesi C, Valyear KF, Culham JC, Kohler S, Obhi SS, Marzi CA, Goodale MA. 2006. Dissociating arbitrary stimulus-response mapping from movement planning during preparatory period: evidence from event-related functional magnetic resonance imaging. *J Neurosci*. 26: 2704-2713.
- Chen R, Classen J, Gerloff C, Celnik P, Wassermann EM, Hallett M, Cohen LG. 1997a. Depression of motor cortex excitability by low-frequency transcranial magnetic stimulation. *Neurology*. 48: 1398-1403.
- Chen R, Cohen LG, Hallett M. 1997b. Role of the ipsilateral motor cortex in voluntary movement. *Can J Neurol Sci*. 24: 284-291.
- Chen YC, Thaler D, Nixon PD, Stern CE, Passingham RE. 1995. The functions of the medial premotor cortex. II. The timing and selection of learned movements. *Exp Brain Res*. 102: 461-473.
- Chouinard PA, Van Der Werf YD, Leonard G, Paus T. 2003. Modulating neural networks with transcranial magnetic stimulation applied over the dorsal premotor and primary motor cortices. *J Neurophysiol*. 90:1071-1083.
- Cunnington R, Windischberger C, Deecke L, Moser E. 2002. The preparation and execution of self-initiated and externally-triggered movement: a study of event-related fMRI. *Neuroimage*. 15: 373-385.

- Deiber MP, Passingham RE, Colebatch JG, Friston KJ, Nixon PD, Frackowiak RS. 1991. Cortical areas and the selection of movement: a study with positron emission tomography. *Exp Brain Res.* 84: 393-402.
- Eliassen JC, Souza T, Sanes JN. 2003. Experience-dependent activation patterns in human brain during visual-motor associative learning. *J Neurosci.* 23: 10540-10547.
- Ferbert A, Priori A, Rothwell JC, Day BL, Colebatch JG, Marsden CD. 1992. Interhemispheric inhibition of the human motor cortex. *J Physiol.* 453: 525-546.
- Friston KJ, Buechel C, Fink GR, Morris J, Rolls E, Dolan RJ. 1997. Psychophysiological and modulatory interactions in neuroimaging. *Neuroimage.* 6:218-229.
- Geyer S, Ledberg A, Schleicher A, Kinomura S, Schormann T, Bürgel U, Klingberg T, Larsson J, Zilles K, Roland PE. 1996. Two different areas within the primary motor cortex of man. *Nature.* 382:805-807.
- Halsband U, Freund HJ. 1990. Premotor cortex and conditional motor learning in man. *Brain.* 113 (Pt 1): 207-222.
- Halsband U, Passingham R. 1982. The role of premotor and parietal cortex in the direction of action. *Brain Res.* 240: 368-372.
- Jankowski J, Scheef L, Huppe C, Boecker H. 2009. Distinct striatal regions for planning and executing novel and automated movement sequences. *Neuroimage.* 44: 1369-1379.
- Jenkins IH, Jahanshahi M, Jueptner M, Passingham RE, Brooks DJ. 2000. Self-initiated versus externally triggered movements. II. The effect of movement predictability on regional cerebral blood flow. *Brain.* 123 (Pt 6): 1216-1228.
- Johansen-Berg H, Rushworth MF, Bogdanovic MD, Kischka U, Wimalaratna S, Matthews PM. 2002. The role of ipsilateral premotor cortex in hand movement after stroke. *Proc Natl Acad Sci USA.* 99:14518-14523.
- Larsson J, Gulyas B, Roland PE. 1996. Cortical representation of self-paced finger movement. *Neuroreport.* 7: 463-468.
- Liu TT, Brown GG. 2007. Measurement of cerebral perfusion with arterial spin labeling: Part 1. Methods. *J Int Neuropsychol Soc.* 13: 517-525.
- Marconi B, Genovesio A, Giannetti S, Molinari M, Caminiti R. 2003. Callosal connections of dorso-lateral premotor cortex. *Eur J Neurosci.* 18: 775-788.
- Mochizuki H, Huang YZ, Rothwell JC. 2004. Interhemispheric interaction between human dorsal premotor and contralateral primary motor cortex. *J Physiol.* 561: 331-338.
- Moisa M, Pohmann R, Ewald L, Thielscher A. 2009. New Coil Positioning Method for Interleaved Transcranial Magnetic Stimulation (TMS)/Functional MRI (fMRI) and Its Validation in a Motor Cortex Study. *J Magn Reson Imaging.* 29:189-197.
- Moisa M, Pohmann R, Uludag K, Thielscher A. 2010. Interleaved TMS/CASL: Comparison of different rTMS protocols. *Neuroimage.* 49: 612-620.
- Mushiake H, Inase M, Tanji J. 1991. Neuronal activity in the primate premotor, supplementary, and precentral motor cortex during visually guided and internally determined sequential movements. *J Neurophysiol.* 66: 705-718.
- O'Shea J, Johansen-Berg H, Trief D, Göbel S, Rushworth MF. 2007. Functionally specific reorganization in human premotor cortex. *Neuron.* 54:479-490.

- Passingham RE, Ramnani N, Rowe JB. 2004. The Motor System. In: Frackowiak RSJ, Friston KJ, Frith CD, Dolan RJ, Price CJ, Zeki S, Ashburner J, Penny W, eds. *Human Brain Function* 2nd ed. Elsevier p 5-32.
- Petrides M. 1986. The effect of periarculate lesions in the monkey on the performance of symmetrically and asymmetrically reinforced visual and auditory go, no-go tasks. *J Neurosci.* 6: 2054-2063.
- Petrides M. 1997. Visuo-motor conditional associative learning after frontal and temporal lesions in the human brain. *Neuropsychologia.* 35: 989-997.
- Picard N, Strick P. 2001. Imaging the premotor areas. *Current Opinion in Neurobiology.* 11: 663-672.
- Richter W, Andersen PM, Georgopoulos AP, Kim SG. 1997. Sequential activity in human motor areas during a delayed cued finger movement task studied by time-resolved fMRI. *Neuroreport.* 8: 1257-1261.
- Rushworth MF, Johansen-Berg H, Göbel SM, Devlin JT. 2003. The left parietal and premotor cortices: motor attention and selection. *Neuroimage.* 20(Suppl 1):S89-S100.
- Sakai K, Hikosaka O, Miyauchi S, Sasaki Y, Fujimaki N, Putz B. 1999. Presupplementary motor area activation during sequence learning reflects visuo-motor association. *J Neurosci.* 19: RC1.
- Schluter ND, Rushworth MF, Passingham RE, Mills KR. 1998. Temporary interference in human lateral premotor cortex suggests dominance for the selection of movements. A study using transcranial magnetic stimulation. *Brain.* 121:785-799.
- Siebner HR, Filipovic SR, Rowe JB, Cordivari C, Gerschlager W, Rothwell JC, Frackowiak RS, Bhatia KP. 2003. Patients with focal arm dystonia have increased sensitivity to slow-frequency repetitive TMS of the dorsal premotor cortex. *Brain.* 126:2710-2725.
- Siebner HR, Bergmann TO, Bestmann S, Massimini M, Johansen-Berg H, Mochizuki H, Bohning DE, Boorman ED, Groppa S, Miniussi C, Pascual-Leone A, Huber R, Taylor PC, Ilmoniemi RJ, De Gennaro L, Strafella AP, Kahkonen S, Kloppel S, Frisoni GB, George MS, Hallett M, Brandt SA, Rushworth MF, Ziemann U, Rothwell JC, Ward N, Cohen LG, Baudewig J, Paus T, Ugawa Y, Rossini PM. 2009. Consensus paper: combining transcranial stimulation with neuroimaging. *Brain Stimul.* 2: 58-80.
- Tomassini V, Jbabdi S, Klein J, Behrens T, Pozzilli C, Matthews P, Rushworth M, Johansen-Berg H. 2007. Diffusion-Weighted Imaging Tractography-Based Parcellation of the Human Lateral Premotor Cortex Identifies Dorsal and Ventral Subregions with Anatomical and Functional Specializations. *J Neurosci.* 27: 10259 –10269.
- Tanji J, Shima K. 1994. Role for supplementary motor area cells in planning several movements ahead. *Nature.* 371: 413-416.
- Tjandra T, Brooks JC, Figueiredo P, Wise R, Matthews PM, Tracey I. 2005. Quantitative assessment of the reproducibility of functional activation measured with BOLD and MR perfusion imaging: implications for clinical trial design. *Neuroimage.* 27: 393-401.
- Toni I, Ramnani N, Josephs O, Ashburner J, Passingham RE. 2001. Learning arbitrary visuomotor associations: temporal dynamic of brain activity. *Neuroimage.* 14: 1048-1057.
- Wang J, Aguirre GK, Kimberg DY, Roc AC, Li L, Detre JA. 2003. Arterial spin labeling perfusion fMRI with very low task frequency. *Magn Reson Med.* 49: 796-802.

- Wang J, Rao H, Wetmore GS, Furlan PM, Korczykowski M, Dinges DF, Detre JA. 2005a. Perfusion functional MRI reveals cerebral blood flow pattern under psychological stress. *Proc Natl Acad Sci U S A*. 102: 17804-17809.
- Wang J, Zhang Y, Wolf RL, Roc AC, Alsop DC, Detre JA. 2005b. Amplitude-modulated Continuous Arterial Spin-labeling 3.0-T Perfusion MR Imaging with a Single Coil: Feasibility Study. *Radiology*. 235:218-228.
- Ward NS, Bestmann S, Hartwigsen G, Weiss MM, Christensen LO, Frackowiak RS, Rothwell JC, Siebner HR. 2010. Low-frequency transcranial magnetic stimulation over left dorsal premotor cortex improves the dynamic control of visuospatially cued actions. *J Neurosci*. 30: 9216-9223.
- Weeks RA, Honda M, Catalan MJ, Hallett M. 2001. Comparison of auditory, somatosensory, and visually instructed and internally generated finger movements: a PET study. *Neuroimage*. 14: 219-230.
- Yousry TA, Schmid UD, Alkadhi H, Schmidt D, Peraud A, Buettner A, Winkler P. 1997. Localization of the motor hand area to a knob on the precentral gyrus - A new landmark. *Brain*. 120: 141-157.
- Zaharchuk G, Ledden PJ, Kwong KK, Reese TG, Rosen BR, Wald LL. 1999. Multislice perfusion and perfusion territory imaging in humans with separate label and image coils. *Magn Reson Med*. 41:1093-1098.
- Zhang W, Sliva AC, Williams DS, Koretsky AP. 1995. NMR measurement of perfusion using arterial spin labeling without saturation of macromolecular spins. *Magn Reson Imaging*. 33:370-376.

Tables

Table 1 Interaction Associative vs. Freely Selected Responses and TMS intensity

Brain Region	Coordinates of peak activity			Z-value of peak activity	Cluster Volume (mm ³)	Cluster Volume Intersection* (mm ³)
	X	Y	Z			
right caudal BA9	42	8	36	3.3	1056	472
right PMd	26	2	46	3.8	1848	880
right PMv (dorsal part)	44	-6	44	3.7	968	-
bilateral anterior CMA	-10	-4	38	3.0	632	-
	6	-8	44	3.0	944	512
right M1	38	-14	38	3.3	512	368
right insula	34	-10	16	3.1	456	-
left S1	-26	-36	64	2.7	328	-
bilateral posterior SMA	0	-38	62	3.5	2508	-

* Intersection volume of the interaction $[TMS_{HIGH} - TMS_{LOW}]_{AK} - [TMS_{HIGH} - TMS_{LOW}]_{FK}$ with the interaction $[TMS_{HIGH} - TMS_{LOW}]_{AK} - [TMS_{HIGH} - TMS_{LOW}]_{PV}$ (blue areas in Fig. 3B).

BA9 - Brodmann area 9; PMd - dorsal premotor cortex; PMv - ventral premotor cortex; CMA - cingulate motor area; M1 - primary motor cortex; S1 - primary somatosensory motor cortex; SMA - supplementary motor area.

Table 2 PPI (Associative > Freely Selected Responses)

Brain Region	Coordinates of peak activity			Z-value of peak activity	Cluster Volume (mm ³)	Cluster Volume Intersection* (mm ³)
	X	Y	Z			
right caudal BA9	40	2	34	2.4	304	96
right M1	36	-12	38	2.3	536	408
bilateral posterior CMA	-10	-26	38	3.1	1024	280
	16	-32	40	3.1	1208	824

* Intersection volume between the PPI results (AK > FK) and the interaction $[TMS_{HIGH} - TMS_{LOW}]_{AK} - [TMS_{HIGH} - TMS_{LOW}]_{FK}$ (blue areas in Fig. 4B). For abbreviations please see legend of Table 1.

Figure Captions

Figure 1 A) Schematic diagram of the experimental design. One motor task was tested per session (either associative or freely selected key presses) while passive viewing was assessed in both sessions. One condition was investigated per experimental run. The order of runs within one session was pseudo-randomized across subjects and the order of sessions was counterbalanced across subjects. Each run consisted of three alternating epochs of task and rest with task epochs lasting 60 s and rest epochs lasting 120 s. B) Brain coverage of the CASL sequence. The field of view contained most of the cortical motor network. C) Reaction times (RTs) for the two different tasks, averaged across TMS intensities. D) Error rates (ERs) for the associative task in dependence on TMS intensity. E) Dependence of RTs during the associative task on TMS intensity. F) RTs during the free selection task in dependence on TMS intensity. (C-F: the error bars represent the standard error across subjects)

Figure 2 Group rCBF activation maps (MNI space); unless indicated otherwise, a threshold of $Z=2.3$ (corresponding to $p = .01$) at the voxel level and an extent threshold of 81 voxel (corresponding to $p = .05$) at the cluster level were used for all figures; abbreviations: AK – associative key presses; FK – freely selected key presses; PV – passive viewing; A) Main effect of key presses (pooled across both tasks) versus passive viewing. B) Freely selected vs. associative key presses (pooled across stimulation intensities). C) TMS main effect.

Figure 3 A) Interaction between motor task and TMS intensity ($[TMS_{HIGH} - TMS_{LOW}]_{AK} - [TMS_{HIGH} - TMS_{LOW}]_{FK}$). B) Overlap of the results depicted in (A) with the interaction between associative key presses vs. passive viewing and TMS intensity ($[TMS_{HIGH} - TMS_{LOW}]_{AK} - [TMS_{HIGH} - TMS_{LOW}]_{PV}$). C) Parameter estimates (proportional to the rCBF changes) in six regions of interest as indicated by the arrows in (A). The error bars represent the standard error across subjects.

Figure 4 Task-dependent changes in the functional coupling between the left PMd and other motor areas, assessed using PPI analyses. A) Overlap between the PPI results indicating increased coupling for associative vs. freely selected movements and the PPI results indicating stronger coupling for associative responses compared to passive viewing. The PPI contrasting associative versus freely selected movements was thresholded at $Z = 1.96$ at the voxel level and a cluster extent threshold of 35 voxel. B) Overlap between the PPI results indicating increased coupling for associative versus freely selected movements and the interaction between associative versus freely selected key presses and TMS intensity (as depicted in Fig. 3A).

Figure 1

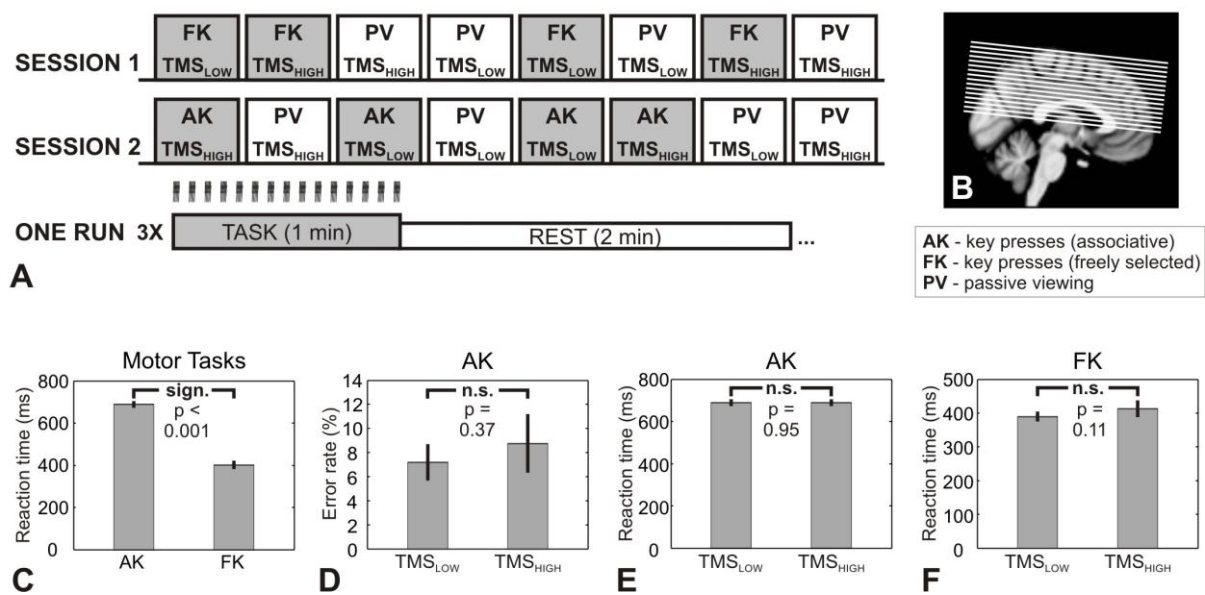


Figure 2

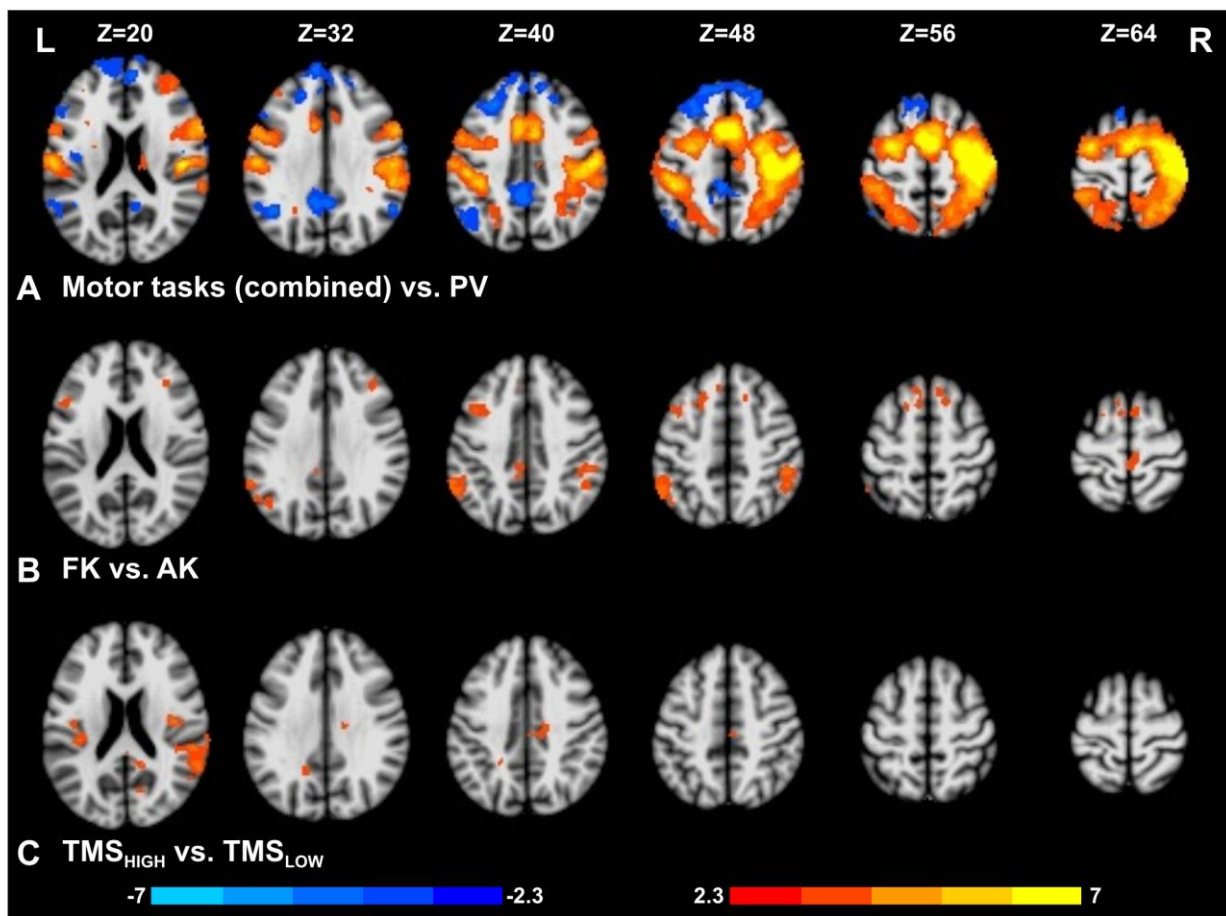


Figure 3

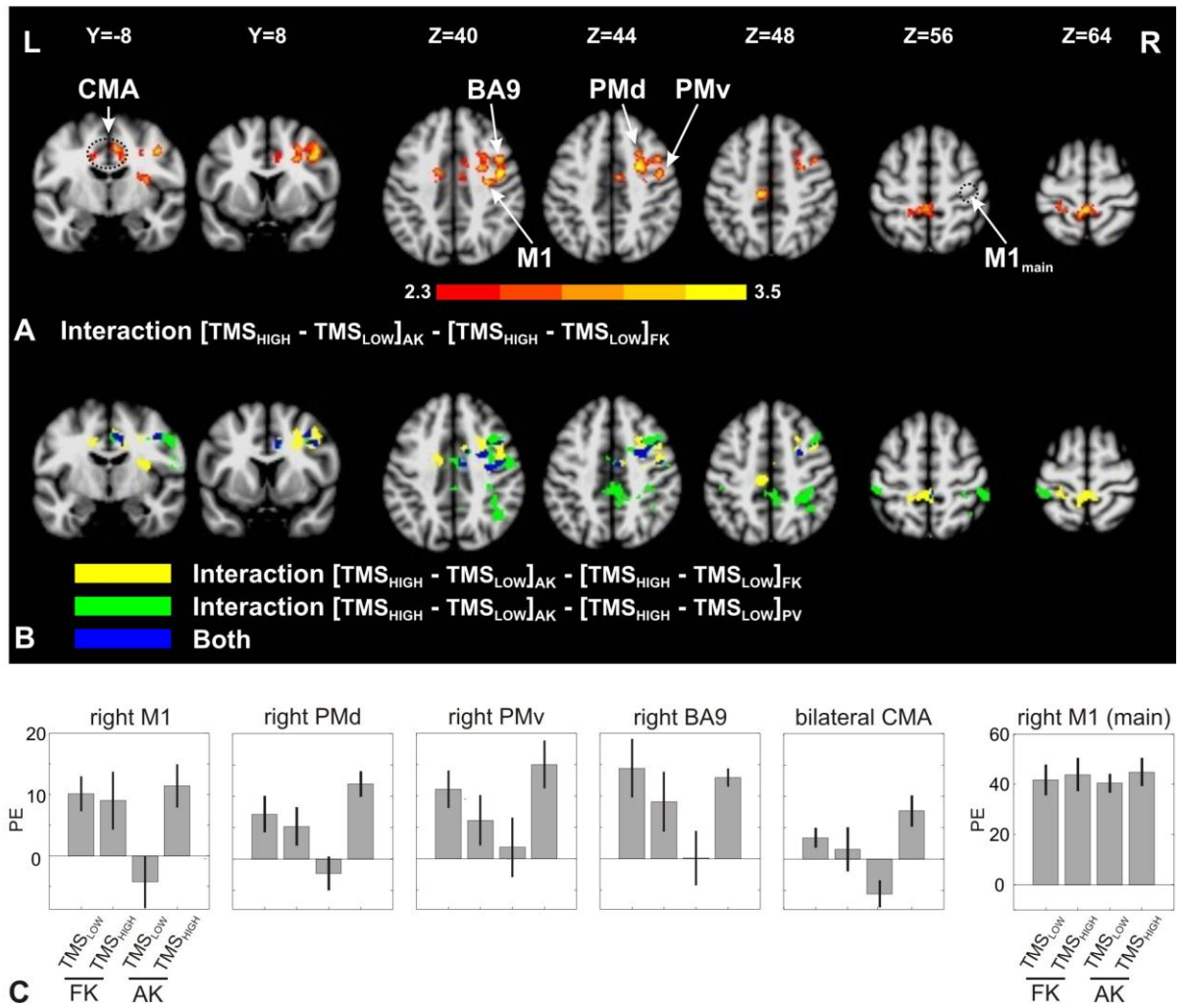
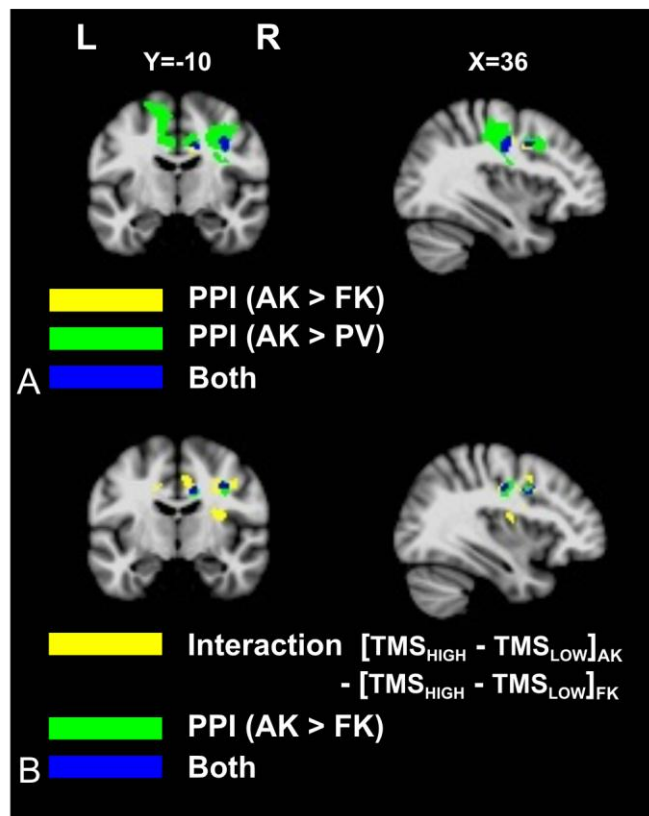


Figure 4



Moisa et al.

Remote motor cortical areas acutely compensate for a transient lesion of left dorsal premotor cortex during arbitrary visuomotor mapping

Supplementary Material

Table S1 Interaction Associative Responses vs. Passive Viewing and TMS intensity

Brain Region	Coordinates of peak activity			Z-value of peak activity	Cluster Volume (mm ³)
	X	Y	Z		
right MFG	32	60	20	2.7	472
right caudal BA9	38	12	40	3.0	2024
right PMd	26	2	46	3.3	1160
right anterior CMA	6	-8	40	3.2	664
	10	20	28	3.2	224
	10	8	34	3.1	220
bilateral posterior CMA	0	-34	44	2.7	1888
right M1	54	-8	40	3.2	1416
right S1(ventral part)	58	-4	24	3.0	760
right S1	34	-36	50	3.2	1408
left S1	-36	-38	66	3.4	2216
right SMG	52	-38	56	3.3	616
right anterior IPS	38	-50	50	3.1	1368

MFG – middle frontal gyrus; BA9 - Brodmann area 9; PMd - dorsal premotor cortex; CMA - cingulate motor area; M1 - primary motor cortex; S1- primary somatosensory cortex; SMG – superior marginal gyrus; IPS – interparietal sulcus.

Table S2 PPI (Associative Responses > Passive Viewing)

Brain Region	Coordinates of peak activity			Z-value of peak activity	Cluster Volume (mm ³)
	X	Y	Z		
right caudal BA9	36	6	38	3.2	608
bilateral SMA (proper/pre)	0	4	60	4.0	5992
right PMd	28	-8	46	3.3	1544
right M1/S1	36	-22	48	3.6	3984
bilateral posterior CMA	8	-24	40	3.6	3376
	-6	-18	42	3.4	3080
left S2 (ventral part)	-58	-22	16	3.3	744

S2- secondary somatosensory motor cortex. For the other abbreviations please see legend of Table S1.

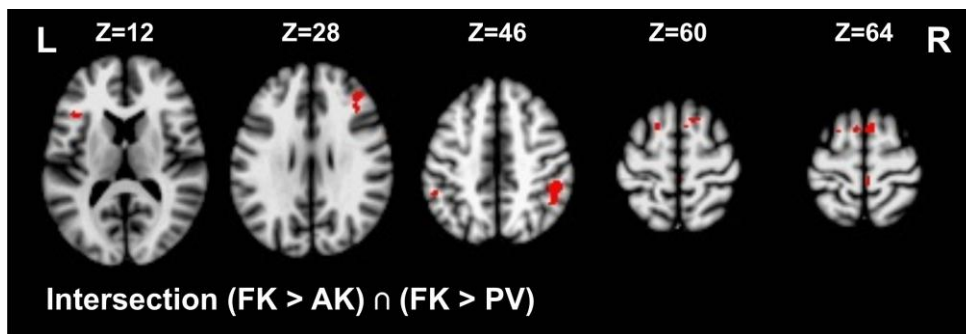


Figure S1 Overlap between the group maps indicating higher rCBF activations for freely selected versus associative responses and freely selected responses versus passive viewing (both were separately thresholded at a voxel level of $Z=2.3$ and an extent threshold of 81 voxel and then intersected; MNI space). Significant rCBF increases occur in the right middle frontal gyrus (MFG), the left inferior frontal gyrus (IFG), the bilateral superior frontal gyri (SFG), the bilateral SMG and the right posterior SMA.

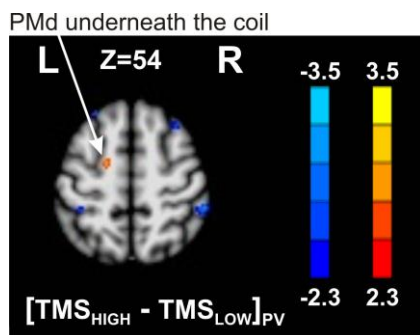


Figure S2 Comparison of TMS_{HIGH} versus TMS_{LOW} , selectively for passive viewing, reveals a significant rCBF increase at the site of stimulation (left PMd; voxel threshold $Z=2.3$, no cluster extent threshold; MNI space).

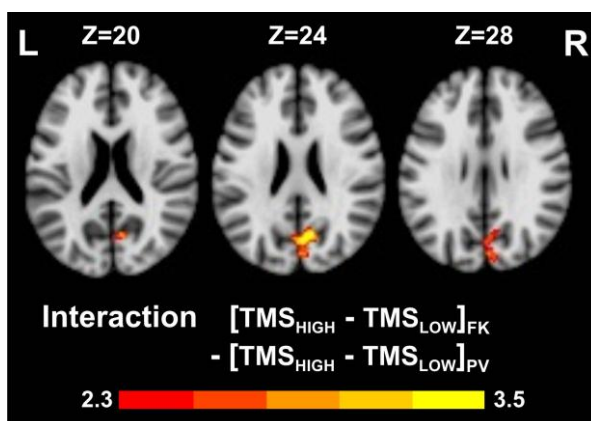


Figure S3 Interaction between freely selected key presses versus passive viewing and TMS intensity ($[TMS_{HIGH} - TMS_{LOW}]_{FK} - [TMS_{HIGH} - TMS_{LOW}]_{PV}$; voxel threshold $Z=2.3$, cluster extent threshold of 81 voxel; MNI space).

Curriculum Vitae

Marius MOISĂ

Fichtenweg 1.1/303,
72076, Tübingen,
Germany

E-mail: marius.moisa@tuebingen.mpg.de
mariusmoisa@yahoo.com



Personal Data:

- Date and place of birth – 30 May 1980, Bacău, Romania
- Nationality – Romanian
- Marital Status – Single

Education:

- 2007 – 2011 **PhD Student**
*Max Planck Institute for Biological Cybernetics,
High-Field Magnetic Resonance Center, Tübingen, Germany.*
Thesis title: “Methodological developments in combining transcranial magnetic stimulation and functional magnetic resonance imaging” (final stage).
- 2002 – 2007 **International Master “Imaging Physics”**
Physics Faculty, University of Siegen, Germany.
Thesis title: “The Detection of Fluorescence X-rays at Synchrotron Radiation Sources for Imaging”.
Degree: **Master of Science**
Grade: **1.1** (very good)
- 1999 – 2004 **Graduate Engineer**
*Faculty of Automatic Control and Computers,
“Politehnica” University, Bucharest, Romania.*
Thesis title: “Detection System for Coronary Angiography with Synchrotron Radiation”.
Degree: **Automatic Control and Computers Engineer**
Grade: **10** (very good, german 1.0)
- 1995 – 1999 **High School Degree**
*Computer Science,
“Ferdinand I National College” Bacău, Romania.*
Grade: **9.04** (good, german 1.52)

Research Awards:

- June 2009 - 15th Annual Meeting of the Organization for Human Brain Mapping, San Francisco, USA (**Trainee Abstract Award**);
- May 2009 - Transcranial Magnetic Stimulation Summer School, London, United Kingdom (**Poster Prize**).

Journal Articles:

Moisa, M., H. R. Siebner, R. Pohmann and A. Thielscher: Interleaved TMS/CASL: Specific Network Effects of Repetitive TMS on the Dorsal Premotor Cortex for Externally versus Internally Guided Movements. (submitted)

Moisa, M., R. Pohmann, K. Uludag and A. Thielscher: Interleaved TMS/CASL: Comparison of different rTMS protocols. *NeuroImage*, 49(1), January 2010

Moisa, M., R. Pohmann, L. Ewald and A. Thielscher: A new coil positioning method for interleaved TMS/fMRI and its validation in a motor cortex study. *Journal of Magnetic Resonance Imaging*, 29(1), January 2009

Selected Conference Articles:

Moisa, M., H. R. Siebner, R. Pohmann and A. Thielscher: Interleaved TMS/CASL: State Dependence of Repetitive TMS Effects on the Dorsal Premotor Cortex. 16th Annual Meeting of the Organization for Human Brain Mapping (Barcelona, Spain), (06 2010)

Moisa, M., H. R. Siebner, R. Pohmann and A. Thielscher: Interleaved TMS/CASL: State Dependence of Repetitive TMS Effects on the Dorsal Premotor Cortex. 18th Annual Meeting of the International Society for Magnetic Resonance in Medicine (Stockholm, Sweden), (05 2010)

Moisa, M., R. Pohmann, K. Uludag and A. Thielscher: Interleaved TMS/CASL: Comparison of different rTMS protocols. 15th Annual Meeting of the Organization for Human Brain Mapping (San Francisco, USA), (06 2009) – **Trainee Abstract Award**

Moisa, M., R. Pohmann, K. Uludag and A. Thielscher: Interleaved TMS/CASL: Comparison of different rTMS protocols. 2009 TMS Summer School (London, United Kingdom), (05 2009) – **Poster Prize**

Moisa, M., R. Pohmann, K. Uludag and A. Thielscher: Interleaved TMS/CASL: A motor cortex study. 3rd International Conference on TMS and tDCS (Göttingen, Germany), (10 2008)

Moisa, M., R. Pohmann and A. Thielscher: A new hardware-software coil positioning system for interleaved TMS/fMRI: A motor cortex stimulation study. 16th Annual Meeting of the International Society for Magnetic Resonance in Medicine (Toronto, Canada), (05 2008)